PEOPLE'S DEMOCRATIC REPUBLIC OF ALGERIA
MINISTRY OF HIGHER EDUCATION AND SCIENTIFIC RESEARCH

UNIVERSITY OF ECHAHID CHEIKH LARBI TEBESSI – TEBESSA
FACULTY OF SCIENCE AND TECHNOLOGY
DEPARTMENT OF ELECTRONICS AND COMMUNICATIONS

THESIS

Presented for obtaining the diploma of
3rd Cycle LMD DOCTORATE

In: TELECOMMUNICATIONS
Speciality: Telecommunications

by:

Ahmed Ould Mohamed Salem

Design and Optimization of Antenna for Next Generation

Discussed publicly on: **15/09/2026**, in front of the jury composed of:

Abdelaziz AOUICHE	Professor	Echahid Cheikh Larbi Tebessi Tebessa University	**Chairman**
Hanane DJELLAB	Professor	Echahid Cheikh Larbi Tebessi Tebessa University	**Supervisor**
Mohamed LASHAB	Professor	Larbi Ben M'hidi – Oum El Bouaghi University	**Co-supervisor**
Mahmoud MAAMRI	MCA	Echahid Cheikh Larbi Tebessi Tebessa University	**Examiner**
Fouzia MAAMRI	MCA	Abbes Laghrour Khenchela University	**Examiner**
Farouk BOUMEHREZ	MCA	08 May 1945 Guelma University	**Examiner**

Acknowledgements

I would like to express my sincere gratitude to my supervisors, Prof. Hanane Djellab and Prof. Mohamed Lashab, for their invaluable guidance, constructive feedback, and unwavering support throughout this doctoral research. Their expertise in antenna design and electromagnetic theory was instrumental in shaping this study.

I would also like to extend my deepest appreciation to the distinguished members of the jury for accepting to review and judge this thesis.

I would also like to sincerely thank Professor Chan Hwang See, School of Computing, Engineering and the Built Environment, Edinburgh Napier University, Edinburgh, UK, for kindly fabricating the antenna prototype used in this thesis.

We gratefully acknowledge the Faculty of Science and Technology, particularly the Department of Electronics and Telecommunications, for providing a stimulating academic environment and valuable knowledge. The high quality of education and the professionalism of the staff have significantly contributed to my academic development.

Finally, I extend my heartfelt appreciation to my family for their unwavering support and encouragement throughout my doctoral study. Most importantly, I dedicate this thesis to the memory of my beloved mother, whose love, sacrifice, and encouragement have been the foundation of all my accomplishments. Although she is no longer with us, her spirit and wisdom continue to guide me. This work is a testament to her enduring legacy and the values she has instilled in me.

Abstract

The rapid evolution of fifth-generation (5G) and beyond fifth-generation (B5G) wireless communication systems has significantly increased the demand for compact, high-performance, and computationally efficient millimeter-wave (mmWave) antenna architectures. However, the design of mmWave Multiple-Input Multiple-Output (MIMO) antennas remains highly challenging due to the simultaneous requirements of high gain, wide bandwidth, compact integration, low mutual coupling, and reduced computational complexity. In addition, conventional full-wave electromagnetic optimization techniques are computationally expensive and time-consuming, particularly for iterative antenna-design procedures. To address these challenges, this doctoral thesis proposes a hybrid electromagnetic and physics-guided artificial intelligence framework for the design, optimization, and rapid synthesis of high-performance mmWave MIMO antennas. The proposed methodology combines advanced electromagnetic engineering techniques with physics-guided neural learning strategies to improve both antenna performance and computational efficiency. In the first part of this work, a compact four-element 28 GHz MIMO antenna system was designed, fabricated, and experimentally validated for 5G mmWave applications. The proposed antenna architecture integrates Defected Ground Structures (DGS) and a Frequency Selective Surface (FSS) superstrate to reduce mutual coupling and enhance radiation performance. The incorporation of the FSS superstrate at an optimized distance of 7 mm improved the antenna gain from 4.8 dBi to 8.4 dBi, corresponding to an enhancement of approximately 75% (+3.6 dBi). In addition, the proposed decoupling configuration achieved port-to-port isolation exceeding 25 dB while maintaining satisfactory MIMO diversity performance. To overcome the computational limitations of conventional full-wave solvers, a dual-network Physics-guided AI framework was developed for inverse antenna synthesis and forward electromagnetic prediction. The inverse synthesis model was trained using 8,000 analytically generated samples derived from Transmission-Line Model (TLM) equations, while the forward analysis model was independently trained using 475 high-fidelity CST full-wave simulation samples. By integrating electromagnetic prior knowledge into the neural learning process, the proposed framework preserves physical consistency while improving prediction accuracy and computational efficiency. The developed framework reduced the antenna synthesis time from several hours of full-wave simulations to only a few milliseconds. The inverse synthesis model achieved sub-millimeter prediction accuracy with a Root Mean Squared Error (RMSE) of W_p ($\approx 0.00156\,\mathrm{mm}$) and

L_p (≈ 0.00169 mm) and a regression coefficient of (R2 = 0.99999), while the forward prediction model limited the relative resonant frequency prediction error to only 0.08% compared with CST full-wave simulation results. Overall, the proposed hybrid electromagnetic–AI framework establishes a scalable and computationally efficient methodology for intelligent antenna synthesis and multi-objective optimization in next-generation wireless communication systems, with strong applicability to future 5G-Advanced and 6G mmWave technologies.

Keywords: Microstrip patch antenna, Millimeter-wave (mmWave), Fifth-generation (5G) communications, Physics-guided AI, Artificial Neural Network (ANN), CST Microwave Studio, Multiple-Input Multiple-Output (MIMO).

ملخص

أدى التطور السريع لأنظمة الاتصالات اللاسلكية من الجيل الخامس (5G) وما بعد الجيل الخامس (B5G) إلى زيادة كبيرة في الطلب على هياكل هوائيات الموجات المليمترية (mmWave) المدمجة، عالية الأداء، وذات الكفاءة الحسابية العالية. ومع ذلك، لا يزال تصميم هوائيات الإدخال والإخراج المتعدد (MIMO) للموجات المليمترية يمثل تحديًا كبيرًا بسبب المتطلبات المتزامنة المتعلقة بتحقيق كسب مرتفع، وعرض نطاق واسع، وتكامل مدمج، وانخفاض الاقتران المتبادل، وتقليل التعقيد الحسابي. بالإضافة إلى ذلك، فإن تقنيات التحسين الكهرومغناطيسي التقليدية المعتمدة على المحاكاة الكاملة للموجات (Full-Wave) تُعد مكلفة حسابيًا وتستغرق وقتًا طويلًا، خاصةً في إجراءات تصميم الهوائيات التكرارية.

ولمواجهة هذه التحديات، تقترح هذه الأطروحة الدكتورالية إطارًا هجينًا يجمع بين الكهرومغناطيسية والذكاء الاصطناعي الموجَّه بالفيزياء، وذلك لتصميم وتحسين والتوليف السريع لهوائيات MIMO عالية الأداء للموجات المليمترية. تجمع المنهجية المقترحة بين تقنيات الهندسة الكهرومغناطيسية المتقدمة واستراتيجيات التعلم العصبي الموجَّه بالفيزياء بهدف تحسين أداء الهوائي والكفاءة الحسابية في آنٍ واحد.

في الجزء الأول من هذا العمل، تم تصميم وتصنيع والتحقق تجريبيًا من نظام هوائي MIMO مدمج مكوَّن من أربعة عناصر يعمل عند تردد 28 GHz لتطبيقات الجيل الخامس ذات الموجات المليمترية. يعتمد الهيكل المقترح للهوائي على دمج بنية الأرضية المعيبة (DGS) وسطح فائق انتقائي للترددات (FSS) بهدف تقليل الاقتران المتبادل وتحسين الأداء الإشعاعي. وقد أدى دمج طبقة الـFSS على مسافة مثلى قدرها 7 مم إلى تحسين كسب الهوائي من 4.8 dBi إلى 8.4 dBi، وهو ما يعادل زيادة تقارب 75% (+6.3 dBi). بالإضافة إلى ذلك، حققت البنية المقترحة للعزل قيمة فصل بين المنافذ تجاوزت 44 dB مع الحفاظ على أداء مرضٍ لتنوع MIMO.

ولتجاوز القيود الحسابية الخاصة بالمحللات الكهرومغناطيسية التقليدية، تم تطوير إطار ذكاء اصطناعي موجَّه بالفيزياء يعتمد على شبكتين عصبيتين للتوليف العكسي للهوائي والتنبؤ الكهرومغناطيسي الأمامي. تم تدريب نموذج التوليف العكسي باستخدام 8,000 عينة مولدة تحليليًا اعتمادًا على معادلات نموذج خط النقل (TLM)، في حين تم تدريب نموذج التحليل الأمامي بشكل مستقل باستخدام 475 عينة عالية الدقة ناتجة عن محاكاة CST الكاملة للموجات. ومن خلال دمج المعرفة الكهرومغناطيسية المسبقة داخل عملية التعلم العصبي، يحافظ الإطار المقترح على الاتساق الفيزيائي مع تحسين دقة التنبؤ والكفاءة الحسابية.

وقد ساهم الإطار المطوَّر في تقليل زمن توليف الهوائي من عدة ساعات من المحاكاة الكاملة للموجات إلى بضعة أجزاء من الألف من الثانية فقط. وحقق نموذج التوليف العكسي دقة تنبؤ دون المليمتر مع خطأ متوسط تربيعي (RMSE) لكل من W_p (≈ 0.00156 mm) وL_p (≈ 0.00169 mm)، ومعامل انحدار بلغ (R2 = 0.99999)، بينما حدَّ نموذج التنبؤ الأمامي من الخطأ النسبي في التنبؤ بتردد الرنين إلى 0.08% فقط مقارنة بنتائج محاكاة CST الكاملة للموجات.

بصورة عامة، يرسّخ الإطار الهجين المقترح بين الكهرومغناطيسية والذكاء الاصطناعي منهجيةً قابلة للتوسع وفعّالة حسابيًا من أجل التوليف الذكي للهوائيات والتحسين متعدد الأهداف في أنظمة الاتصالات اللاسلكية من الجيل القادم، مع قابلية تطبيق قوية على تقنيات الموجات المليمترية المستقبلية للجيل الخامس المتقدم (5G-Advanced) والجيل السادس (6G).

الكلمات المفتاحية: هوائي الرقعة الميكروستريب، الموجات المليمترية (mmWave)، اتصالات الجيل الخامس (5G)، الذكاء الاصطناعي الموجه بالفيزياء، الشبكة العصبية الاصطناعية (ANN)، CST Microwave Studio، متعدد المداخل والمخارج (MIMO).

Résumé

L'évolution rapide des systèmes de communication sans fil de cinquième génération (5G) et au-delà de la cinquième génération (B5G) a considérablement accru la demande en architectures d'antennes à ondes millimétriques (mmWave) compactes, performantes et à haute efficacité computationnelle. Cependant, la conception des antennes MIMO (Multiple-Input Multiple-Output) pour les ondes millimétriques demeure particulièrement complexe en raison des exigences simultanées de gain élevé, de large bande passante, d'intégration compacte, de faible couplage mutuel et de réduction de la complexité computationnelle. De plus, les techniques conventionnelles d'optimisation électromagnétique basées sur les simulations électromagnétiques complètes (full-wave) sont coûteuses en ressources de calcul et nécessitent un temps d'exécution important, notamment dans les procédures itératives de conception d'antennes.

Afin de répondre à ces défis, cette thèse de doctorat propose un cadre hybride combinant l'électromagnétisme et l'intelligence artificielle guidée par la physique pour la conception, l'optimisation et la synthèse rapide d'antennes MIMO mmWave à hautes performances. La méthodologie proposée associe des techniques avancées d'ingénierie électromagnétique à des stratégies d'apprentissage neuronal guidées par les lois physiques afin d'améliorer simultanément les performances des antennes et l'efficacité computationnelle.

Dans la première partie de ce travail, un système d'antenne MIMO compact à quatre éléments fonctionnant à 28 GHz a été conçu, fabriqué et validé expérimentalement pour des applications 5G mmWave. L'architecture proposée intègre des structures de masse défectueuse (DGS : Defected Ground Structures) ainsi qu'une surface sélective en fréquence (FSS : Frequency Selective Surface) utilisée comme superstrat afin de réduire le couplage mutuel et d'améliorer les performances de rayonnement. L'intégration du superstrat FSS à une distance optimale de 7 mm a permis d'augmenter le gain de l'antenne de 4.8 dBi à 8.4 dBi, correspondant à une amélioration d'environ 75% (+3.6 dBi). En outre, la configuration de découplage proposée a permis d'obtenir une isolation entre ports supérieure à 25 dB tout en maintenant des performances satisfaisantes en diversité MIMO.

Pour surmonter les limitations computationnelles des solveurs électromagnétiques conventionnels, un cadre d'intelligence artificielle guidée par la physique reposant sur deux réseaux neuronaux a été développé pour la synthèse inverse des antennes et la prédiction électromagnétique directe. Le modèle de synthèse inverse a été entraîné à l'aide de 8 000 échantillons générés analytiquement à partir des équations du modèle de ligne de transmission (TLM : Transmission-Line Model), tandis que le modèle d'analyse directe a été entraîné indépendamment à l'aide de 475 échantillons haute fidélité issus des simulations électromagnétiques complètes réalisées sous CST. En intégrant des connaissances électromagnétiques a priori

dans le processus d'apprentissage neuronal, le cadre proposé garantit la cohérence physique tout en améliorant la précision des prédictions et l'efficacité computationnelle.

Le cadre développé a permis de réduire le temps de synthèse des antennes, passant de plusieurs heures de simulations full-wave à seulement quelques millisecondes. Le modèle de synthèse inverse a atteint une précision de prédiction submillimétrique avec une erreur quadratique moyenne (RMSE) de W_p ($\approx 0.00156\,\text{mm}$) et L_p ($\approx 0.00169\,\text{mm}$), ainsi qu'un coefficient de régression (R2 = 0.99999), tandis que le modèle de prédiction directe a limité l'erreur relative de prédiction de la fréquence de résonance à seulement 0.08% par rapport aux résultats des simulations full-wave sous CST.

Globalement, le cadre hybride électromagnétisme–intelligence artificielle proposé établit une méthodologie évolutive et efficace sur le plan computationnel pour la synthèse intelligente et l'optimisation multi-objectifs des antennes dans les systèmes de communication sans fil de nouvelle génération, avec une forte applicabilité aux futures technologies mmWave de la 5G-Advanced et de la 6G.

Mots-clés : Antenne patch microruban, Ondes millimétriques (mmWave), Communications de cinquième génération (5G), Intelligence artificielle guidée par la physique, Réseau de neurones artificiels (ANN), CST Microwave Studio, Entrées multiples sorties multiples (MIMO).

Contents

List of Figures

List of Tables

Abbreviations

5G Fifth Generation
6G Sixth Generation
AI Artificial Intelligence
ANN Artificial Neural Network
BW Bandwidth
CEM Computational Electromagnetics
CST Computer Simulation Technology
DG Diversity Gain
DGS Defected Ground Structure
EBG Electromagnetic Band Gap
ECC Envelope Correlation Coefficient
FSS Frequency Selective Surface
GUI Graphical User Interface
IoT Internet of Things
LM Levenberg-Marquardt
MAE Mean Absolute Error
MEG Mean Effective Gain
MIMO Multiple-Input Multiple-Output
ML Machine Learning
MLP Multilayer Perceptron
mmWave Millimeter Wave
MPA Microstrip Patch Antenna
MSE Mean Squared Error
RBF Radial Basis Function
ReLU Rectified Linear Unit
RF Random Forest
RMSE Root Mean Squared Error
SISO Single-Input Single-Output
SVM Support Vector Machine
SVR Support Vector Regression
TLM Transmission-Line Model

VNA Vector Network Analyzer

Chapter 1

General Introduction

1.1 Background and Challenges of 5G/mmWave Communications

The exponential growth of global mobile data traffic, driven by emerging applications such as ultra-high-definition video streaming, Internet of Things (IoT) networks, autonomous transportation systems, and immersive virtual and augmented reality technologies, has significantly accelerated the evolution of wireless communication systems from first-generation (1G) to fifth-generation (5G) networks and beyond [1, 2]. To satisfy the stringent requirements of ultra-high data rates, massive connectivity, and ultra-low latency, 5G and emerging sixth-generation (6G) communication systems increasingly rely on the millimeter-wave (mmWave) frequency spectrum, formally designated in 3GPP standards as Frequency Range 2 (FR2), spanning approximately 24 GHz to 52 GHz[3].

Despite the substantial bandwidth resources offered by mmWave frequencies, their practical deployment introduces major propagation challenges. Compared with conventional sub-6 GHz systems, mmWave signals experience severe free-space path loss, atmospheric attenuation caused by oxygen and water vapor absorption, and high sensitivity to physical blockages and environmental obstructions [4].

Consequently, the realization of reliable mmWave communication links requires the integration of advanced Multiple-Input Multiple-Output (MIMO) technologies, highly directive antenna architectures, and efficient beamforming strategies capable of compensating for these propagation impairments [2].

1.2 Scientific Problem and Technical Challenges

The deployment of compact mmWave massive MIMO systems introduces increasingly stringent and often conflicting electromagnetic, hardware, and computational constraints. Although mmWave technologies provide substantial improvements in spectral efficiency, channel capacity, and ultra-high data-rate transmission, several critical challenges continue to hinder their practical implementation in next-generation wireless communication systems. These limitations arise primarily from severe propagation losses, compact antenna integration constraints, mutual coupling effects, and the high computational complexity associated with full-wave electromagnetic optimization techniques.

1.2.1 Antenna Design Bottleneck

The design of compact multiband and high-gain antenna systems constitutes a highly nonlinear and multi-objective optimization problem. In order to compensate for the severe free-space path loss encountered at mmWave frequencies, particularly at 28 GHz and 38 GHz, antenna structures must simultaneously provide high gain, strong directivity, compact size, and wide operational bandwidth [5].

Traditionally, antenna optimization relies on Computational Electromagnetics (CEM) simulation tools, such as CST Microwave Studio and HFSS, which are based on rigorous numerical techniques including the Finite Element Method (FEM) and the Finite Difference Time Domain (FDTD) method. Although these full-wave solvers provide highly accurate electromagnetic predictions, they remain computationally intensive and time-consuming, especially when addressing complex multi-parameter optimization problems. Consequently, conventional iterative trial-and-error optimization methodologies have become increasingly inefficient for modern mmWave antenna synthesis and design[6, 7].

1.2.2 Mutual Coupling in MIMO Systems

To achieve the high spectral efficiency and channel capacity targeted by 5G and beyond-5G communication systems without significantly increasing transmission power, multiple antenna elements must be integrated within the limited physical dimensions of modern wireless devices and compact base stations[8]. However, reducing the inter-element spacing inevitably intensifies electromagnetic interactions between adjacent antenna elements, leading to strong mutual coupling.

Excessive mutual coupling degrades radiation efficiency, distorts radiation characteristics, and significantly increases the Envelope Correlation Coefficient (ECC), thereby reducing the spatial diversity gain required for efficient MIMO operation [9, 10]. Consequently, maintaining high port-to-port isolation, typically exceeding 25 dB, while preserving compactness and radiation performance, remains one of the most critical design challenges in mmWave MIMO antenna engineering.

1.2.3 Need for Intelligent Design Frameworks

The simultaneous requirements of antenna miniaturization, high gain, wide bandwidth, strong isolation, and reduced computational complexity transform modern antenna engineering into a highly constrained and computationally demanding optimization problem. Although conventional full-wave electromagnetic solvers provide high modeling accuracy, their computational inefficiency limits their applicability for rapid antenna synthesis and large-scale multi-objective optimization, particularly when dealing with complex electromagnetic structures such as Frequency Selective Surfaces (FSS) and Defected Ground Structures (DGS). In this context, Artificial Intelligence (AI) and Machine Learning (ML) techniques have emerged as promising alternatives for accelerating electromagnetic optimization through surrogate modeling and intelligent synthesis methodologies. Nevertheless, conventional data-driven approaches frequently suffer from limited physical interpretability, poor generalization capability, and the inherent ambiguity associated with black-box learning models [11, 12].

Consequently, this work adopts a physics-guided AI framework that combines analytical electromagnetic knowledge with CST-generated datasets to improve computational efficiency, prediction accuracy, and electromagnetic consistency for mmWave antenna design applications. Unlike conventional black-box Artificial Neural Networks (ANNs), the proposed methodology incorporates analytical information derived from electromagnetic theory and Transmission-Line Models (TLMs) directly into the neural learning process. This strategy improves physical consistency while preserving the computational efficiency of ANN-based surrogate modeling. As a result, the proposed framework establishes a computationally efficient and physically reliable methodology for intelligent mmWave antenna synthesis and electromagnetic prediction.

1.3 Research Questions

To address the aforementioned challenges, this thesis seeks to answer the following fundamental research questions:

1. How can compact MIMO antenna arrays be designed to operate efficiently in the 5G mmWave band (e.g., 28 GHz) while intrinsically achieving high gain and superior port-to-port isolation without excessively increasing the device footprint?
2. How can advanced electromagnetic decoupling structures, such as Frequency Selective Surfaces (FSS) and Defected Ground Structures (DGS), be optimally integrated into MIMO systems to mitigate mutual coupling and improve diversity metrics (ECC, DG)?
3. How can Artificial Intelligence and Machine Learning techniques be synergized with foundational electromagnetic physics to bypass the computational bottlenecks of traditional full-wave simulators?

4. Can a unified physics-guided AI framework be developed to simultaneously perform rapid inverse antenna synthesis and accurate forward electromagnetic prediction while preserving physical consistency and computational efficiency?

1.4 Objectives of the Thesis

Motivated by the identified scientific gaps and the previously formulated research questions, this thesis aims to develop an integrated electromagnetic and artificial intelligence-assisted framework for the design, optimization, and rapid synthesis of high-performance mmWave MIMO antennas. The principal objectives of this research are summarized as follows:

- **Develop Compact High-Performance mmWave MIMO Antennas**: Design, optimize, fabricate, and experimentally validate a compact 28 GHz MIMO antenna architecture integrating Defected Ground Structures (DGS) and Frequency Selective Surface (FSS) techniques to achieve high gain, strong port-to-port isolation, and enhanced diversity performance.
- **Bridge Computational Electromagnetics and Artificial** Intelligence: Develop a robust AI-assisted optimization framework capable of reducing the computational complexity associated with conventional full-wave electromagnetic simulations through efficient surrogate modeling and intelligent parameter prediction.
- **Enable Intelligent Multi-Objective Antenna Synthesis:** Propose an automated inverse design methodology capable of generating optimized antenna geometries from predefined electromagnetic specifications while ensuring high computational efficiency, prediction accuracy, and physical consistency.

1.5 Main Contributions

This doctoral research contributes to bridging the gap between computational electromagnetics and intelligent optimization methodologies for next-generation mmWave antenna engineering. The principal scientific contributions of this thesis are summarized as follows:

1. **Design and Experimental Validation of a High-Isolation mmWave MIMO Antenna:** A compact four-element 28 GHz MIMO antenna integrating Defected Ground Structures (DGS) and a Frequency Selective Surface (FSS) superstrate was designed, optimized, fabricated, and experimentally validated. The proposed antenna architecture achieved significant gain enhancement and inter-element isolation exceeding 25 dB across the targeted operating band while maintaining excellent MIMO diversity performance metrics.
2. **Development of a Physics-Guided AI Framework for Antenna Synthesis and Analysis** A hybrid physics-guided AI optimization framework was developed by

combining analytical Transmission-Line Model (TLM) equations with high-fidelity CST full-wave electromagnetic simulations. The proposed framework simultaneously performs inverse antenna synthesis and forward electromagnetic prediction while significantly reducing computational cost and antenna-design time. The developed framework achieved sub-millimeter dimensional prediction accuracy together with resonant-frequency prediction errors below 0.1% compared with CST full-wave simulation results.

1.6 Organization of the Thesis

To ensure a coherent and systematic presentation of the research work, this thesis is organized into six chapters as follows:

- **Chapter 1: General Introduction.** Introduces the scientific background of 5G and mmWave communication systems, presents the main research challenges, and outlines the research questions, objectives, and scientific contributions of the thesis.
- **Chapter 2: Fundamentals of Antennas and MIMO Systems.** Presents the theoretical foundations required for this study, including antenna theory, microstrip antenna principles, and the fundamental concepts and performance metrics associated with MIMO communication systems.
- **Chapter 3: State of the Art and Research Gap.** Provides a comprehensive review of existing literature on mmWave MIMO antennas, mutual coupling reduction techniques, and AI-assisted electromagnetic optimization methods, leading to the identification of current research limitations and scientific gaps.
- **Chapter 4: Design and Experimental Validation of a 28 GHz MIMO Antenna.** Details the design methodology, electromagnetic optimization, fabrication process, and experimental validation of the proposed high-isolation mmWave MIMO antenna integrating DGS and FSS structures.
- **Chapter 5: ANN-Based Antenna Synthesis and Optimization.** Describes the proposed physics-guided AI framework, including dataset generation, ANN architectures, training methodologies, electromagnetic validation, and intelligent antenna synthesis procedures.
- **Chapter 6: General Conclusion and Future Work.** Summarizes the principal findings and contributions of the thesis and outlines future research directions related to intelligent electromagnetic optimization and next-generation wireless communication systems..

Part I

Foundations and State of the Art

Chapter 2

Fundamentals of Antennas and MIMO Structures

2.1 Introduction

This chapter establishes the theoretical and conceptual foundations necessary for the analysis, design, and optimization of advanced antenna systems, with particular emphasis on microstrip patch antennas (MPAs) and Multiple-Input Multiple-Output (MIMO) technologies. In the context of the rapid evolution of wireless communication systems toward fifth-generation (5G) and emerging sixth-generation (6G) networks, antenna systems have become fundamental enabling components for next-generation communication infrastructures. Their role is critical in achieving ultra-high data rates, enhanced link reliability, improved spectral efficiency, and low-latency communication without requiring additional transmit power or excessive spectrum allocation [13].

The chapter begins with an overview of the evolution of cellular communication systems, spanning from first-generation (1G) analog networks to the prospective sixth-generation (6G) paradigm [14]. This technological progression reflects the continuous transformation of wireless systems from conventional voice-oriented architectures toward highly intelligent, data-centric, and massively connected communication ecosystems. Furthermore, this evolution highlights substantial advancements in key performance indicators (KPIs), communication architectures, and emerging application domains, including the Internet of Things (IoT), autonomous transportation systems, immersive extended reality (XR), and holographic communications [15].Such a historical and technological perspective provides essential insight into the increasingly stringent requirements imposed on modern radio-frequency (RF) systems, particularly in terms of antenna miniaturization, wideband operation, high radiation efficiency, and adaptive beam management [14].

Subsequently, the chapter investigates the frequency spectrum allocations associated with 5G and future 6G communication systems, including the sub-6 GHz, millimeter-wave (mmWave), and Terahertz (THz) frequency bands[16] .Although the exploitation of high-frequency spectrum bands provides access to large underutilized bandwidths capable of supporting terabit-per-second (Tbps) data rates, these frequency ranges introduce severe propagation impairments, including high free-space path loss, molecular absorption,atmospheric attenuation, and strong sensitivity to environmental blockages. Consequently, overcoming these limitations requires the development of highly directive antenna architectures, advanced beamforming mechanisms, and sophisticated signal processing techniques capable of maintaining reliable and high-capacity communication links [8, 17].

To address these challenges, this chapter introduces microstrip patch antennas (MPAs), which are widely adopted in modern wireless systems due to their low-profile geometry, lightweight structure, low fabrication cost, and compatibility with planar and integrated circuit technologies [18].The discussion covers the fundamental operating principles of MPAs, common geometrical configurations, and various feeding mechanisms. In addition, essential antenna performance parameters are rigorously analyzed, including radiation pattern, directivity, gain, impedance bandwidth, efficiency, and polarization characteristics, all of which play a crucial role in evaluating antenna performance in practical wireless applications.

The chapter further explores Multiple-Input Multiple-Output (MIMO) antenna systems, which constitute one of the core enabling technologies of high-capacity wireless communication systems [14]. Fundamental MIMO concepts, including spatial multiplexing and diversity techniques, are comprehensively discussed. In particular, spatial multiplexing enables the simultaneous transmission of multiple independent data streams through multipath propagation environments, thereby significantly enhancing spectral efficiency and channel capacity. Moreover, critical MIMO performance metrics are examined, including isolation, Envelope Correlation Coefficient (ECC), Diversity Gain (DG), Total Active Reflection Coefficient (TARC), Mean Effective Gain (MEG), and channel capacity. These parameters are essential for evaluating the electromagnetic interaction between antenna elements and ensuring efficient, low-correlation, and independent channel operation in compact MIMO architectures.

Finally, the chapter presents an overview of advanced mutual coupling reduction and decoupling techniques used in compact MIMO antenna arrays, including Defected Ground Structures (DGS), Electromagnetic Band Gap (EBG) structures, and Frequency Selective Surfaces (FSS). These techniques play a fundamental role in improving port-to-port isolation, enhancing radiation efficiency, and preserving diversity performance in densely integrated antenna systems[9].

Overall, this chapter provides a comprehensive theoretical framework that supports the subsequent design, analysis, and optimization of high-performance antenna systems for next-generation wireless communication applications. Furthermore, it establishes the scientific foundation necessary for the development of intelligent and physics-guided antenna optimization methodologies presented in the following chapters.

2.2 Evolution of Cellular Networks (1G → 6G)

The evolution of wireless communication systems has been driven by the continuous increase in mobile data tra ffic and the growing demand for high-speed, reliable, and low-latency wireless connectivity[14] . Modern wireless networks have progressively evolved from conventional voice-oriented systems toward highly interconnected and data-centric communication infrastructures capable of supporting emerging applications such as the Internet of Things (IoT), autonomous transportation systems, immersive extended reality (XR), and intelligent industrial automation [15].

Fig. 2.1 illustrates the evolution of cellular communication networks from first-generation (1G) systems to future 6G networks, highlighting the major technological advancements, operating frequency bands, transmission data rates, and representative application domains associated with each generation of mobile communications.

In this context, fifth-generation (5G) and Beyond 5G (B5G) networks introduce major technological advancements, including Massive Multiple-Input Multiple-Output (Massive MIMO), beamforming, edge computing, and millimeter-wave (mmWave) communications [19].

These technologies enable multi-gigabit-per-second transmission rates, massive connectivity, and improved spectral efficiency, thereby satisfying the increasing requirements of next-generation wireless applications.

However, the growing complexity of future communication systems introduces significant challenges related to electromagnetic propagation, antenna miniaturization, mutual coupling reduction, and computational optimization. Consequently, the development of compact, high-performance, and computationally efficient antenna architectures has become a major research direction in modern wireless communications.

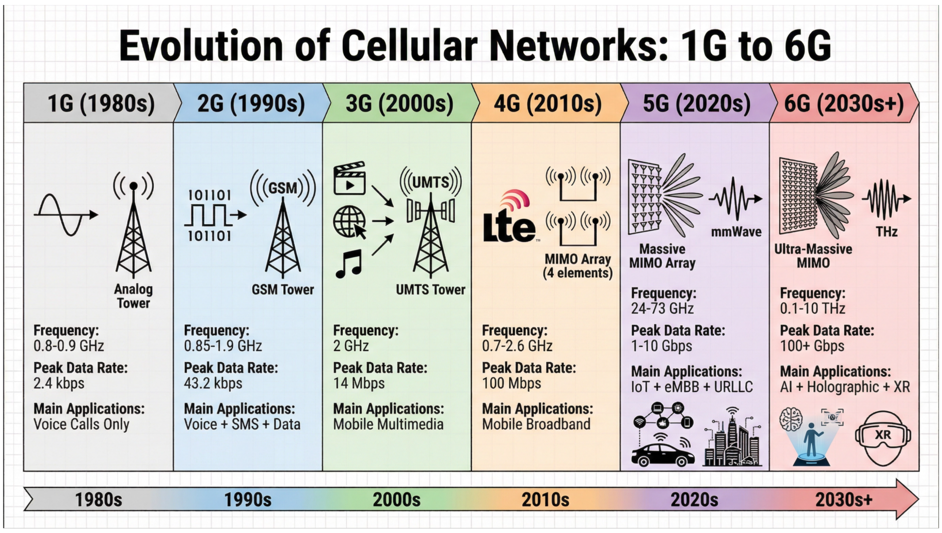

Figure 2.1: *Evolution of cellular networks from 1G to 6G and their corresponding technological advancements.*

2.2.1 Evolutionary Trends and Emerging Requirements

The transition toward 5G and future 6G networks is characterized by increasingly stringent requirements in terms of spectral efficiency, latency reduction, energy efficiency, and network scalability [15]. In addition to enhanced mobile broadband (eMBB), future wireless systems are expected to support ultra-reliable low-latency communications (URLLC) and massive machine-type communications (mMTC), enabling applications such as smart cities, autonomous vehicles, industrial automation, and immersive wireless environments. Future 6G systems are also expected to integrate advanced technologies such as Artificial Intelligence (AI), Ultra-Massive MIMO, Reconfigurable Intelligent Surfaces (RIS), and Terahertz (THz) communications in order to develop intelligent, adaptive, and ultra-high-capacity wireless networks.

To satisfy these demanding requirements, wireless communication systems are progressively shifting toward higher-frequency spectrum allocations, as summarized in Table 2.1.

Table 2.1: *Spectrum allocation tiers for 5G and 6G*

Tier	**Frequency Range**	**Main Application**
Low-Band	< 3 GHz	Wide-area coverage
Mid-Band	3–10 GHz	Coverage and capacity balance
mmWave Band	24–71 GHz	High-capacity and ultra-high-speed communications
Sub-THz/THz Band	100 GHz–10 THz	Future 6G ultra-high-data-rate applications

As shown in table 2.1, future wireless communication systems are progressively migrating toward mmWave and THz frequency bands to support ultra-high data rates, massive connectivity, and next-generation intelligent wireless applications.

2.2.2 Transition Toward High-Frequency Communications

The progressive saturation of conventional sub-6 GHz frequency bands has accelerated the transition toward millimeter-wave (mmWave) and Terahertz (THz) frequency spectra [16]. These high-frequency bands provide large underutilized bandwidths capable of supporting ultra-high data rates and massive wireless connectivity.

However, mmWave and THz communications suffer from severe propagation limitations, including high free-space path loss, atmospheric attenuation, molecular absorption, and strong sensitivity to environmental blockages [8, 17]. These impairments significantly degrade communication range and link reliability compared with conventional microwave systems.

Consequently, future wireless communication systems require compact and highly directive antenna architectures, advanced beamforming techniques, and efficient electromagnetic optimization strategies capable of maintaining reliable and high-performance wireless links under challenging propagation environments.

2.2.3 Emerging Enabling Technologies

To address the limitations of future wireless communication systems, several emerging technologies have become fundamental components of 5G and future 6G infrastructures. Among these technologies, Massive MIMO systems significantly improve spectral efficiency and network capacity through the simultaneous transmission of multiple data streams.

Similarly, beamforming techniques, Reconfigurable Intelligent Surfaces (RIS), and physics-guided AI-assisted optimization methods provide efficient solutions for improving wireless coverage, reducing interference, and enhancing communication reliability

2.2.4 Technical Challenges and Implications for Antenna Design

Despite the significant advancements achieved in modern wireless communications, the design of compact mmWave MIMO antenna systems remains highly challenging due to the simultaneous requirements of high gain, wide bandwidth, compact integration, low mutual coupling, high radiation efficiency, and reduced computational complexity. In compact MIMO configurations, the reduced spacing between antenna elements intensifies electromagnetic interactions, leading to mutual coupling effects that degrade antenna efficiency, alter radiation characteristics, and increase signal correlation between antenna ports.

Furthermore, conventional full-wave electromagnetic solvers, such as CST Microwave Studio and HFSS, require substantial computational resources and long optimization times for complex and multidimensional antenna synthesis problems. Consequently, there is an increasing need for intelligent and physics-guided optimization frameworks capable of accelerating antenna design while preserving electromagnetic accuracy and physical consistency.

2.3 Fundamentals of Microstrip Patch Antennas

2.3.1 Overview of Microstrip Antennas

Microstrip patch antennas (MPAs) have become one of the most widely adopted antenna technologies in modern wireless communication systems due to their low-profile structure, lightweight characteristics, low fabrication cost, and compatibility with planar and integrated circuit technologies [20, 21]. Their compact geometry and ease of integration make them particularly suitable for fifth-generation (5G), millimeter-wave (mmWave), Internet of Things (IoT), and portable wireless communication applications, where antenna miniaturization and high integration density are critical design requirements.

A conventional microstrip antenna consists of a metallic radiating patch printed on a dielectric substrate backed by a conductive ground plane, as illustrated in Fig. 2.2. Depending on the targeted operating frequency and radiation characteristics, different geometrical configurations can be employed, including rectangular, circular, triangular, elliptical, and fractal geometries.

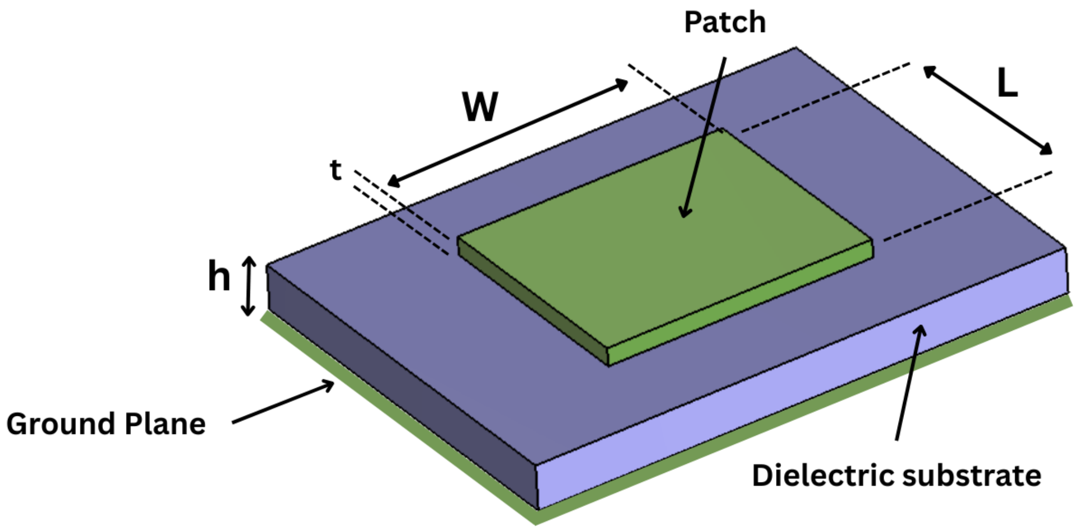

Figure 2.2: *Structure of a rectangular microstrip patch antenna*

Among these configurations, rectangular and circular microstrip antennas remain the most widely utilized structures because of their analytical simplicity, ease of fabrication, stable radiation performance, and low cross-polarization characteristics [18, 22]. Various geometrical configurations of microstrip patch antennas are illustrated in Fig. 2.3.

Despite their numerous advantages, conventional microstrip antennas inherently suffer from several limitations, including narrow impedance bandwidth, relatively low gain, reduced radiation efficiency, and surface-wave losses, particularly at high operating frequencies [18]. These limitations become more critical in compact mmWave MIMO systems, where high isolation, reduced mutual coupling, compact integration, and computationally efficient optimization are simultaneously required.

Consequently, advanced electromagnetic techniques such as Defected Ground Structures (DGS), Electromagnetic Band-Gap (EBG) structures, metasurfaces, and Frequency Selective Surfaces (FSS) have been extensively investigated to enhance antenna performance and mitigate mutual coupling effects in modern compact MIMO antenna architectures.

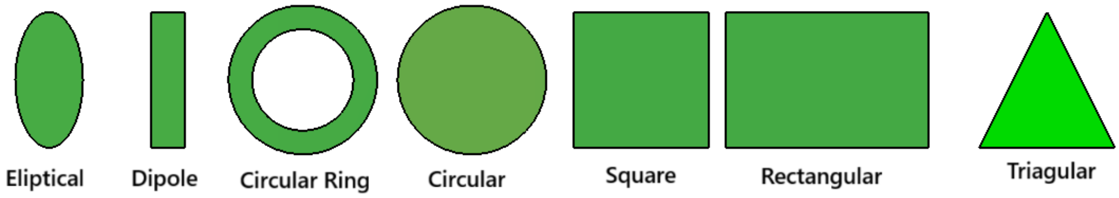

Figure 2.3: *Different geometrical configurations of microstrip patch antennas*

2.3.2 Design Methodology of a Rectangular Patch

Due to their inherently narrow bandwidth and strong dependence on the resonant frequency, precise determination of the geometrical parameters is essential in the de-sign of rectangular microstrip antennas [18]. The design process typically begins with the specification of the target resonant frequency (fr), substrate thickness (h), and dielectric constant (ϵr) [23]. These parameters directly influence the antenna dimensions, impedance matching, radiation efficiency, and bandwidth performance, which become particularly critical in compact mmWave MIMO antenna systems.

2.3.2.1 Patch Width (W):

The patch width mainly influences the radiation efficiency, input impedance, and bandwidth characteristics of the antenna. It is calculated using the following expression [18]:

$$W = \frac{c}{2f_r\sqrt{\frac{\epsilon_r+1}{2}}} \tag{2.1}$$

where C denotes the speed of light in free space, f_r is the resonant frequency, and ϵ_r represents the dielectric constant of the substrate material. An increase in the patch width generally improves the radiation efficiency and bandwidth performance of the antenna; however, excessive enlargement may increase the overall antenna dimensions, which becomes a critical limitation in compact mmWave MIMO systems.

2.3.2.2 Effective Dielectric Constant (ϵ_{reff}):

Due to fringing-field effects, part of the electromagnetic field propagates in both the dielectric substrate and surrounding air. Consequently, the antenna behaves as if it were operating with an effective dielectric constant lower than the actual substrate permittivity. The effective dielectric constant is expressed as [23]:

$$\epsilon_{reff} = \frac{\epsilon_r+1}{2} + \frac{\epsilon_r-1}{2}\left(1+12\frac{h}{W}\right)^{-1/2} \tag{2.2}$$

where:

- ϵ_{reff} is the effective relative permittivity,
- ϵ_r is the dielectric constant of the substrate,
- h is the height of the dielectric substrate,
- W is the width of the patch.

The effective dielectric constant directly affects the electromagnetic propagation velocity and resonant characteristics of the antenna structure.

2.3.2.3 Length Extension (ΔL):

Fringing fields electrically increase the effective length of the radiating patch beyond its physical dimensions. The corresponding length extension is approximated by [18]:

$$\Delta L = 0.412h \frac{(\epsilon_{reff} + 0.3)\left(\frac{W}{h} + 0.264\right)}{(\epsilon_{reff} - 0.258)\left(\frac{W}{h} + 0.8\right)} \tag{2.3}$$

where ΔL is the length extension due to the fringing fields, h is the substrate thickness, ϵ_{reff} is the effective dielectric constant, and W is the width of the patch.

Accurate estimation of fringing effects becomes increasingly important at mmWave frequencies, where small geometrical variations can significantly affect antenna performance and resonant frequency stability.

2.3.2.4 Physical Length (L):

The actual physical length of the rectangular patch antenna is determined using the following equation [23]:

$$L = \frac{C}{2f_r\sqrt{\epsilon_{reff}}} - 2\Delta L \tag{2.4}$$

where L is the actual physical length of the patch, C is the speed of light in free space, f_r is the target resonant frequency, ϵ_{reff} is the effective dielectric constant, and ΔL is the length extension due to the fringing effects.

These analytical equations provide an initial approximation of the antenna dimensions prior to full wave electromagnetic optimization. Although analytical models offer valuable physical insight and rapid preliminary estimation, accurate design of compact mmWave antenna systems generally requires full-wave electromagnetic simulations to account for complex coupling effects and high-frequency propagation phenomena.

2.3.3 Feeding Techniques

Following the geometrical design, an appropriate feeding mechanism must be selected to efficiently excite the antenna and ensure proper impedance matching. Several feeding techniques have been proposed, each offering specific advantages in terms of bandwidth, fabrication complexity, and radiation performance.

1. **Microstrip Line Feed**
   This is one of the simplest and most widely used feeding techniques. A microstrip transmission line, typically designed with a characteristic impedance of 50 Ω, is directly connected to the radiating patch, as shown in Fig. 2.4. Matching can be improved using a quarter-wave transformer section.

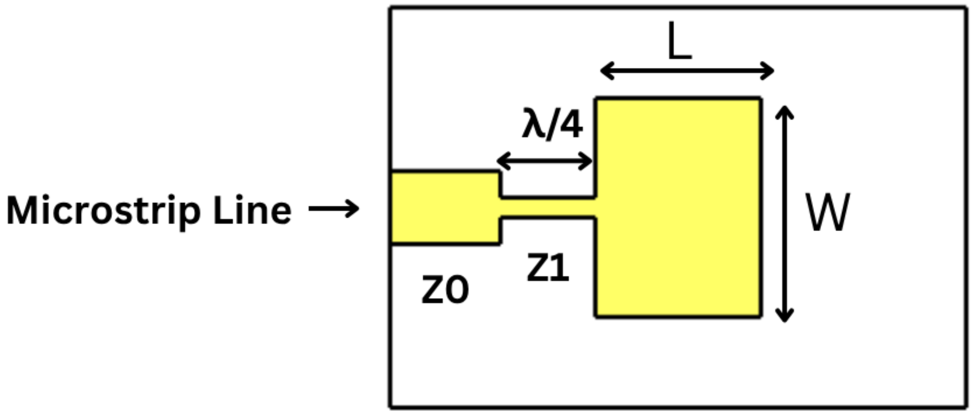

Figure 2.4: *Microstrip line feeding technique*

   where Z_0 denotes the characteristic impedance of the feed line and Z_1 represents the impedance of the quarter-wave matching section.

2. **Aperture-Coupled Feed**
   The aperture-coupled feeding technique is a non-contact method in which electromagnetic energy is coupled from a feed line to the radiating patch through an □□□□□ (aperture) etched in the ground plane. This technique, introduced by D. M. Pozar, enables improved isolation between the feed and the radiating element, thereby enhancing bandwidth and radiation performance [24]. The structure is illustrated in Fig. 2.5.

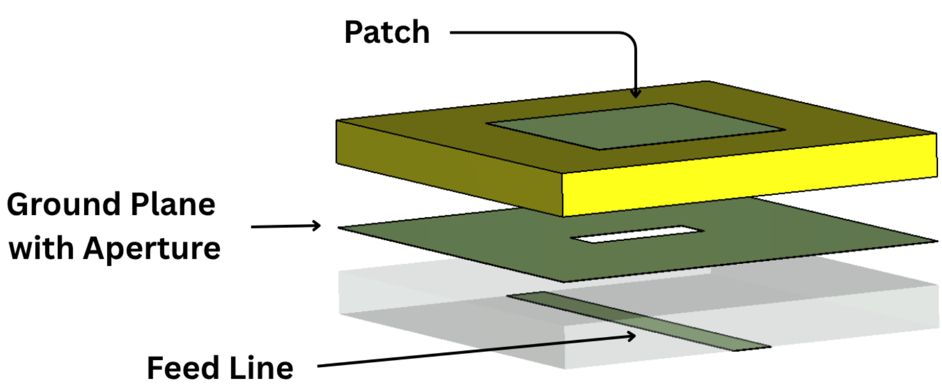

Figure 2.5: *Aperture-coupled microstrip patch antenna*

3. **Coaxial (Probe) Feed**
   In this technique, a coaxial connector is used to directly feed the patch at a location where the input impedance matches approximately 50 Ω. The inner conductor is connected to the patch, while the outer conductor is connected to the ground plane, as depicted in Fig. 2.6 [25].

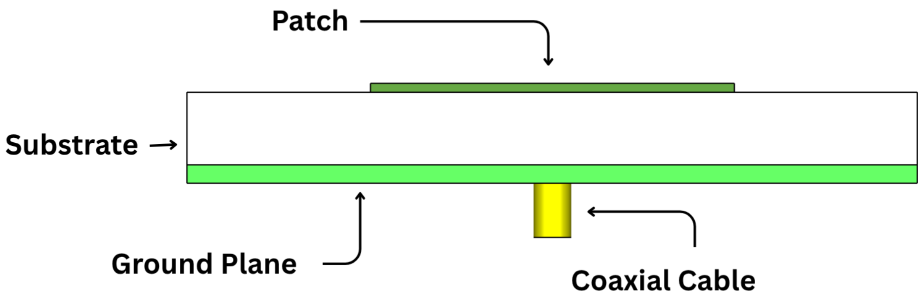

Figure 2.6: *Coaxial probe-fed microstrip patch antenna*

2.3.4 Fundamental Antenna Parameters

2.3.4.1 Radiation Pattern and Beamwidth

According to IEEE definitions, the radiation pattern represents the spatial distribu-tion of radiated energy as a function of direction [18].Although inherently three-dimensional, radiation characteristics are commonly represented using two-dimensional cuts in the azimuth and elevation planes, as illustrated in (Fig. 2.7).

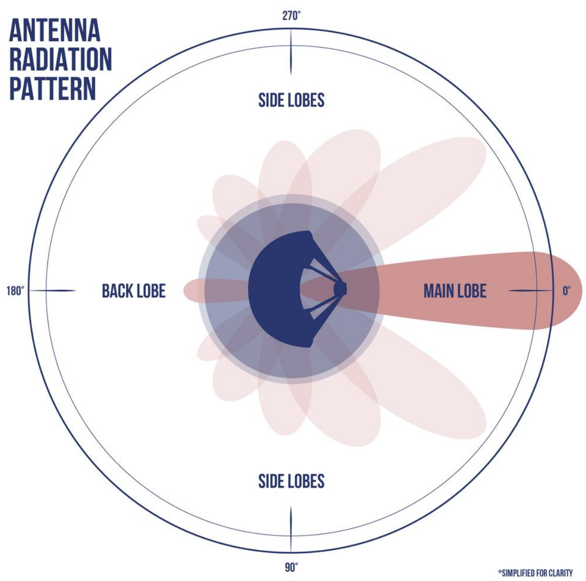

Figure 2.7: *Radiation pattern of an antenna*

The radiation pattern generally consists of a main lobe, side lobes, and a back lobe

[26].Two important beamwidth parameters are commonly defined:

- **Half-Power Beamwidth (HPBW):** separation between the points where the radiated power decreases by 3 dB relative to the maximum radiation level.
- **First-Null Beamwidth (FNBW):** Angular separation between the first nulls surrounding the main lobe. These beamwidth parameters are illustrated in.fig. 2.8

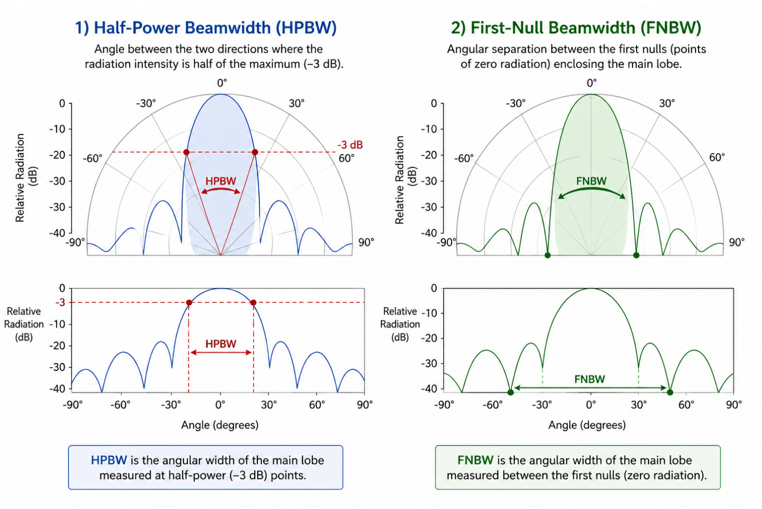

Figure 2.8: *Illustration of HPBW and FNBW*

2.3.4.2 Directivity, Gain, and Efficiency

Directivity (D) quantifies the ability of an antenna to concentrate radiated power in a given direction relative to an isotropic radiator [27]:

$$D(\theta, \phi) = \frac{U(\theta, \phi)}{U_{av}} \tag{2.5}$$

where $U(\theta, \phi)$ denotes the radiation intensity and U_{av} represents the average radiated power density.

The antenna gain incorporates both directivity and radiation efficiency, accounting for internal losses within the antenna structure:

$$G = e_{cd} \cdot D \tag{2.6}$$

where e_{cd} denotes the radiation efficiency coefficient. The relationship between directivity, efficiency, and gain is illustrated in Fig. 2.9.

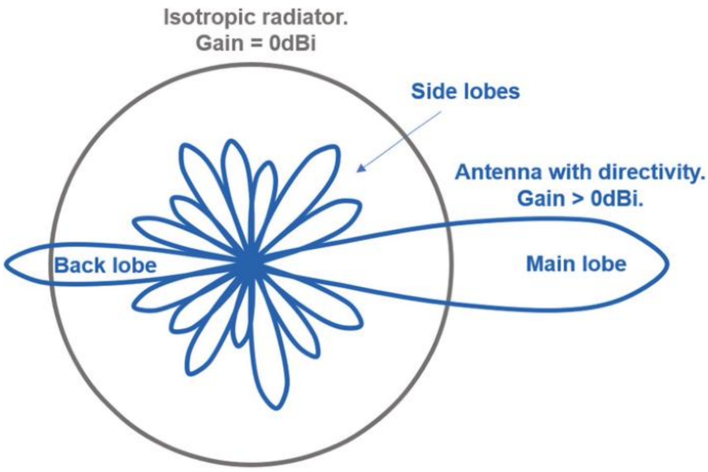

Figure 2.9: *Relationship between directivity, efficiency, and gain*

2.3.4.3 Input Impedance, Return Loss, and VSWR

Efficient power transfer requires proper impedance matching between the antenna input impedance and the feeding transmission line [28]. Any impedance mismatch results in reflected power, quantified through the return loss parameter [29]. In practical antenna systems, a return loss below -10 dB and a VSWR below 2 are generally considered acceptable[18, 30].

2.3.4.4 Bandwidth

Bandwidth defines the frequency range over which the antenna satisfies specified performance requirements [18]. It is commonly classified into:

- **Impedance Bandwidth:** Frequency range where $S_{11} \leq -10$ dB [21].
- **Pattern Bandwidth:** Frequency range over which the radiation characteristics remain stable.The variation of the reflection coefficient (S11) with frequency is illustrated in Fig.2.10

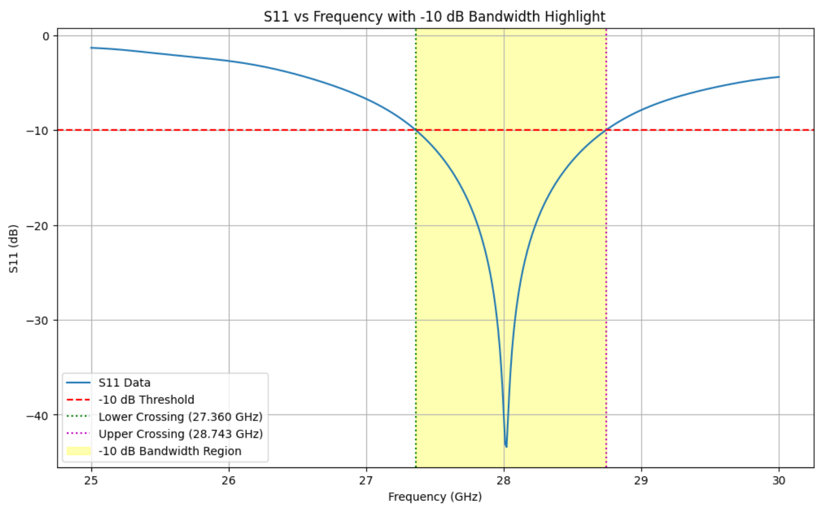

Figure 2.10: *Reflection coefficient (S_{11}) versus frequency*

2.3.4.5 Polarization

Polarization describes the orientation and temporal behavior of the electric field vector radiated by the antenna [31]. Antennas may exhibit linear, circular, or elliptical polarization [26].

Efficient wireless communication requires polarization matching between transmitting and receiving antennas. Any polarization mismatch results in power loss quantified through the Polarization Loss Factor (PLF). Circular polarization is particularly advantageous in mobile and satellite communication systems because of its robustness against orientation misalignment. These antenna characteristics become particularly critical in compact mmWave MIMO systems, where high gain, wide bandwidth, low mutual coupling, and efficient radiation performance must be simultaneously achieved under strict size and integration constraints.

2.4 MIMO Antenna Systems

2.4.1 Introduction

The use of multiple antennas at both the transmitter and receiver has emerged as a fundamental paradigm in modern wireless communication systems, significantly enhancing system performance in terms of capacity, reliability, and spectral efficiency [32].Although the concept of Multiple-Input Multiple-Output (MIMO) systems dates back to the 1970s, where it was initially investigated in the context of multi-pair tele-phone cables, it has gained widespread adoption in contemporary wireless standards due to advances in signal processing and antenna technologies.

MIMO antenna systems enable high data rate transmission across a wide range of applications, including base stations, automotive communication systems, handheld devices, satellite links, and radar systems. They are now integral to numerous wireless

technologies such as Wireless Local Area Networks (WLAN), WiMAX, GSM, LTE, Global Positioning System (GPS), and, more recently, 5G and beyond [33].

The transition toward MIMO architectures has been largely motivated by the inherent limitations of conventional Single-Input Single-Output (SISO) systems. In particular, SISO systems struggle to achieve gigabit-per-second (Gbps) data rates without requiring excessively large bandwidths or high transmit power. Furthermore, their performance is severely degraded in non-line-of-sight (NLOS) environments due to multipath fading and interference. As demonstrated in [34], achieving high spectral efficiency with SISO systems requires impractically high signal-to-noise ratio (SNR) levels, thereby limiting coverage range and system robustness.

In contrast, MIMO systems exploit the spatial dimension by employing multiple antennas to transmit and receive independent data streams. This enables significant improvements in channel capacity, which can theoretically increase linearly with the number of antenna elements under favorable propagation conditions [33].

In modern mmWave and 5G communication systems, MIMO technology has become particularly important for compensating propagation losses, improving link robustness, and enabling highly directive beamforming capabilities. However, the integration of multiple antenna elements within compact platforms introduces significant challenges related to mutual coupling, antenna miniaturization, and electromagnetic optimization complexity, which constitute major research issues in compact mmWave MIMO antenna design.

2.4.2 Core Concepts

The performance improvements achieved by MIMO systems mainly originate from spatial multiplexing and diversity mechanisms. Unlike conventional SISO architectures, MIMO systems employ multiple antenna elements at both the transmitter and receiver to improve channel capacity, communication reliability, and spectral efficiency.

In Spatial Multiplexing (SM), a high-data-rate stream is divided into multiple parallel data streams transmitted simultaneously over the same frequency band, thereby increasing transmission throughput without requiring additional bandwidth. In contrast, diversity techniques transmit redundant signal replicas across multiple antennas to mitigate multipath fading and improve link reliability.

MIMO systems also exploit multipath propagation characteristics to separate and reconstruct independent transmitted signals at the receiver [35]. Depending on the number of transmitting and receiving antennas, different MIMO configurations can be implemented, including 2×2, 4×4, and Massive MIMO architectures.

Although increasing the number of antenna elements improves spectral efficiency and beamforming capability, it also introduces significant challenges related to mutual coupling, hardware complexity, and compact antenna integration, particularly in mmWave communication systems.

2.4.3 Applications

MIMO technology is now widely deployed across various application domains:

- **Consumer Devices:** Smartphones, tablets, and portable communication systems [36]
- **Network Infrastructure:** 5G base stations (gNodeB) and WLAN access points [37]
- **Advanced Systems:** Vehicle-to-everything (V2X) communication, satellite systems, radar, and healthcare monitoring platforms [38]

The rapid expansion of these applications has considerably increased the demand for compact, high-performance, and computationally efficient MIMO antenna architectures capable of operating reliably under complex and high-frequency propagation environments.

2.4.4 From Conventional MIMO to Massive and Ultra-Massive MIMO

MIMO technology has evolved considerably to satisfy the increasing performance requirements of next-generation wireless communication systems. Conventional MIMO architectures, typically employing a limited number of antenna elements, have progressively evolved toward Massive MIMO (m-MIMO) systems, where large-scale antenna arrays are deployed at the base station [13]. This evolution enables highly directive beamforming, improved spectral efficiency, and significant reduction of inter-user interference [39]. For future sixth-generation (6G) wireless systems operating in the Terahertz (THz) frequency range, the concept of Ultra-Massive MIMO (UM-MIMO) is currently being investigated [15]. Due to the severe propagation losses encountered at THz frequencies, UM-MIMO systems rely on extremely dense antenna arrays composed of sub-wavelength radiating elements, often incorporating advanced materials and plasmonic nanostructures. These architectures aim to achieve ultra-high-capacity communications, enhanced spatial multiplexing, and ultra-narrow beam steering capabilities [39].

However, the integration of large numbers of antenna elements within compact high-frequency platforms significantly increases electromagnetic coupling effects, antenna design complexity, and computational optimization requirements. Consequently, the development of compact, high-isolation, and computationally efficient MIMO antenna architectures has become a major research challenge in modern mmWave and THz communication systems.

2.5 Performance Metrics of MIMO Antennas

In addition to conventional antenna parameters such as gain, radiation efficiency, and radiation pattern, MIMO antenna systems require dedicated performance metrics to evaluate electromagnetic coupling effects, signal correlation, and overall system performance [40]. These parameters are essential for assessing the capability of MIMO antennas to support efficient diversity and multiplexing operations in practical wireless communication environments.

2.5.1 Isolation Between Antenna Elements

Isolation quantifies the level of electromagnetic coupling between antenna elements and is commonly evaluated using scattering parameters (S12, S21). High isolation is required to ensure independent operation of the antenna elements and to reduce mutual coupling effects.

$$S_{ji} = \frac{V_j^-}{V_i^+} \tag{2.7}$$

Low values isolation (low $|S_{ij}|$) indicate weak electromagnetic coupling and improved MIMO performance. In compact mmWave antenna systems, achieving high isolation represents one of the most critical design challenges.

2.5.2 Envelope Correlation Coefficient (ECC)

The Envelope Correlation Coefficient (ECC) measures the level of correlation between antenna elements. Lower ECC values indicate better diversity performance and improved signal independence.

$$\mathrm{ECC}(i, j, N) = \frac{\left|\sum_{n=1}^{N} S_{in}^{*} S_{nj}\right|}{\sqrt{\prod_{k \in \{i,j\}} \left[1 - \sum_{n=1}^{N} |S_{in}|^2\right]}} \tag{2.8}$$

In practical MIMO systems, an ECC value lower than 0.5 is generally considered acceptable[33, 41].

2.5.3 Diversity Gain (DG)

Diversity Gain quantifies the improvement in signal reliability and is directly related to ECC:

$$DG = 10\sqrt{1 - |ECC|^2} \tag{2.9}$$

An ideal MIMO system achieves a DG close to 10 dB.

2.5.4 Mean Effective Gain (MEG)

Mean Effective Gain (MEG) evaluates the average received power of an antenna element in a multipath propagation environment:

$$MEG_i = 0.5 \left[1 - \sum_{j=1}^{N} |S_{ij}|^2\right] \tag{2.10}$$

A balanced system requires $|MEG_i - MEG_j| < 3$ dB [41].

2.5.5 Total Active Reflection Coefficient (TARC)

The Total Active Reflection Coefficient (TARC) provides a realistic evaluation of reflected power in multiport antenna systems by considering simultaneous excitation of all antenna elements:

$$TARC = \frac{\sqrt{\sum_{i=1}^{N} |b_i|^2}}{\sqrt{\sum_{i=1}^{N} |a_i|^2}} \tag{2.11}$$

For optimal performance, TARC should remain below -10 dB across the operating band [40].

2.5.6 Channel Capacity Loss (CCL)

Channel Capacity Loss (CCL) quantifies the degradation in channel capacity caused by correlation and mutual coupling effects within the MIMO system:

$$CCL = -\log_2 \det(\Psi^R) \tag{2.12}$$

To maintain high system performance, CCL should remain below 0.4 bits/s/Hz [42].

These performance metrics play a fundamental role in the design and evaluation of compact mmWave MIMO antenna systems, where achieving high isolation, low correlation, and efficient multiport operation simultaneously remains a major electromagnetic and optimization challenge.

2.6 Conclusion

This chapter established the theoretical foundations necessary for understanding the requirements and challenges of next-generation wireless communication systems. The evolution toward 5G and emerging 6G networks operating at mmWave and THz frequency bands enables ultra-high data rates and enhanced spectral efficiency; however, it also introduces severe propagation losses and atmospheric attenuation [13, 43] . To overcome these limitations, advanced antenna technologies have become essential components of modern wireless systems. In this context, microstrip patch antennas (MPAs) represent attractive solutions due to their low-profile structure, low fabrication cost, ease of integration, and compatibility with integrated circuits [18]. Nevertheless, conventional single-antenna configurations remain insufficient to satisfy the increasing demands of high-capacity wireless communications. Consequently, MIMO and Massive MIMO architectures have emerged as key enabling technologies for improving channel capacity, communication reliability, and spectral efficiency through spatial multiplexing and diversity techniques[43]. Despite these advantages, the implementation of compact mmWave MIMO antenna systems introduces critical challenges related to mutual coupling, antenna miniaturization, and computational complexity. In particular, strong electromagnetic coupling between closely spaced antenna elements degrades radiation efficiency and diversity performance [35]. Therefore, maintaining high isolation and low Envelope Correlation Coefficient (ECC) values is essential for efficient MIMO operation. Furthermore, the simultaneous requirements of compact size, high gain, wide bandwidth, and low mutual coupling result in highly complex electromagnetic optimization problems. Traditional trial-and-error and full-wave simulation approaches become increasingly time-consuming and computationally expensive when applied to modern high-frequency antenna systems. Consequently, intelligent and physics-guided optimization methodologies are becoming increasingly important for the design and synthesis of compact high-performance

MIMO antennas. In this context, the next chapter presents a comprehensive review of recent mmWave MIMO antenna designs, mutual coupling reduction techniques, Frequency Selective Surfaces (FSS), and Artificial Intelligence (AI)-based optimization approaches in order to identify the main research gaps addressed in this thesis [11].

Chapter 3

State of the Art and Research Gap

3.1 Introduction

The transition toward millimeter-wave (mmWave) frequency bands in fifth-generation (5G) New Radio (NR) systems enables access to large underutilized spectrum resources capable of supporting multi-gigabit-per-second data rates and ultra-low-latency communications. However, mmWave signal propagation is inherently affected by severe free-space path loss, atmospheric attenuation, and high sensitivity to environmental blockage [5].

To overcome these propagation limitations and maintain reliable wireless communication links, the integration of advanced Multiple-Input Multiple-Output (MIMO) antenna technologies has become essential. In particular, compact high-gain and highly directive MIMO antenna architectures are increasingly required to improve link robustness, enhance spectral efficiency, and compensate for propagation losses in modern 5G and emerging 6G wireless systems [44].

Despite significant progress in mmWave antenna engineering, the simultaneous achievement of compact size, high gain, wide bandwidth, low mutual coupling, and reduced computational complexity remains a major research challenge. Consequently, numerous electromagnetic decoupling techniques and intelligent optimization methodologies have recently been investigated to improve the performance of compact MIMO antenna systems.

In parallel, the increasing complexity of modern antenna structures has accelerated the adoption of Artificial Intelligence (AI) and Machine Learning (ML)-based approaches as efficient alternatives to conventional full-wave electromagnetic optimization techniques. These intelligent methodologies aim to reduce computational cost while enabling rapid and accurate antenna synthesis.

Therefore, this chapter presents a comprehensive review of recent advances in high-gain mmWave MIMO antennas, mutual coupling reduction techniques, Frequency Selective Surfaces (FSS), and AI-assisted antenna optimization methods. The chapter also identifies the principal limitations and research gaps that motivate the contributions developed in this thesis.

3.2 High-Gain MIMO Antennas for 5G/mmWave

3.2.1 Recent MIMO Antenna Designs for 28/38 GHz Bands

A considerable body of research has focused on the design of compact high-gain Multiple-Input Multiple-Output (MIMO) antenna arrays operating within the Frequency Range 2 (FR2) spectrum, particularly targeting the 28 GHz and 38 GHz bands for fifth-generation (5G) applications. Sehrai et al. [45] proposed a wideband MIMO antenna specifically designed to maintain stable high-gain performance across mmWave frequencies.

To address multi-band operational requirements, Aghoutane et al.[46]developed a dual-band four-port MIMO antenna array operating at 28/37 GHz, demonstrating high gain and excellent isolation characteristics suitable for next-generation mobile communication systems.

Various structural enhancement techniques have also been investigated to achieve an optimal trade-off between compactness and electromagnetic performance.Ghosh et al.[47] introduced a highly isolated high-gain four-port MIMO antenna integrating Complementary Split Ring Resonators (CSRR) and Defected Ground Structures (DGS) to suppress mutual coupling. Similarly, Tiwari et al. [5] proposed a wideband quad-port MIMO antenna employing diamond-shaped slots combined with DGS, achieving a peak gain of 18.2 dBi and isolation exceeding 25 dB over the 24–40 GHz frequency range.Furthermore, Khouyaoui et al. [48]emphasized the practical realization of high-gain microstrip patch antenna arrays for 28 GHz mmWave 5G applications, including both simulation and fabrication aspects.

Despite these improvements, most reported high-gain mmWave MIMO antennas still suffer from several limitations, including increased structural complexity, limited compactness, fabrication difficulty, and narrow operational bandwidths. Moreover, simultaneously achieving high gain, strong isolation, and compact integration remains particularly challenging in portable and densely integrated 5G platforms.

3.2.2 Advanced Gain Enhancement Techniques

To improve antenna directivity without significantly increasing the physical dimensions of the radiating structure, numerous studies have investigated the integration of advanced electromagnetic structures. Mohamed et al. [49]demonstrated substantial gain enhancement in 5G mmWave sys-tems by employing a reflective FSS positioned beneath the radiating element. This configuration enables constructive interference, thereby improving the overall radiation efficiency and directivity.

Adopting an alternative strategy, Choi et al. [50] incorporated advanced meta-material structures into a dipole array antenna, achieving improved gain performance specifically within the 5G mmWave frequency bands.

More recently, Shaban [51] proposed a 28 GHz four-port MIMO antenna in which each port consists of a 1×8 series-fed array. By integrating a carefully engineered metamaterial unit cell as a decoupling mechanism, the design achieved a peak gain of 13 dBi while reducing mutual coupling to below −40 dB. Furthermore, the antenna exhibited an exceptionally low Envelope Correlation Coefficient (ECC) of 0.00012 and a Channel Capacity Loss (CCL) of only 0.147 bit/s/Hz, highlighting the effective-ness of metamaterial-based approaches in enhancing both gain and isolation in high-performance MIMO systems.

Nevertheless, many gain enhancement approaches rely on multilayer configurations, periodic metamaterials, or complex resonant surfaces, which may increase fabrication difficulty, dimensional sensitivity, and computational optimization cost at mmWave frequencies. In addition, several existing techniques remain difficult to integrate into highly compact portable wireless devices..

3.2.3 Integration of Machine Learning in Antenna Design

As the complexity of millimeter-wave (mmWave) MIMO antenna systems continues to increase, conventional full-wave electromagnetic simulation techniques become increas-ingly computationally intensive and time-consuming. Consequently, recent research has demonstrated a clear paradigm shift toward the adoption of Artificial Intelligence (AI)-based methodologies to accelerate the antenna design process.

In particular, machine learning (ML) techniques have been widely explored as ef-ficient surrogate models capable of capturing the complex nonlinear relationships between antenna geometrical parameters and their electromagnetic performance. For example, Haque et al. [52] employed machine learning algorithms to accurately pre-dict and optimize the gain of broadband high-performance MIMO antenna arrays for 5G mmWave applications. Their approach significantly reduced the design time while maintaining high prediction accuracy, highlighting the potential of ML-driven frame-works in modern antenna engineering.

Despite these advantages, conventional ML and ANN-based approaches remain strongly dependent on large training datasets generated using computationally intensive full-wave simulations. Furthermore, most existing models operate as black-box systems with limited physical interpretability and reduced generalization capability outside the training domain. These limitations restrict their robustness for complex inverse electromagnetic design problems and motivate the development of physics-guided and data-efficient intelligent optimization frameworks for next-generation antenna synthesis

3.2.4 Comparative Analysis of Existing High-Gain mmWave MIMO Antennas

The Table 3.1 summarizes the principal characteristics and limitations of representative high-gain mmWave MIMO antennas reported in the literature.

Table 3.1: *Performance Comparison of Recent High-Gain mmWave MIMO Antenna Designs*

Ref.	Frequency	Gain	Isolation	Technique	Main Limitation
[45]	mmWave	High	Moderate	Wideband MIMO	Limited compactness
[46]	28/37 GHz	High	High	Dual-band MIMO	Structural complexity
[47]	mmWave	High	Improved	CSRR + DGS	Fabrication complexity
[5]	24–40 GHz	18.2 dBi	> 44 dB	DGS + Slot design	Large structural complexity
[51]	28 GHz	13 dBi	< -40 dB	Metamaterial decoupling	Multilayer complexity

The comparative analysis reveals that existing mmWave MIMO antenna designs generally achieve performance improvement at the expense of increased structural complexity, fabrication difficulty, or computational optimization cost. Therefore, developing compact, high-isolation, and computationally efficient MIMO antenna architectures remains an open research challenge for future 5G and 6G wireless systems.

3.3 Mutual Coupling Reduction Techniques

The deployment of Multiple-Input Multiple-Output (MIMO) technology is essential for achieving the high data rates and spectral efficiency required by fifth-generation (5G) and emerging sixth-generation (6G) wireless communication systems. However, the integration of multiple antenna elements within the limited physical space of modern portable devices and densely packed base stations inevitably results in strong electro-magnetic interactions between adjacent antennas [9].

As highlighted by Nadeem and Choi [53], this mutual coupling (MC) degrades ra-diation efficiency, distorts radiation patterns, and significantly increases the Envelope Correlation Coefficient (ECC), thereby reducing channel capacity and overall system performance. Although digital signal processing and calibration techniques can par-tially compensate for these effects, physical decoupling approaches implemented at the antenna level are generally preferred due to their simplicity, effectiveness, and low computational overhead [53]..

In recent years, a wide range of innovative decoupling techniques has been proposed to mitigate mutual coupling in compact MIMO antenna systems. These techniques can be broadly classified into the following categories:

3.3.1 Defected Ground Structures (DGS)

Defected Ground Structures (DGS) consist of introducing intentional discontinuities in the metallic ground plane of a microstrip antenna in the form of etched slots or non-conductive patterns. These engineered defects modify the current distribution and electromagnetic behavior of the ground plane, thereby influencing the antenna performance.

According to the comprehensive review by Jemaludin et al. [35], DGS structures act as spatial band-stop filters that effectively suppress the propagation of surface waves between adjacent radiating elements. This suppression mechanism reduces electromagnetic coupling and improves isolation in MIMO systems.

Nadeem and Choi [53] further demonstrated that periodic DGS configurations—such as S-shaped and dumbbell-shaped slots—can significantly inhibit the flow of in-duced surface currents by confining them within localized regions of the substrate. As a result, these structures can achieve substantial isolation enhancement, typically ranging from 20 dB to 40 dB, without increasing the overall antenna size [40, 53].

Despite their effectiveness, DGS structures may increase back radiation, degrade bandwidth performance, and disturb surface current distribution in compact mmWave systems. In addition, their performance strongly depends on defect geometry and substrate characteristics, which increases electromagnetic optimization complexity. These limitations become more critical in highly compact mmWave MIMO platforms, where maintaining both miniaturization and wideband isolation remains challenging.

3.3.2 Electromagnetic Band Gap (EBG) and Metamaterials

When Defected Ground Structures (DGS) alone are insufficient to achieve the desired level of isolation, researchers often employ more sophisticated periodic structures such as Electromagnetic Band Gap (EBG) structures and metamaterials. These engineered surfaces exhibit unique electromagnetic properties that enable effective suppression of surface wave propagation and reduction of mutual coupling.

Fadehan et al. [54] proposed a Modified **EBG** structure for ultra-wideband (UWB) MIMO antennas, achieving an isolation level of -23 dB across a wide frequency range while maintaining an ultra-compact footprint of 19×24 mm^2. This demonstrates the effectiveness of EBG-based approaches in achieving compact and high-performance antenna designs.

In parallel, metamaterial-inspired structures—particularly Split Ring Resonators (SRR) and Complementary Split Ring Resonators (CSRR)—have been extensively investigated for mutual coupling suppression. Selvaraju et al. [55] showed that embedding CSRRs within the ground plane or positioning them between adjacent antenna elements creates a single-negative metamaterial region. This region acts as an electromagnetic barrier that significantly attenuates surface wave propagation, resulting in enhanced isolation levels, often exceeding -20 dB. Such characteristics make metamaterial-based techniques highly suitable for compact and densely integrated 5G MIMO antenna arrays [40, 55].

Nevertheless, EBG and metamaterial structures generally require complex periodic geometries and multilayer configurations, which may increase fabrication difficulty, dimensional sensitivity, and the computational cost of full-wave simulations, particularly in highly miniaturized mmWave systems.

Consequently, more compact and computationally efficient decoupling approaches are still required for next-generation mmWave MIMO antenna platforms.

3.3.3 Parasitic Elements and Neutralization Lines

The incorporation of parasitic (dummy) elements is a well-established technique for mitigating mutual coupling in compact MIMO antenna systems. As reported by Jayaraman et al. [40], parasitic structures—such as unconnected metallic strips, inverted-F elements, or stubs—are strategically positioned between adjacent driven antennas. These elements interact electromagnetically with the radiating structures through inductive or capacitive coupling, generating secondary fields with opposite phase to the coupled signals, thereby enabling effective field cancellation [53].

A closely related technique involves the use of Neutralization Lines (NLs), where adjacent antenna elements are interconnected through thin conductive traces or lumped components. This configuration introduces an additional controlled coupling path that produces counter-phase currents, effectively compensating for the direct electromagnetic coupling between antenna elements. When properly optimized, neutralization lines can significantly enhance isolation without compromising radiation characteristics [35].

Building upon these concepts, Li et al. [56] recently proposed a Parasitic Decoupling Network (PDN), which employs sections of transmission lines combined with reactive components to establish controlled power propagation paths. This approach enables precise cancellation of undesired coupling effects while preserving pattern diversity and overall antenna performance.

Despite their effectiveness, parasitic elements and neutralization lines may increase structural complexity and exhibit high sensitivity to geometrical dimensions and optimization conditions. Furthermore, some configurations may distort current distribution and degrade wideband radiation performance in compact mmWave MIMO systems

3.3.4 Decoupling Networks

Decoupling networks (DNs) employ passive microwave circuit elements—such as transmission lines, directional couplers, and lumped capacitors or inductors—to mitigate mutual coupling between closely spaced antenna elements [53]. These networks are designed to counteract the mutual admittance between antenna ports and improve isolation performance in MIMO systems.

According to Ramos et al. [9], the fundamental operating principle of a decoupling network consists in transforming the complex cross-admittance between coupled antennas into a purely imaginary component, thereby suppressing real power transfer between ports. This transformation effectively minimizes electromagnetic interaction and enhances port isolation.

Despite their effectiveness, conventional DNs are often constrained by limited operational bandwidth and increased design complexity, as they may require additional substrate area for implementation. However, recent developments—such as Coupled Resonator Decoupling Networks (CRDN) and dummy-load-based configurations—have demonstrated significant potential in achieving wideband isolation while maintaining compact form factors suitable for modern 5G antenna systems [53].

However, these approaches frequently increase hardware complexity, insertion losses, and integration constraints, which may limit their applicability in highly miniaturized portable devices and future mmWave and THz communication platforms.

3.3.5 Comparative Analysis of Mutual Coupling Reduction Techniques

Table 3.2 summarizes the main characteristics, advantages, and limitations of representative mutual coupling reduction techniques reported in the literature [40, 53, 56, 56].

Table 3.2: *Comparative Analysis of Mutual Coupling Reduction Techniques for Compact mmWave MIMO Antenna Systems*

Technique	Advantages	Limitations	Typical Isolation
DGS	Compact and easy integration	Back radiation and bandwidth degradation	20–40 dB
EBG	Strong surface-wave suppression	Fabrication complexity	$>$ 20 dB
Metamaterials	High isolation performance	Multilayer complexity	$>$ 30 dB
Neutralization Lines	Compact implementation	Optimization sensitivity	Moderate–High
Decoupling Networks	Effective wideband isolation	Additional circuitry and insertion losses	High

The comparative analysis indicates that most existing decoupling techniques achieve isolation improvement at the expense of increased structural complexity, fabrication difficulty, or computational optimization cost. Therefore, developing compact, wideband, and computationally efficient decoupling methodologies remains a major challenge for next-generation mmWave MIMO antenna systems.

3.4 Frequency Selective Surfaces (FSS) in Antenna Design

3.4.1 Fundamental Concepts and Filtering Mechanisms

Frequency Selective Surfaces (FSSs) are spatial electromagnetic filters composed of two-dimensional periodic arrays of metallic patches or apertures printed on a dielectric substrate [57]. These structures exhibit frequency-dependent transmission and reflection characteristics, which can be precisely controlled through the geometry of the unit cell, inter-element spacing, and substrate properties.

By appropriately engineering these parameters, an FSS can be designed to selectively transmit, reflect, or absorb incident electromagnetic waves at specific resonant frequencies [57, 58]. This frequency-selective behavior makes FSSs highly suitable for a wide range of applications in modern wireless and electromagnetic systems.

According to Babinet's principle, arrays composed of metallic patches generally exhibit band-stop (capacitive) behavior, reflecting incident waves, whereas their complementary structures—formed by apertures—demonstrate band-pass (inductive) characteristics, allowing electromagnetic waves to propagate through the surface [59].

Owing to their unique spatial filtering properties, FSS structures have become a fundamental component in advanced electromagnetic applications, including radome design, radar cross-section (RCS) reduction, electromagnetic shielding, and antenna performance enhancement [57].

Despite their advantages, conventional planar FSS structures often suffer from limited angular stability, polarization sensitivity, and relatively large unit-cell dimensions, particularly at lower operating frequencies. These limitations become increasingly critical in compact and highly integrated mmWave communication systems.

3.4.2 FSS for Gain and Directivity Enhancement

One of the most significant applications of FSS in modern wireless communication systems lies in their ability to enhance antenna gain and radiation directivity. When an FSS is positioned at an optimized distance from the primary radiating element—typically an integer multiple of $\lambda/2$ or $\lambda/4$—a resonant structure known as a Fabry–Perot cavity is formed [59].

In this configuration, the FSS operates as a partially reflective surface that redirects downward or scattered electromagnetic waves back toward the antenna. These reflected waves constructively interfere with the directly radiated fields, resulting in a reinforced radiation pattern and a highly directive main lobe [58]. Consequently, a substantial improvement in antenna gain can be achieved without increasing the physical dimensions of the radiating element.

For instance, Chen and Tao [60] employed a dual-band FSS composed of double rectangular ring elements to enhance both the bandwidth and gain of a V-slot patch antenna. More recently, a 2025 study demonstrated the effectiveness of a decagonal FSS reflector integrated with a MIMO antenna for 5.9 GHz vehicle-to-everything (V2X) communications [58]. By positioning the FSS array at a distance of $3/4\lambda$ from the antenna, optimal phase alignment was achieved, leading to constructive interference and a significant gain enhancement from 2.7 dBi to 7.4 dBi, while maintaining an omnidirectional radiation pattern above the radiating element [58].

Nevertheless, many FSS-based gain enhancement techniques rely on multilayer resonant structures and precise phase alignment conditions, which may increase fabrication complexity, profile thickness, and sensitivity to dimensional tolerances. Furthermore, maintaining stable performance over wide bandwidths and large incidence angles remains a major challenge for compact mmWave antenna systems.

3.4.3 Advanced FSS Topologies: Miniaturization and Reconfigurability

To satisfy the stringent requirements of 5G and future 6G communication systems, modern FSS structures have evolved beyond conventional planar periodic surfaces. Recent research has mainly focused on antenna miniaturization, angular stability, and frequency reconfigurability. Miniaturized and fractal FSS structures employ space-filling geometries — such as Minkowski, Sierpinski, and Peano curves — or meandered conductive lines to increase the effective electrical length within a compact physical area[57]. These configurations reduce the resonant frequency while improving multiband performance and angular stability [57, 59].

Active and tunable FSSs (AFSSs) integrate active electronic components — including PIN diodes and varactor diodes — within the unit-cell structure [57]. By controlling the bias voltage, the electromagnetic response of the surface can be dynamically reconfigured, enabling adaptive filtering and smart electromagnetic control [57, 59].

Three-dimensional (3D) FSS structures have also been investigated to achieve steeper frequency selectivity and improved out-of-band rejection by incorporating vertical metallic vias or multilayer configurations [57].

Although advanced FSS topologies provide improved electromagnetic performance and reconfigurability, they generally introduce higher fabrication complexity, increased optimization difficulty, and additional integration constraints. In compact mmWave systems, these issues become particularly critical due to fabrication tolerances and computational optimization requirements.

3.4.4 Equivalent Circuit Modeling (ECM)

Because full-wave electromagnetic simulations of complex periodic structures are computationally expensive and time-consuming, Equivalent Circuit Modeling (ECM) is widely employed for efficient FSS analysis [61, 62]. As described by Costa et al. [61] and Amini et al. [62], an FSS can be represented using lumped-element circuit models in which metallic strips behave as inductive elements (L), while gaps between adjacent elements behave as capacitive elements (C). By accurately determining these equivalent parameters, the transmission and reflection characteristics of multilayer FSS structures can be rapidly predicted using transmission-line theory [61].

Despite their computational efficiency, conventional ECM approaches may exhibit limited accuracy when modeling highly complex, multilayer, or strongly coupled mmWave structures. Consequently, advanced intelligent and physics-guided electromagnetic modeling techniques are increasingly required to improve prediction accuracy while reducing computational cost for modern FSS-assisted antenna systems.

3.4.5 Comparative Analysis of FSS-Based Techniques in Antenna Design

Table 3.3 summarizes the principal characteristics, advantages, and limitations of representative FSS-based approaches reported in the literature [57, 62]. The comparative analysis

Table 3.3: *Comparative Analysis of FSS-Based Techniques for Antenna Performance Enhancement*

Technique	Advantages	Limitations	Main Application
Conventional Planar FSS	Simple implementation	Limited angular stability	Basic filtering
Reflective FSS	Gain enhancement	Profile thickness	High-directivity antennas
Fractal/ Miniaturized FSS	Compact size and multiband response	Complex geometry	Compact mmWave systems
Active/Tunable FSS	Dynamic reconfigurability	Biasing complexity	Adaptive wireless systems
3D FSS Structures	Improved selectivity	Fabrication complexity	Wideband filtering

indicates that FSS structures provide significant potential for antenna gain enhancement, filtering, and electromagnetic control. However, most advanced FSS configurations remain constrained by fabrication complexity, dimensional sensitivity, and computational optimization challenges. Therefore, developing compact, high-performance, and computationally efficient FSS-assisted antenna architectures remains an important research direction for future mmWave and 6G communication systems.

3.5 ANN-Based Techniques in Antenna Design: Review and Limitations

As the complexity of modern wireless communication systems continues to increase, the design of antennas subject to multiple constraints—such as multiband operation, high gain, and stringent miniaturization requirements—has become increasingly challenging. Conventional Computational Electromagnetics (CEM) tools, including CST Microwave Studio and HFSS, rely on rigorous numerical techniques such as the Finite Element Method (FEM) and the Finite Difference Time Domain (FDTD) method[7].

Although these full-wave simulation tools provide highly accurate electromagnetic analysis, they are computationally intensive and time-consuming, rendering iterative trial-and-error design approaches inefficient and impractical for complex antenna struc-tures [6?].

To address these limitations, Artificial Neural Networks (ANNs) have been widely adopted as efficient and flexible surrogate modeling techniques. These data-driven models are capable of capturing the complex nonlinear relationships between antenna geometrical parameters and their corresponding electromagnetic performance, thereby significantly accelerating the design and optimization process [11, 23].

Nevertheless, despite their computational advantages, conventional ANN-based methodologies still suffer from several important limitations related to data dependency, physical interpretability, and generalization capability, particularly for complex mmWave antenna synthesis problems.

3.5.1 Forward and Reverse Modeling: Analysis vs. Synthesis

In antenna design applications, Artificial Neural Network (ANN) methodologies are generally classified into two principal categories: forward modeling (analysis) and reverse modeling (synthesis) [23, 63].

In forward modeling, the ANN predicts the electromagnetic performance of an antenna using its physical and material parameters as inputs. Typical predicted quantities include resonant frequency (fr), return loss (S11), gain, and bandwidth, while the input parameters generally include antenna dimensions and substrate properties [63].

Conversely, reverse modeling addresses the inverse antenna synthesis problem, where the ANN predicts the geometrical parameters required to achieve predefined electromagnetic characteristics. In this approach, desired electrical specifications — such as resonant frequency and bandwidth — are provided as inputs, while the ANN predicts the corresponding antenna dimension [23, 64].

Bhagat et al. [64] demonstrated the effectiveness of both forward and reverse ANN modeling techniques across multiple antenna geometries, including rectangular, cir- cular, and equilateral triangular microstrip antennas. Their results showed excellent agreement with full-wave electromagnetic simulations, achieving prediction errors be-low 1.5%.

Despite their effectiveness, reverse ANN models remain particularly sensitive to the non-uniqueness of inverse electromagnetic problems, where multiple antenna geometries may produce similar electromagnetic responses. This ambiguity often degrades prediction stability and optimization reliability.

3.5.2 Common ANN Architectures and Algorithms

Among the various Artificial Neural Network (ANN) architectures employed in an-tenna design, the Multilayer Perceptron (MLP) remains the most widely adopted. Typically trained using feed-forward backpropagation algorithms, the MLP benefits from efficient optimization techniques such as the Levenberg–Marquardt (LM) algo-rithm[23, 65]. The LM algorithm is particularly favored due to its fast convergence rate and robust learning performance, making it well-suited for modeling complex nonlinear relationships in antenna design problems . In addition to MLP-based models, Radial Basis Function (RBF) neural networks have gained considerable attention in recent years. RBF networks employ Gaussian activation functions in the hidden layer, enabling localized approximation of nonlinear functions. Several studies have demonstrated that RBF-based models can achieve higher prediction accuracy and reduced training time compared to conventional MLP architectures, particularly in the optimization of microstrip patch antenna dimensions[63, 64].However, the selection of ANN architecture parameters — including the number of hidden layers, neurons, and activation functions — often relies on empirical trial-and-error procedures rather than physics-based optimization principles. Consequently, the optimization process may become unstable and computationally inefficient for highly complex electromagnetic structures.

3.5.3 Limitations and Research Challenges

Despite the significant advantages of Artificial Neural Networks (ANNs) in accelerating antenna analysis and optimization, several major challenges still limit their widespread and reliable application in modern electromagnetic design problems.

One of the primary limitations is the high computational cost associated with training dataset generation. ANN models require large and representative datasets to achieve acceptable prediction accuracy. However, these datasets are generally generated using computationally expensive full-wave electromagnetic simulations performed with software tools such as CST Microwave Studio and HFSS [7**?**].Consequently, generating thousands of training samples for complex three-dimensional antenna structures becomes highly time-consuming.

Another major challenge arises from the non-uniqueness of inverse electromagnetic problems. In reverse modeling applications, multiple geometrical antenna configurations may correspond to similar electromagnetic responses, leading to inconsistent training datasets and unstable prediction behavior [65].

Furthermore, conventional ANN models behave as black-box systems with limited physical interpretability. Although these models can provide accurate predictions, they generally fail to capture the underlying electromagnetic mechanisms governing antenna operation, such as surface current distribution, near-field interactions, and wave propagation phenomena [23].

In addition, ANN models often exhibit limited generalization capability outside the training domain. Due to the curse of dimensionality, their predictive performance typically deteriorates when applied to unseen antenna topologies or parameter ranges beyond the training dataset [11].

These limitations demonstrate that purely data-driven ANN approaches remain insufficient for highly complex mmWave antenna synthesis problems. Consequently, there is an increasing need for physics-guided, data-efficient, and computationally robust intelligent optimization frameworks capable of preserving electromagnetic consistency while reducing simulation cost.

3.6 Comparative Analysis of Existing Approaches

A comprehensive review of the literature indicates that Artificial Neural Networks (ANNs) encompass a wide variety of architectures and training algorithms, each characterized by distinct computational complexities, convergence behaviors, and prediction capabilities. Consequently, different ANN methodologies involve inherent trade-offs between prediction accuracy, computational cost, training time, generalization capability, and implementation complexity.

To provide a structured overview of the state-of-the-art, Table 3.4 presents a comparative analysis of the most widely employed ANN-based methodologies in antenna analysis and synthesis. The comparison highlights their principal characteristics, advantages, limitations, and suitability for different electromagnetic design scenarios.

Table 3.4: *Comparative Analysis of Various ANN Methods Used in Antenna Design*

ANN Architecture / Algorithm	Description & Characteristics	Key Advantages	Limitations	References
MLP with Levenberg-Marquardt (LM-ANN)	Feed-forward Multilayer Perceptron (MLP) trained using the Levenberg-Marquardt backpropagation algorithm.	Exceptionally fast convergence; highly accurate for forward modeling (analysis) and simple parameter mapping.	Prone to getting trapped in local minima; suffers from the non-uniqueness problem in synthesis; relies on large datasets.	[23, 63, 66]
Radial Basis Function (RBF) Network	Utilizes Gaussian activation functions (radial basis) in the hidden layer rather than standard sigmoidal functions.	Superior approximation capabilities for synthesis (reverse modeling); often yields higher accuracy than standard MLPs (e.g., $> 99\%$).	Performance heavily depends on the correct tuning of the spread constant; can be memory-intensive.	[67, 68]
Knowledge-Based Neural Networks (KBNN)	Integrates existing analytical or empirical microwave formulas directly into the ANN structure (e.g., Prior Knowledge Input).	Drastically reduces the required training dataset size; excellent extrapolation accuracy outside the predefined training bounds.	Requires prior domain knowledge/formulas, which may not exist for highly complex, novel, or fractal geometries.	[69]
Deep Neural Networks (DNN) & CNN	Deep architectures with multiple hidden layers; CNNs use convolutional layers for spatial feature extraction.	Excellent for Massive MIMO beamforming, array spatial pattern recognition, and complex multi-parameter prediction.	Exorbitant computational cost for training; purely ”black-box”; demands massive datasets ($> 10,000$ samples) to avoid overfitting.	[7, 70]
MLP with SCG or RPROP	MLP trained using Scaled Conjugate Gradient (SCG) or Resilient Backpropagation (RPROP) algorithms.	More memory-efficient than LM; RPROP effectively handles vanishing gradients without manual learning rate tuning.	Generally exhibits lower accuracy in complex synthesis tasks compared to RBF and LM-trained networks.	[23, 63]

The comparative analysis indicates that ANN-based approaches significantly accelerate antenna analysis and optimization processes. However, most existing methodologies remain strongly dependent on large simulation datasets and lack robust physical interpretability and generalization capability. Consequently, physics-guided and computationally efficient intelligent optimization frameworks are increasingly required for next-generation mmWave and 6G antenna design applications.

3.7 Identified Research Gaps and Motivation

A comprehensive review of the state-of-the-art literature indicates that, despite significant progress in millimeter-wave (mmWave) antenna technologies, Multiple-Input Multiple-Output

(MIMO) systems, and Artificial Intelligence (AI)-assisted optimization methodologies, several critical challenges remain unresolved. The evolution toward 5G-Advanced and emerging sixth-generation (6G) wireless networks introduces increasingly stringent and often conflicting requirements related to compactness, gain enhancement, isolation improvement, bandwidth, and computational efficiency.

Although numerous electromagnetic decoupling techniques and intelligent optimization approaches have been proposed, existing methodologies still struggle to simultaneously satisfy the performance, compactness, and computational constraints of modern wireless communication systems

3.7.1 Identified Research Gaps

Based on a comprehensive comparative analysis of existing approaches, the primary research gaps can be broadly classified into two categories: physical limitations in antenna design and computational bottlenecks in optimization methodologies.

- **Trade-off Between Miniaturization, High Gain, and High Isolation:** To compensate for the severe free-space path loss and atmospheric attenuation encountered at mmWave and Terahertz (THz) frequencies, antennas must exhibit high gain and strong directivity [71]. Simultaneously, achieving ultra-high data rates requires the integration of multiple antenna elements within highly constrained physical dimensions, which intensifies mutual coupling (MC) effects and degrades the Envelope Correlation Coefficient (ECC) [35].
  Although techniques such as EBG structures,DGS, and FSS have demonstrated effectiveness in mitigating mutual coupling, they often introduce additional design complexity, bandwidth limitations, or increased physical footprint. These drawbacks conflict with the stringent compactness and performance requirements of modern 5G and IoT portable devices [72].
  Consequently, achieving compact, high-gain, and highly isolated MIMO antenna systems remains a major challenge for next-generation 5G and 6G portable wireless devices.
- **Computational Inefficiency of Traditional EM Solvers:** The design of compact multiband MIMO antenna systems represents a high-dimensional and multi-objective electromagnetic optimization problem. Conventional Computational Electromagnetics (CEM) tools — such as CST Microwave Studio and HFSS — rely on rigorous numerical techniques including the Finite Element Method (FEM) and the Finite Difference Time Domain (FDTD) method [6, 73].
  Although these full-wave simulation tools provide highly accurate electromagnetic analysis, they remain computationally expensive and time-consuming for complex antenna structures. Consequently, exhaustive parametric sweeps and iterative trial-

and-error optimization procedures become increasingly impractical for modern antenna synthesis problems[6, 73]
Therefore, computationally efficient surrogate-assisted and intelligent optimization methodologies are increasingly required to accelerate antenna design while preserving electromagnetic accuracy.

– **Limitations in Current Machine Learning (ML)-Based Antenna Design:** Although Machine Learning (ML) techniques, particularly Artificial Neural Networks (ANNs), have been introduced to accelerate antenna design, several critical limitations persist:
    1. *Single-Geometry Confinement:* Many existing ML-based studies focus on a single antenna geometry (e.g., rectangular patch antennas), lacking a generalized framework capable of capturing the influence of diverse geometrical configurations—such as circular, triangular, or fractal structures—on antenna performance [73].
    2. *Non-Uniqueness in Inverse Design:* Synthesis (inverse modeling) approaches frequently suffer from the non-uniqueness problem, where multiple distinct geometrical configurations correspond to identical electromagnetic responses. This ambiguity complicates model training and degrades convergence stability [11].
    3. *High Data Generation Cost and Lack of Interpretability:*ML models re-quire large training datasets to achieve high accuracy; however, generating such datasets using full-wave EM simulations is computationally expensive. Moreover, conventional ANN models operate as black-box systems, offering limited physical insight and reduced extrapolation capability beyond the training domain [73].
    4. *Lack of Multi-Objective Optimization Frameworks:* Current ML-based approaches often focus on optimizing a single performance metric. There remains a significant gap in the development of intelligent frameworks capable of simultaneously optimizing multiple critical parameters—such as gain, return loss (S_{11}), and mutual coupling (e.g., S_{21})—within a unified design strategy [72].

These limitations highlight the necessity for integrated and physics-guided intelligent optimization frameworks capable of combining electromagnetic accuracy, computational efficiency, and multi-objective optimization capability for next-generation MIMO antenna systems.

Figure 3.1 summarizes the principal research challenges identified in the literature and illustrates the proposed AI-assisted electromagnetic optimization framework considered in this thesis for compact high-performance mmWave MIMO antenna systems. The framework integrates compact antenna architectures, advanced electromagnetic decoupling techniques, surrogate-assisted modeling, and intelligent multi-objective optimization methodologies.

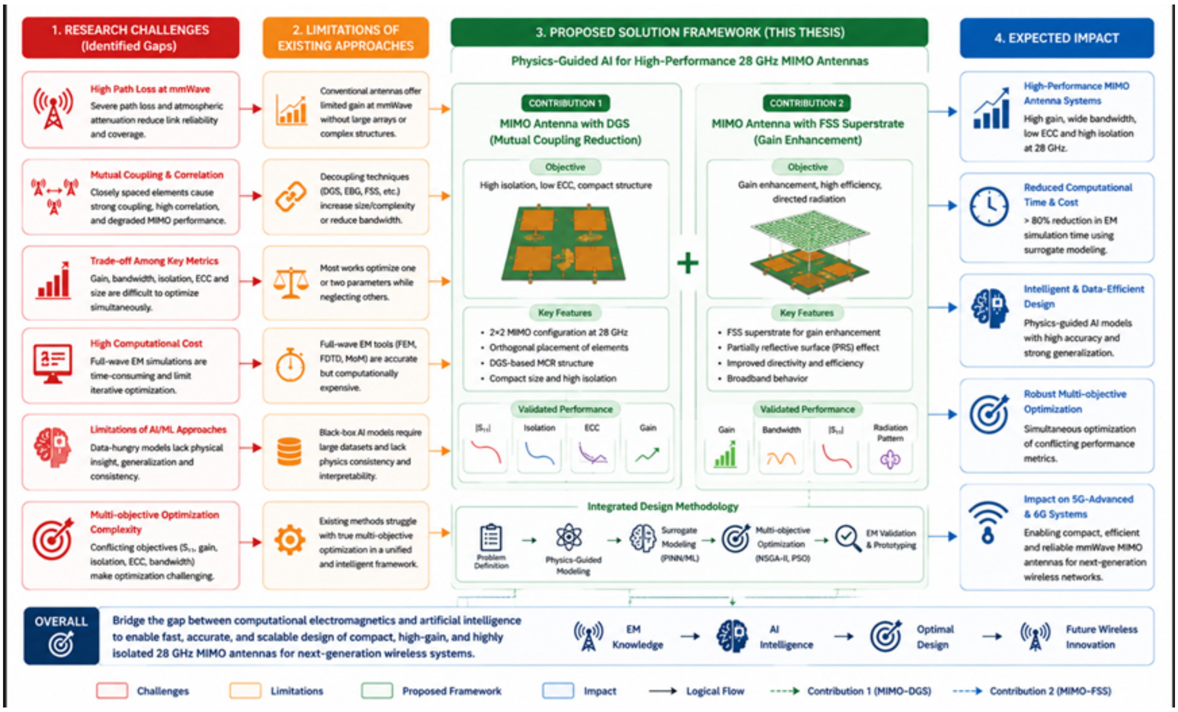

Figure 3.1: *Research Challenges and Proposed Solution Framework for Compact 28 GHz MIMO Antenna Systems*

The proposed framework presented in Fig.3.1 establishes the scientific foundation for the intelligent antenna design methodologies developed in the subsequent chapters. By combining electromagnetic modeling with physics-guided AI techniques, the proposed approach aims to achieve compact, high-gain, and highly isolated MIMO antenna systems while significantly reducing computational optimization cost.

3.8 Conclusion

This chapter has presented a comprehensive state-of-the-art review of the principal electromagnetic and computational challenges associated with next-generation wireless communication systems. The analysis demonstrates that millimeter-wave (mmWave) MIMO antenna systems are essential for meeting the stringent requirements of 5G-Advanced and emerging 6G networks in terms of high data rates, spectral efficiency, and low latency [35].

The review further highlights that simultaneously achieving high gain, compact size, and strong isolation remains a major challenge in modern MIMO antenna design. Although advanced decoupling techniques — including Defected Ground Structures (DGS), Electromagnetic Band Gap (EBG) structures, and Frequency Selective Surfaces (FSS) — have demonstrated effective mutual coupling suppression and gain enhancement capabilities, these approaches often introduce increased structural complexity, fabrication constraints, and computational optimization cost [57, 58].

In addition, conventional full-wave Computational Electromagnetics (CEM)-based optimization methodologies remain computationally expensive for high-dimensional and multi-objective antenna synthesis problems [6, 7].

Although Artificial Neural Networks (ANNs) and Machine Learning (ML)-based approaches have significantly accelerated antenna analysis and optimization, most existing models still suffer from limited physical interpretability, high data dependency, and weak generalization capability outside the training domain [69, 70].

Consequently, the analysis presented in this chapter highlights the necessity for intelligent, physics-guided, and computationally efficient optimization frameworks capable of simultaneously addressing electromagnetic performance, compactness, and multi-objective optimization requirements in modern MIMO antenna systems. The identified limitations and research gaps establish the scientific foundation for the intelligent electromagnetic optimization methodologies proposed in the subsequent chapters.

Part II

Contribution 1: MIMO–FSS Antenna Design

Chapter 4

Design and Experimental Validation of a 28 GHz MIMO Antenna

4.1 Introduction

The rapid deployment of fifth-generation (5G) wireless communication systems has accelerated the exploitation of millimeter-wave (mmWave) frequency bands, particularly the 28 GHz spectrum, to satisfy the increasing demand for ultra-high data rates, massive connectivity, and low-latency communication services [74].

However, despite the large available bandwidth offered by mmWave frequencies, signal propagation at these bands is severely affected by high free-space path loss, atmospheric attenuation, and sensitivity to blockage effects [14].To address these propagation limitations while maintaining high spectral efficiency and reliable wireless links, Multiple-Input Multiple-Output (MIMO) antenna technology has emerged as a key enabling solution for modern 5G and beyond wireless systems.

Nevertheless, the design of compact mmWave MIMO antennas remains particularly challenging due to the strong mutual coupling that arises between closely spaced antenna elements in highly integrated platforms. In addition to mutual coupling effects, conventional microstrip patch antennas operating at mmWave frequencies generally suffer from limited gain and reduced radiation efficiency, which further degrades communication reliability in practical 5G environments. Consequently, advanced electromagnetic enhancement and decoupling techniques are increasingly required to simultaneously improve gain, isolation, and overall MIMO performance.In this context, this chapter presents the design, optimization, fabrication, and experimental validation of a compact four-element (2×2) microstrip patch MIMO antenna operating at 28 GHz. To enhance the electromagnetic performance of the proposed system, two complementary techniques are integrated. First, an orthogonal antenna arrangement combined with a dedicated Mutual Coupling Reduction (MCR) structure is employed to improve port-to-port isolation and spatial diversity performance[75]. Second, a Frequency Selective Surface (FSS) superstrate composed of periodic unit cells is positioned above the antenna array to enhance forward gain and radiation directivity[76].

The proposed antenna system is designed and analyzed using CST Microwave Studio, followed by experimental fabrication and measurement validation. The electromagnetic performance is evaluated through key parameters including reflection and transmission coefficients (S-parameters), gain enhancement, radiation characteristics, radiation efficiency, surface current distribution, and MIMO diversity metrics such as the Envelope Correlation Coefficient (ECC). The obtained results demonstrate that the proposed MIMO–FSS configuration provides an effective and compact solution for next-generation 5G mmWave wireless communication applications[77, 78].

4.2 Design Methodology

This section presents the systematic design procedure adopted for the proposed 28 GHz MIMO antenna system. The design process was carried out progressively, starting from the development of a single microstrip patch antenna element, followed by the implementation of a compact four-element MIMO configuration and the integration of a mutual coupling reduction (MCR) mechanism. A progressive optimization strategy was adopted in order to simultaneously achieve compactness, high gain, proper impedance matching, and strong inter-element isolation at the target 28 GHz frequency band.

4.2.1 Single Element Design

The proposed MIMO system was initially developed from a single microstrip patch antenna element specifically optimized for 28 GHz millimeter-wave applications. The primary objective of the single-element design phase was to establish a stable resonant structure capable of providing efficient impedance matching, acceptable bandwidth, and suitable radiation characteristics prior to MIMO integration. Microstrip patch antennas were selected due to their low-profile geometry, ease of fabrication, low cost, and compatibility with planar integrated circuits, which make them highly suitable for compact 5G wireless communication devices.

4.2.1.1 Substrate and Material Properties

The antenna was fabricated using a Rogers RT/duroid 5880 (RT885) substrate, selected for its low dielectric loss and stable electromagnetic characteristics at high frequencies. This substrate is widely employed in mmWave antenna design because of its low loss tangent and excellent performance stability within high-frequency operating bands. The principal substrate parameters are summarized as follows:

- **Relative Permittivity**(ϵ_r): 2.2
- **Substrate Thickness (h)**: 0.51 mm

The relatively low dielectric constant contributes to improved radiation efficiency and reduced surface-wave losses, which are critical parameters in mmWave antenna applications.

4.2.1.2 Design Equations

The geometrical dimensions of the single-patch antenna were calculated using conventional microstrip antenna design equations [18].These analytical expressions provide the initial dimensions required to achieve resonance at the target frequency of 28 GHz.

- **Patch Width (Wp):** The width of the radiating patch was calculated using the conventional microstrip antenna design equation:

$$W_p = \frac{c}{2f_r}\sqrt{\frac{2}{\epsilon_r + 1}} \tag{4.1}$$

  where:**C** is the speed of light, $/f_r$ is the resonant frequency, and ϵ_r is the substrate relative permittivity.
  The patch width significantly influences the antenna radiation efficiency, input impedance, and bandwidth characteristics. A suitable choice of Wp contributes to improved radiation performance and stable antenna operation at the target frequency.
- **Effective Dielectric Constant (ϵ_{eff}):** Due to fringing-field effects, part of the electromagnetic field propagates in air, leading to an effective dielectric constant given by:

$$\epsilon_{eff} = \frac{\epsilon_r + 1}{2} + \frac{\epsilon_r - 1}{2}\left(1 + 12\frac{h}{W_p}\right)^{-1/2} \tag{4.2}$$

  where:
  - ϵ_r is the substrate relative permittivity,
  - h is the substrate thickness,
  - Wp is the patch width.

  The effective dielectric constant directly influences the resonant frequency, effective wavelength, and electromagnetic field distribution within the antenna structure.
- **Effective Length (Leff):**The effective resonant length is expressed as:

$$L_{eff} = \frac{c}{2f_r\sqrt{\epsilon_{eff}}} \tag{4.3}$$

  where:
  - ϵ_eff is the effective dielectric constant.
  - C is the speed of light in free space,
  - f_r is the target resonant frequency,

  The effective patch length determines the resonant behavior of the antenna and is directly related to the operating frequency of the microstrip patch structure.
- **Length Extension (ΔL):** Due to fringing-field effects at the radiating edges of the

patch, the effective electrical length of the antenna becomes slightly greater than its physical length. The corresponding length extension is calculated using:

$$\Delta L = 0.412h\frac{(\epsilon_{eff} + 0.3)(\frac{W_p}{h} + 0.264)}{(\epsilon_{eff} - 0.258)(\frac{W_p}{h} + 0.8)} \tag{4.4}$$

where:

– h is the substrate thickness,
– ϵ_{eff} is the effective dielectric constant,
– W_p is the patch width.

The length extension parameter compensates for the fringing electromagnetic fields and plays an important role in accurately determining the resonant frequency of the antenna.

– **Actual Length of the Patch (Lp):** • The actual physical length of the radiating patch is obtained by subtracting the fringing-field length extensions from the effective resonant length:

$$L_p = L_{eff} - 2\Delta L \tag{4.5}$$

where:

– L_eff is the effective patch length,
– δ_L is the length extension caused by fringing fields.

The physical patch length is one of the most critical antenna parameters, as it directly controls the resonant frequency and overall electromagnetic behavior of the microstrip patch antenna.

– **Microstrip Feed Line Design**

The microstrip feed line was designed to provide proper impedance matching between the excitation source and the radiating patch antenna. At millimeter-wave (mmWave) frequencies, accurate feed-line dimensioning is essential to minimize reflection losses, improve power transfer efficiency, and ensure stable antenna performance. The dimensions of the feed line mainly depend on the characteristic impedance (Z0), substrate thickness (h), and relative permittivity (ϵ_r)) of the dielectric material [20].

– **Feed Line Width (W):** The width of the microstrip transmission line is calculated according to the ratio (W/h)

– case 1: For $W/h \leq 2$:

$$\frac{W}{h} = \frac{8e^A}{e^{2A} - 2}, \tag{4.6}$$

where:

$$A = \frac{Z_0}{60}\sqrt{\frac{\epsilon_r + 1}{2}} + \frac{\epsilon_r - 1}{\epsilon_r + 1}\left(0.23 + \frac{0.11}{\epsilon_r}\right). \tag{4.7}$$

– case 2: For $W/h > 2$:

$$\frac{W}{h} = \frac{2}{\pi}(B-1-\ln(2B-1)+\frac{\epsilon_r-1}{2\epsilon_r}(\ln(B-1)+0.39-\frac{0.61}{\epsilon_r})) \quad (4.8)$$

where:

$$B = \frac{377\pi}{2Z_0\sqrt{\epsilon_r}}. \quad (4.9)$$

and:

– W is the feed-line width,
– h is the substrate thickness,
– Z0 is the characteristic impedance,
– ϵ_r is the substrate relative permittivity.

The feed-line width directly affects the characteristic impedance of the transmission line and therefore plays a critical role in achieving efficient impedance matching and minimizing return losses.

– **Feed Line Length (L):** For a given frequency:

$$L = \frac{c}{2f\sqrt{\epsilon_{\text{eff}}}}, \quad (4.10)$$

where:

– C is the speed of light in free space,
– fr is the resonant frequency,
– ϵ_{eff} is the effective dielectric constant.

The feed-line length contributes to phase stability and proper electromagnetic energy transmission toward the radiating patch element.

4.2.1.3 Antenna Geometry Optimization

The proposed single-element antenna was designed using Equations 4.10–4.1. Figure 4.1 presents the optimized geometry of the microstrip patch antenna, including the front, back, and side views.

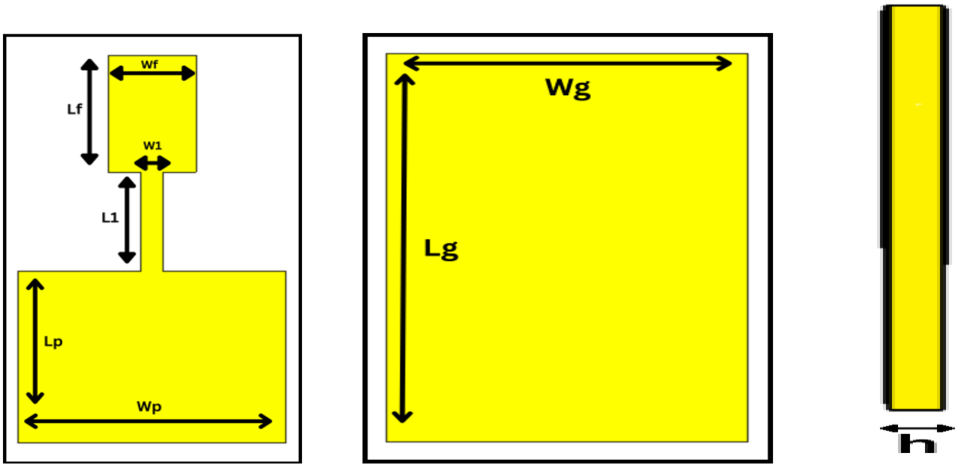

(a) *front view* **(b)** *back view* **(c)** *side view*

Figure 4.1: *Geometry of the Proposed Single Microstrip Patch Antenna(a) Front view, (b) Back view, and (c) Side view*

The antenna consists of a rectangular radiating patch fed by a microstrip transmission line printed on a Rogers RT/duroid 5880 substrate, while a full metallic ground plane is located on the opposite side. The antenna dimensions were optimized using CST Microwave Studio in order to achieve efficient impedance matching, stable resonance at 28 GHz, and suitable radiation performance for compact 5G mmWave applications. The optimized dimensions are: Lf = 6 mm, Wf = 1.38 mm, W1 = 0.35 mm,L1=1.8 mm LP = 3.13 mm,Wp=4.19 mm , Wg = 7.6 mm, Lg=11 mm , and substrate thickness h = 0.51mm.

4.2.1.4 Parametric Optimization of the Antenna Geometry

To improve the electromagnetic performance of the proposed antenna, several geometrical modifications were investigated for both the radiating patch and the ground-plane structure. The optimization process aimed to achieve stable resonance at 28 GHz, enhanced impedance matching, and improved bandwidth characteristics suitable for 5G mmWave applications.

Figure 4.2 illustrates the different antenna configurations analyzed during the parametric optimization process. Various patch geometries and ground-plane configurations were progressively modified and evaluated using CST Microwave Studio in order to identify the optimal antenna structure.

The investigated modifications mainly affected the surface current distribution and fringing electromagnetic fields, which directly influence the reflection coefficient (S11), resonance stability, and radiation performance of the antenna.

The comparative analysis enabled the selection of the optimal antenna configuration providing efficient impedance matching and stable resonance behavior at 28 GHz

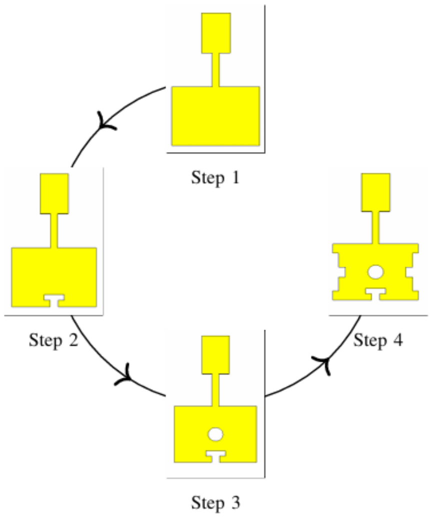

(a) *Different patch geometries*

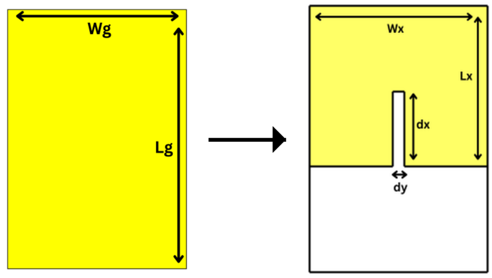

(b) *different ground-plane configurations*

Figure 4.2: *Investigated Antenna Configurations During the Optimization Process (a) Different patch geometries and (b) different ground-plane configurations.*

Figure 4.3 presents the simulated reflection coefficient (S11) for the different antenna configurations investigated during the optimization process. The results show that the geometrical modifications significantly affect the resonance behavior and impedance matching performance of the antenna.

Among all investigated structures, Configuration 04 provides the best performance, achieving a minimum reflection coefficient of approximately −31 dB near 28 GHz. This result confirms efficient impedance matching and stable resonance at the target operating frequency. Consequently, Configuration 04 was selected as the optimal antenna geometry for the subsequent MIMO and FSS integration stages.

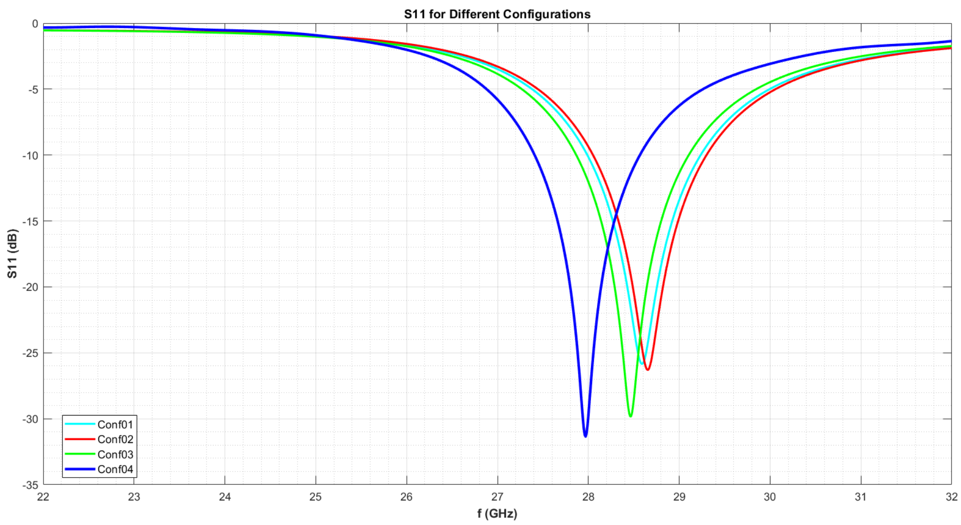

Figure 4.3: *Simulated Reflection Coefficient (S11) for Different Antenna Configurations*

To further highlight the influence of the geometrical modifications, a comparative summary of the investigated antenna configurations is presented in Table 4.1.

Table 4.1: *Comparative Analysis of the Investigated Antenna Configurations*

Configuration	**Main Modification**	**Resonance Behavior**	**Minimum S_{11}**	**Remarks**
Config. 01	Initial patch geometry	Resonance shifted from target frequency	Moderate matching	Limited impedance matching performance
Config. 02	Modified patch structure	Improved resonance stability	Improved S_{11}	Better matching than Config. 01
Config. 03	Ground-plane modification	Resonance close to 28 GHz	Acceptable matching	Enhanced bandwidth characteristics
Config. 04	**Optimized patch and ground structure**	**Stable resonance at 28 GHz**	**≈ -31 dB**	**Best overall electromagnetic performance**

The comparative analysis demonstrates that the geometrical modifications applied to the radiating patch and ground-plane structure significantly affect the antenna resonance behavior and impedance matching characteristics. As observed in Fig.4.3, Configuration 04 provides the best performance with stable resonance and improved impedance matching at the target operating frequency. Although the obtained bandwidth remains suitable for 5G mmWave applications, additional bandwidth enhancement techniques may still be required for ultra-wideband communication scenarios. Nevertheless, the obtained results validate the effectiveness of the adopted parametric optimization methodology for compact high-performance antenna design.

Figure 4.4 presents the final optimized geometry of the proposed antenna after the parametric optimization process.

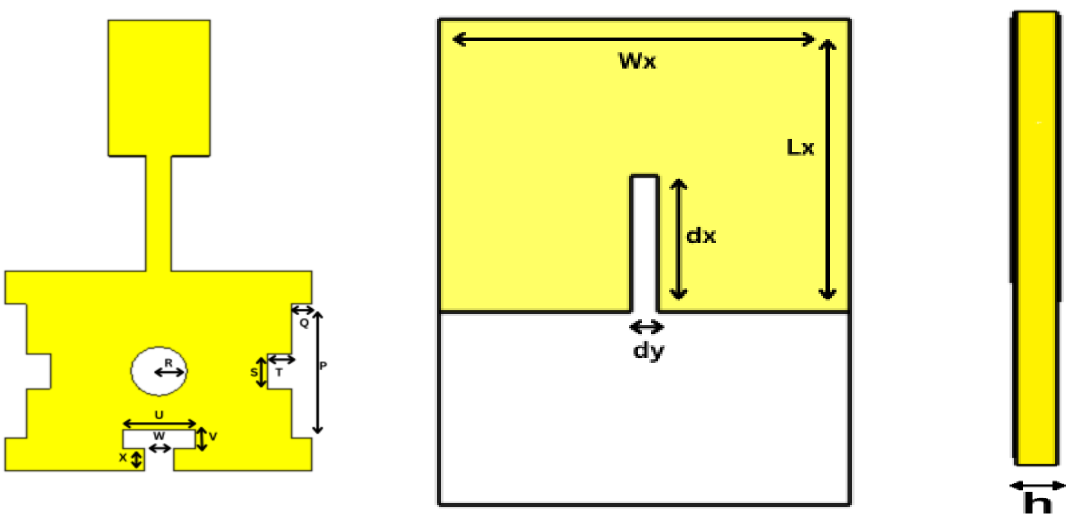

Figure 4.4: *Optimized Geometry of the Proposed Single Antenna Element*

The optimized geometrical parameters are: $P = 2.09$ mm, $Q = 0.28$ mm, $S = 0.55$ mm, $T = 0.33$ mm, $U = 1$ mm, $V = 0.3$ mm, $W = 0.4$ mm, $X = 0.35$ mm, $Lx = 6.62$ mm, $Wx = 7.6$ mm, $dx = 3.09$ mm, $dy = 0.48$ mm The optimized antenna geometry provides improved current distribution, stable resonance characteristics, and efficient impedance matching, making it suitable for compact 5G mmWave MIMO applications.

Following the optimization of the single-element antenna, the proposed structure was extended to a compact multiport MIMO configuration for enhanced spatial diversity and high-data-rate operation.

4.2.2 MIMO Configuration

To satisfy the increasing requirements of 5G wireless communication systems in terms of high data rates, spectral efficiency, and communication reliability, a Multiple-Input Multiple-Output (MIMO) antenna configuration was developed using the optimized single antenna element presented in the previous section.

The proposed 2×2 MIMO configuration exploits spatial diversity to improve channel capacity and transmission reliability while maintaining compact antenna dimensions suitable for 5G mmWave applications. However, the compact integration of multiple antenna elements at millimeter-wave frequencies inherently increases electromagnetic coupling between adjacent radiating elements. Such coupling may degrade impedance matching, radiation efficiency, isolation performance, and MIMO diversity characteristics such as ECC.

To overcome these limitations, a dedicated mutual coupling reduction (MCR) structure was incorporated into the proposed antenna array[75].

The adopted design was optimized to simultaneously achieve compactness, high isolation, stable resonance behavior, and efficient radiation performance at the target 28 GHz operating frequency. Therefore, additional electromagnetic decoupling techniques were investigated and optimized, as discussed in the following section.

4.2.2.1 4-Element Array Design

The proposed MIMO antenna system consists of four identical microstrip patch antenna elements arranged in a compact 2×2 array configuration. The adopted arrangement was selected to improve spatial diversity and communication reliability while maintaining compact antenna dimensions suitable for portable 5G mmWave devices.

The overall dimensions of the complete MIMO structure are 32.5×32.5×0.51 mm. Despite the compact size of the antenna array, the proposed configuration provides sufficient spatial separation between the radiating elements to support efficient multiport operation.

Figure 4.5 illustrates the geometry of the proposed four-element MIMO antenna before introducing the mutual coupling reduction mechanism. The front view shown in Fig.4.5a presents the arrangement and orientation of the four radiating elements, whereas the 3D view illustrated in Fig.4.5b provides a global representation of the antenna structure and substrate configuration.

The orthogonal arrangement of the antenna elements contributes to polarization diversity and partially reduces electromagnetic interaction between adjacent radiators. However, due to the compact inter-element spacing at millimeter-wave frequencies, additional mutual coupling reduction techniques remain necessary to further improve the isolation performance of the proposed antenna array.

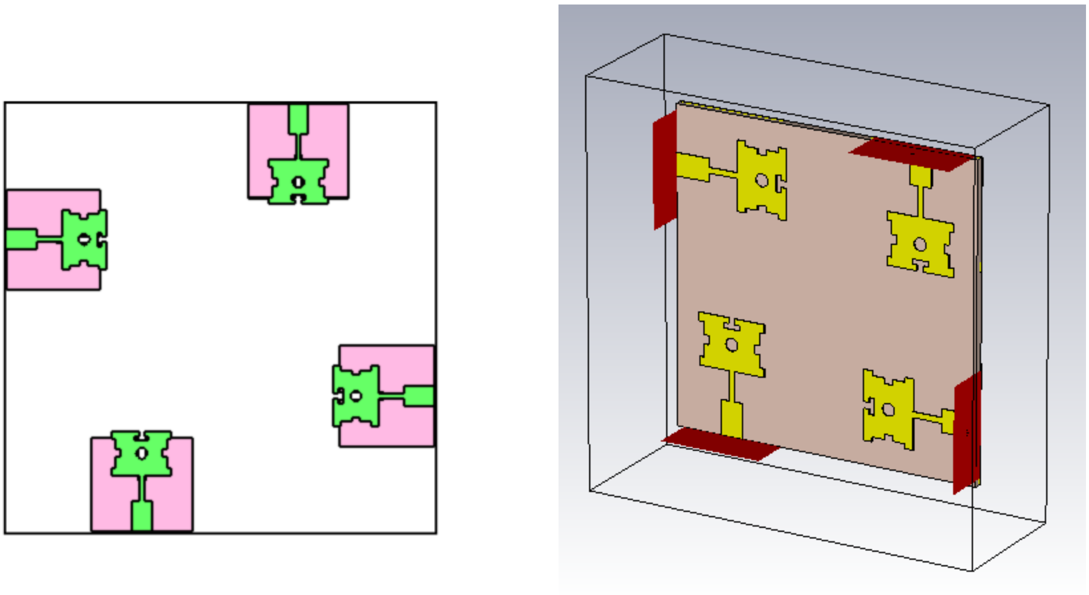

(a) *front view* **(b)** *3D view*

Figure 4.5: *Proposed Four-Element MIMO Antenna Without Mutual Coupling Reduction*

4.2.3 Mutual Coupling Reduction Strategy

One of the principal challenges in compact MIMO antenna systems is the strong electromagnetic interaction between closely spaced antenna elements. At millimeter-wave frequencies, the reduced inter-element spacing considerably intensifies near-field coupling and surface-wave interactions, which may significantly degrade impedance matching, radiation efficiency, and diversity performance.

To overcome these limitations, a dedicated Mutual Coupling Reduction (MCR) structure was incorporated into the proposed MIMO antenna system. The adopted decoupling mechanism was designed to suppress unwanted surface currents and improve the isolation performance between adjacent radiating elements.

4.2.3.1 Orthogonal Placement for Mutual Coupling Reduction

The proposed MIMO antenna employs an orthogonal arrangement of the radiating elements in combination with a dedicated coupling reduction structure in order to enhance isolation performance and spatial diversity characteristics [75].

Figure 4.6 illustrates the geometry of the proposed MIMO antenna integrated with the MCR mechanism. The front view shown in Fig. 4.6(a) presents the compact antenna array together with the inserted decoupling structure located between the radiating elements. Meanwhile, Fig. 4.6(b) provides a detailed view of the proposed coupling reduction structure and its optimized geometrical parameters. The orthogonal placement of the antenna elements contributes to polarization diversity and partially suppresses electromagnetic coupling between adjacent radiators. In addition, the introduced MCR structure modifies the surface current distribution and reduces the propagation of coupling currents between antenna ports. The optimized dimensions of the coupling reduction structure are: ex=0.3 mm, lcy=7 mm, lcx=0.8 mm, rc=1.02. The combined effect of orthogonal element placement and the proposed MCR structure enables improved isolation performance while preserving compact antenna dimensions suitable for 5G mmWave applications.

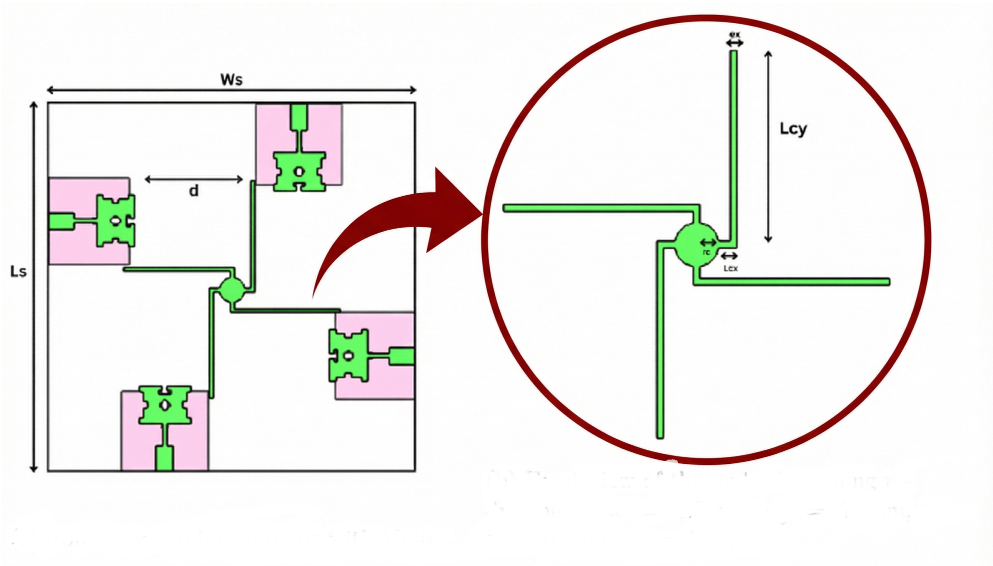

Figure 4.6: *The MIMO antenna with the mutual coupling reduction*

4.2.3.2 S-Parameters Analysis and Simulated Performance

The electromagnetic performance of the proposed 28 GHz MIMO antenna was rigorously evaluated using CST Microwave Studio through full-wave electromagnetic simulations. The scattering parameters (S-parameters) were employed to characterize the antenna performance in terms of impedance matching, operational bandwidth, and inter-element isolation. In MIMO antenna systems, the reflection coefficients (S11,S22,S33,S44) describe the impedance matching quality of each antenna port, whereas the transmission coefficients (S21,S31,S41) quantify the level of electromagnetic coupling between adjacent antenna elements. Accurate analysis of the S-parameters is essential for evaluating the effectiveness of the proposed mutual coupling reduction mechanism and validating the suitability of the antenna for 5G mmWave applications. In particular, low reflection coefficients and reduced transmission coefficients indicate efficient impedance matching and high isolation performance, respectively. The simulated S-parameter results obtained for the proposed MIMO antenna are presented and discussed in the following subsections.

4.2.3.2.1 Reflection Coefficient (S11)

The The reflection coefficient (S11)) represents the amount of electromagnetic power reflected back toward the antenna input port. A lower (S11) value indicates improved impedance matching and more efficient power transmission between the excitation source and the antenna. Figure 4.7presents the simulated reflection coefficients (S11,S22,S33,S44) of the proposed MIMO antenna before the integration of the Frequency Selective Surface (FSS). The obtained results show that all antenna ports exhibit similar resonance behavior due to the symmetrical configuration of the proposed antenna array. The reflection coefficients remain below the conventional −10 dB impedance-matching criterion over the frequency range from approximately 27.5 GHz to 28.7 GHz, resulting in an operational bandwidth of about 1.21 GHz. Furthermore, the antenna exhibits stable resonance around the target 28 GHz operating frequency, where the minimum reflection coefficient reaches approximately −26 dB. These results confirm that the proposed MIMO antenna achieves efficient impedance matching and satisfactory bandwidth performance suitable for 5G mmWave communication systems. Although the obtained bandwidth is appropriate for the targeted application, additional bandwidth enhancement techniques may still be investigated for future ultra-wideband mmWave communication scenarios.

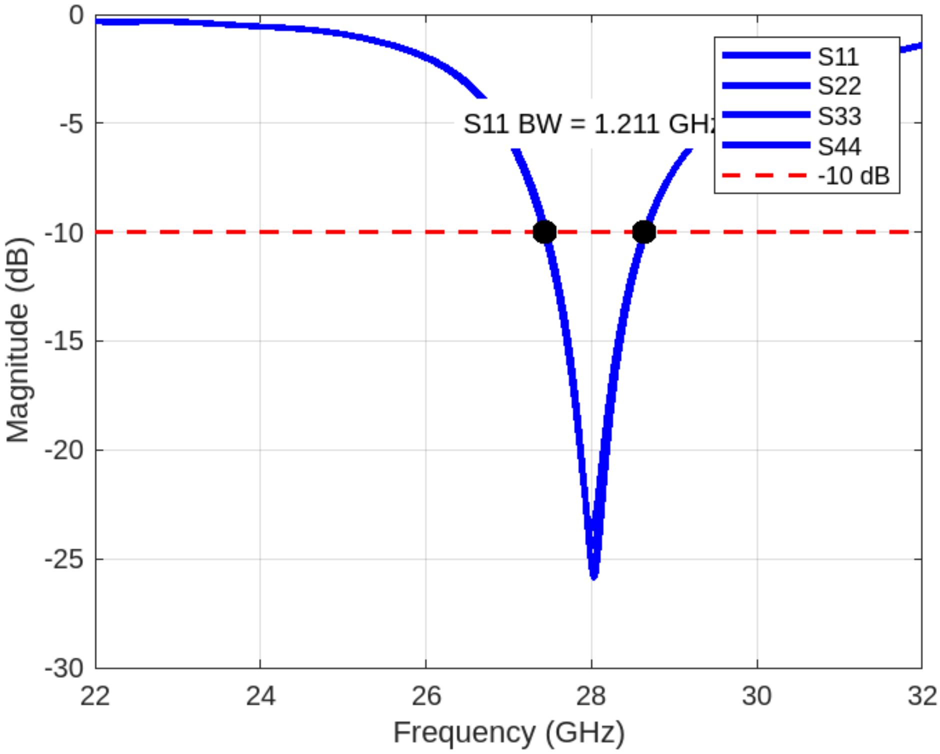

Figure 4.7: *Reflection Coefficients (S11,S22,S33,S44) of the Proposed MIMO Antenna Without FSS*

4.2.3.2.2 Transmission Coefficient

The transmission coefficients (S21,S31,S41,...) quantify the level of electromagnetic coupling between the antenna elements. In MIMO systems, low transmission coefficients are essential for achieving high port isolation and efficient spatial diversity performance. Figure 4.8 compares the simulated transmission coefficients of the proposed MIMO antenna before and after integrating the Mutual Coupling Reduction (MCR) mechanism. Figure 4.8a corresponds to the antenna configuration without the MCR structure, whereas Fig. 4.8b presents the transmission coefficients obtained after introducing the proposed decoupling mechanism.

The obtained results clearly demonstrate that the integration of the MCR structure significantly improves the isolation performance of the antenna system. Without the coupling reduction mechanism, the transmission coefficients remain close to approximately −21 dB near the target operating frequency. After integrating the proposed MCR structure, the transmission coefficients decrease substantially, reaching values below approximately −24 dB and even lower for certain antenna ports.

This improvement confirms that the proposed decoupling structure effectively suppresses surface-current propagation and reduces electromagnetic coupling between adjacent antenna elements. The enhanced isolation performance contributes directly to improved MIMO diversity characteristics, reduced signal interference, and more stable antenna operation within the targeted 28 GHz frequency band. Although the obtained isolation performance is already suitable for compact 5G mmWave applications, additional advanced decoupling techniques could still be explored in future work to further enhance isolation and bandwidth performance in ultra-dense MIMO environments [79].

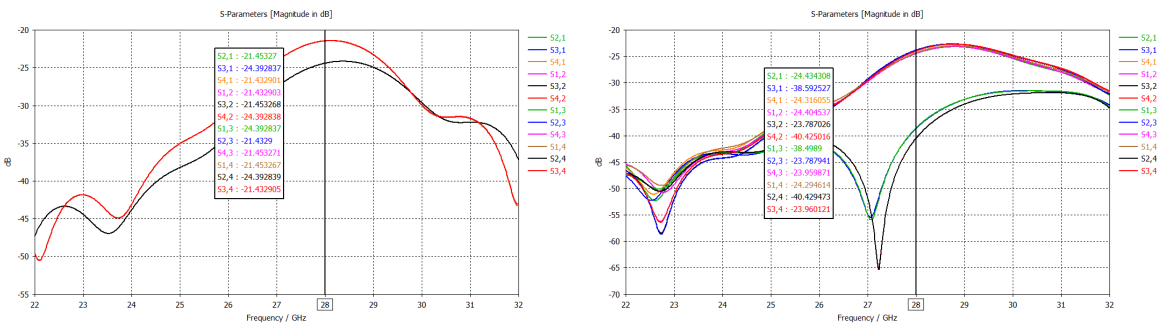

(a) *Without mutual coupling reduction* **(b)** *with mutual coupling reduction*

Figure 4.8: *Simulated Transmission Coefficients of the Proposed MIMO Antenna*

4.3 FSS Modeling and Integration into the Antenna

To further enhance the electromagnetic performance of the proposed MIMO antenna system, a Frequency Selective Surface (FSS) structure was designed and integrated above the antenna array. Frequency Selective Surfaces are periodic electromagnetic structures composed of conductive unit cells capable of controlling the transmission and reflection properties of electromagnetic waves at specific frequency bands. In antenna engineering, FSS structures are widely employed to improve gain, directivity, bandwidth characteristics, and radiation efficiency, particularly in millimeter-wave applications where severe free-space path loss represents a major challenge[76].

In the proposed design, the FSS structure consists of 6×6 periodic unit cells (36 cells in total) positioned at an optimized distance of 7 mm above the MIMO antenna array. The adopted configuration acts as a partially reflective surface that redirects and concentrates the radiated electromagnetic energy toward the desired direction, thereby improving the forward gain and radiation characteristics of the antenna system.

The FSS unit cells were fabricated using a Rogers RT/duroid 5880 substrate with a relative permittivity of $\epsilon_r = 2.2$ and a substrate thickness of 0.51 mm. In addition, the absence of a metallic ground plane on the backside of the FSS substrate contributes to reducing the overall antenna profile while maintaining efficient electromagnetic interaction with the radiating structure.

The periodic arrangement of the FSS unit cells enables stable electromagnetic resonance behavior and efficient control of electromagnetic wave propagation near the target 28 GHz operating frequency. Consequently, the proposed FSS structure provides an effective electromagnetic enhancement mechanism for improving the gain and radiation directivity of compact MIMO antenna systems designed for 5G mmWave applications.

4.3.1 FSS Unit Cell Design

The proposed FSS unit cell was designed using a concentric split-ring resonator geometry in order to achieve selective electromagnetic resonance near the target 28 GHz operating frequency.

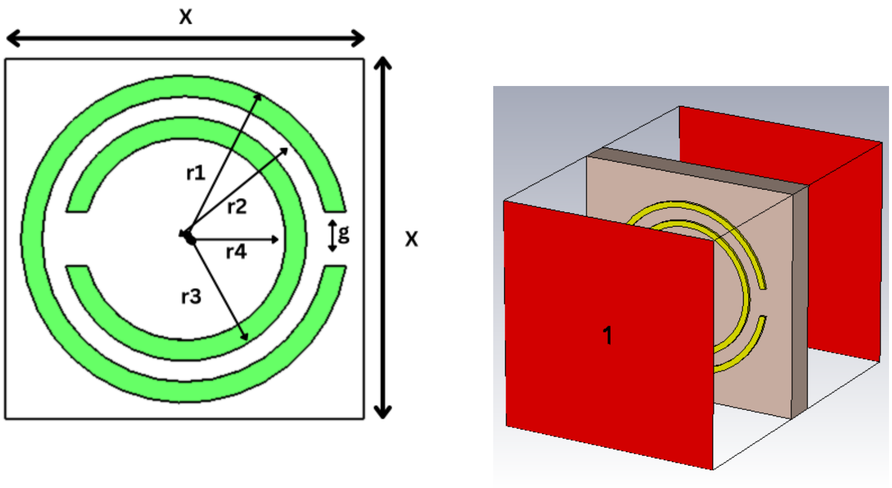

(a) *Unit cell FSS.* **(b)** *front-viewl*

Figure 4.9: *Geometry and Simulation Configuration of the Proposed FSS Unit Cell (a) FSS unit cell geometry and (b) simulation setup of the unit cell.*

The proposed unit cell consists of concentric circular split-ring structures printed on a Rogers RT/duroid 5880 substrate. The geometrical parameters controlling the electromagnetic response of the structure are denoted by X, r1, r2, r3, r4, and g, as illustrated in Fig.4.9a. The optimized geometrical dimensions of the proposed FSS unit cell are: r1 = 1.57 mm, r2=1.37 mm, r3=1.17 mm, r4=1.97 mm, with a substrate thickness of: h=0.51 mm. Figure 4.9b presents the unit-cell simulation configuration implemented in CST Microwave Studio for evaluating the electromagnetic behavior of the proposed FSS structure under periodic boundary conditions.

The adopted circular split-ring resonator configuration enables compact electromagnetic resonance behavior while maintaining stable filtering characteristics at millimeter-wave frequencies. In addition, the resonant response of the proposed FSS structure is mainly governed by the equivalent inductive and capacitive effects generated by the split-ring resonator geometry. The concentric arrangement of the split-ring structures contributes to improving the electromagnetic field confinement and resonance stability around the target operating frequency. Consequently, the proposed FSS unit cell provides suitable electromagnetic characteristics for gain enhancement and radiation control in 5G mmWave antenna applications.

4.3.2 Electromagnetic Response of the FSS Unit Cell

The reflection and transmission coefficients of the FSS unit cell were analyzed to evaluate its electromagnetic filtering characteristics at millimeter-wave frequencies. Figure 4.10 presents the simulated scattering parameters of the proposed FSS unit cell. The obtained results demonstrate a strong resonance behavior around the target 28 GHz frequency, where the transmission coefficient exhibits a significant attenuation level.

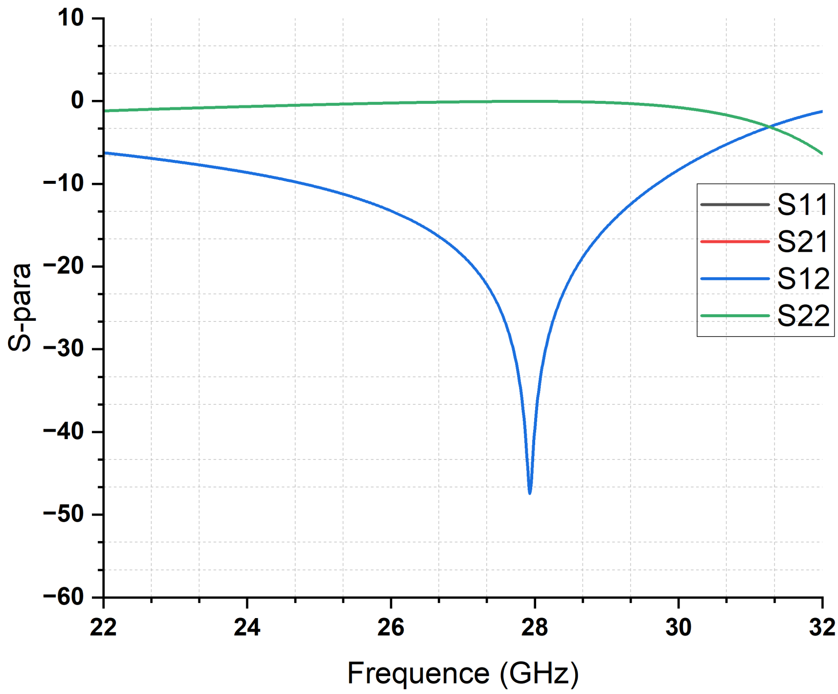

Figure 4.10: *Simulated Scattering Parameters of the Proposed FSS Unit Cell*

The obtained response confirms that the proposed FSS structure behaves as an effective frequency-selective resonator capable of controlling electromagnetic wave propagation around the targeted operating frequency. The resonance observed near 28 GHz indicates that the proposed FSS structure effectively suppresses undesired wave propagation outside the targeted operating band. Furthermore, the strong resonant behavior validates the suitability of the proposed FSS structure for gain enhancement and electromagnetic field control in 5G mmWave antenna applications. The resonant behavior of the proposed FSS structure is mainly governed by the equivalent inductive and capacitive effects generated by the split-ring resonator geometry. These electromagnetic effects contribute to the selective filtering characteristics observed near the target operating frequency

4.3.3 FSS Superstrate Configuration

Figure 4.11 illustrates the final configuration of the proposed Frequency Selective Surface composed of 36 periodic unit cells arranged in a 6×6 matrix.

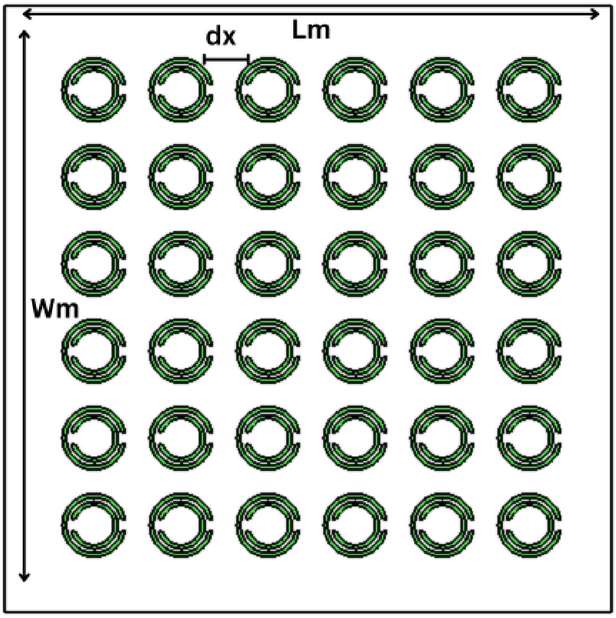

Figure 4.11: *Geometry of the Proposed Frequency Selective Surface (FSS)*
$Lm = Wm = 30.07mm, dx = 1.22mm$

The overall dimensions of the FSS structure are: $Lm = Wm = 30.07\,mm$ with an inter-element spacing of: $dx = 1.22\,mm$.

The periodic arrangement of the FSS unit cells enables stable electromagnetic resonance behavior and uniform field distribution across the entire superstrate surface. This periodic configuration contributes to improving the interaction between the radiated electromagnetic waves and the partially reflective FSS structure. Consequently, the proposed FSS superstrate provides stable electromagnetic filtering characteristics and efficient control of the radiated fields generated by the MIMO antenna array. The adopted configuration therefore contributes to improving the antenna gain and radiation directivity while maintaining compact antenna dimensions suitable for 5G mmWave applications.

4.3.4 Integration of the FSS with the MIMO Antenna

After validating the electromagnetic response of the FSS unit cell and the complete superstrate configuration, the proposed FSS structure was integrated with the MIMO antenna array. The final proposed antenna system consists of a four-element MIMO antenna integrated with the designed FSS superstrate positioned 7 mm above the antenna array. Figure 4.12 illustrates the integration of the FSS structure with the proposed MIMO antenna configuration. Figure 4.12a presents the 3D representation of the complete antenna system, while Fig. 4.12b shows the relative positioning between the MIMO antenna and the FSS layer.

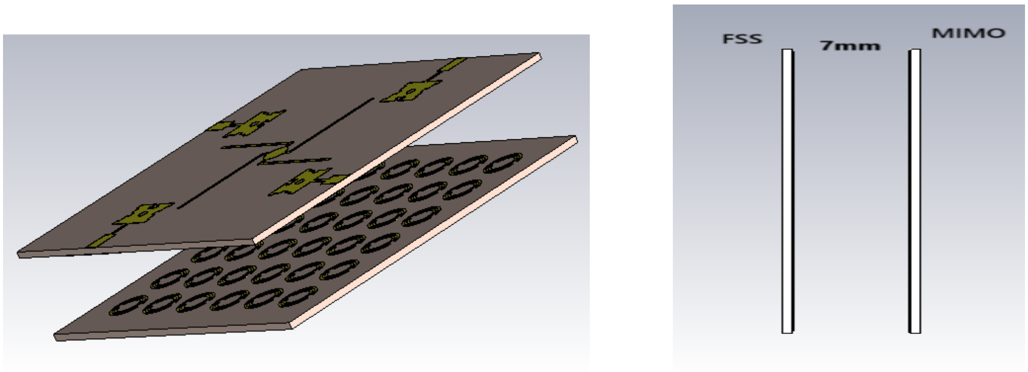

(a) *3D view* **(b)** *Front view*

Figure 4.12: *Proposed MIMO Antenna Integrated with the Frequency Selective Surface (FSS) (a) 3D view and (b) front view.*

The optimized separation distance of 7 mm between the antenna array and the FSS superstrate enables constructive electromagnetic interaction between the radiated waves and the partially reflective FSS surface. The selected separation distance was optimized to maximize constructive electromagnetic interference and improve the coupling between the radiated fields and the FSS resonant structure.

Consequently, the proposed configuration significantly enhances the antenna forward gain and improves the radiation directivity while preserving compact antenna dimensions suitable for 5G mmWave applications.

The integration of the proposed FSS structure therefore establishes an effective electromagnetic enhancement mechanism for improving the overall performance of compact MIMO antenna systems operating at 28 GHz.

Although the proposed FSS structure significantly improves the antenna gain and radiation directivity, the introduction of the superstrate may slightly increase fabrication complexity and alignment sensitivity at millimeter-wave frequencies.

Overall, the proposed FSS-integrated MIMO configuration provides an effective solution for enhancing antenna gain and radiation directivity while maintaining compact antenna dimensions suitable for next-generation 5G mmWave wireless communication systems.

4.4 Simulation Setup (CST Microwave Studio)

The proposed MIMO antenna integrated with the Frequency Selective Surface (FSS) was simulated and analyzed using CST Microwave Studio to evaluate its electromagnetic performance at the target 28 GHz operating frequency.

The complete antenna structure, including the four-element MIMO array, the Mutual Coupling Reduction (MCR) structure, and the FSS superstrate, was modeled using optimized geometrical and material parameters. Open boundary conditions were applied to emulate free-space propagation, while 50 Ω excitation ports were used to evaluate the antenna scattering parameters and radiation characteristics.

Adaptive mesh refinement was employed to ensure numerical accuracy and stable convergence at millimeter-wave frequencies.The simulation setup was configured to analyze the antenna performance in terms of reflection coefficients, transmission coefficients, gain, radiation efficiency, radiation patterns, surface current distribution, and Envelope Correlation Coefficient (ECC). The corresponding simulated electromagnetic results are presented and discussed in the following section.

4.5 Simulated Results and Performance Analysis

This section presents the simulated electromagnetic results of the proposed MIMO antenna integrated with the Mutual Coupling Reduction (MCR) structure and the Frequency Selective Surface (FSS). The antenna performance was evaluated in terms of impedance matching, port isolation, gain enhancement, radiation characteristics, surface current distribution, and MIMO diversity performance at the target 28 GHz operating frequency.

The obtained results are discussed to demonstrate the effectiveness of the proposed antenna design for compact high-performance 5G mmWave applications.

4.5.1 S-Parameters

The scattering parameters (S-parameters) were analyzed to evaluate the impedance matching and isolation performance of the proposed MIMO antenna integrated with the Mutual Coupling Reduction (MCR) structure and the Frequency Selective Surface (FSS). In compact multiport MIMO systems operating at millimeter-wave frequencies, the reflection coefficients characterize the impedance matching quality of each antenna port, whereas the transmission coefficients quantify the electromagnetic coupling between adjacent radiating elements. These parameters play a fundamental role in determining the operational bandwidth, power-transfer efficiency, isolation capability, and overall electromagnetic stability of the antenna system.

4.5.1.1 Reflection Coefficients (S11,S22,S33,S44)

The impedance-matching performance of the developed MIMO antenna was evaluated through the simulated reflection coefficients (S11,S22,S33,S44), as illustrated in Fig. 4.13.

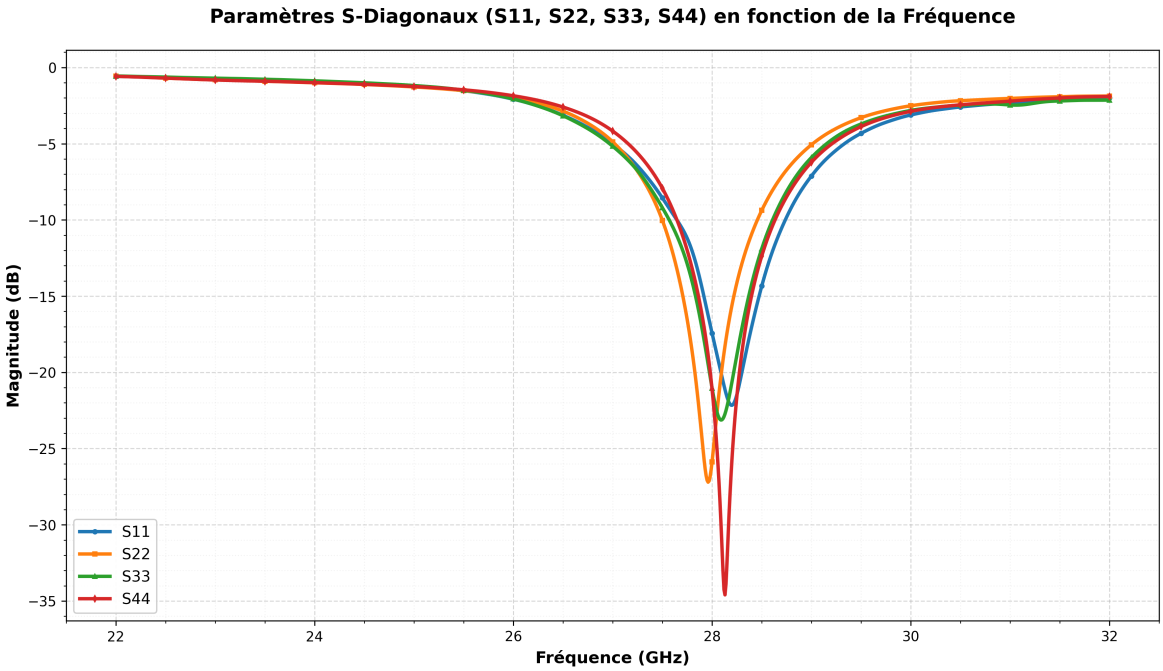

Figure 4.13: *Reflection coefficients ($S_{11}, S_{22}, S_{33}, S_{44}$) with MCR and FSS.*

The simulated electromagnetic responses confirm efficient antenna resonance around the target 28 GHz operating frequency, with all reflection coefficients remaining below the conventional −10 dB impedance-matching criterion over the operating bandwidth of approximately 1.320 GHz.

As observed in Fig.4.13, S11 reaches approximately −22 dB, while S22 achieves a deeper resonance close to −27 dB, indicating efficient impedance matching and reduced reflected power for Ports 1 and 2. Similarly, S33 and S44 exhibit minimum values of approximately −23 dB and −35 dB, respectively, where the deeper resonance observed for S44 indicates stronger electromagnetic field confinement and more efficient energy transfer. Furthermore, the close similarity between the four reflection-coefficient responses confirms the symmetrical electromagnetic behavior and stable multiport operation of the developed MIMO antenna structure.

The achieved resonance stability and impedance-matching performance are mainly attributed to the optimized patch geometry, the orthogonal arrangement of the antenna elements, the proposed MCR structure, and the constructive electromagnetic interaction introduced by the FSS superstrate, which enhances electromagnetic field confinement and resonance stability despite the compact inter-element spacing .

4.5.1.2 Transmission Coefficients

Figure 4.14 presents the simulated transmission coefficients of the proposed MIMO antenna integrated with the Mutual Coupling Reduction (MCR) structure and the Frequency Selective Surface (FSS).

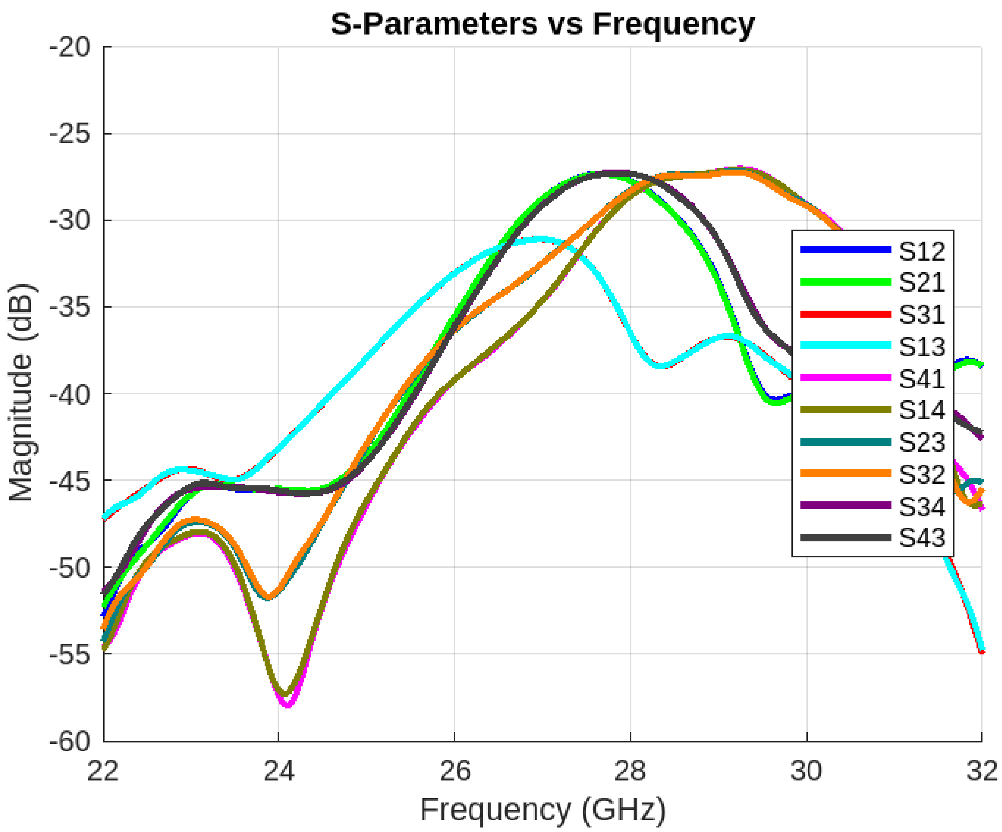

Figure 4.14: *Simulated Transmission Coefficients of the Proposed MIMO Antenna with MCR and FSS.*

The transmission coefficients remain below the conventional −20 dB isolation criterion throughout the operating bandwidth, confirming excellent electromagnetic isolation between the antenna ports[80].

As observed in Fig. 4.14, the adjacent coupling coefficient S21reaches approximately −28 dB near the target 28 GHz operating frequency, indicating very weak near-field coupling and minimal undesired power transfer between neighboring antenna elements. Similarly, S31 , and S43 exhibit isolation levels better than −27 dB, while several transmission responses remain below −30 dB outside the resonance region. The achieved high-isolation performance is mainly attributed to the orthogonal arrangement of the antenna elements and the proposed MCR structure, which suppress near-field electromagnetic interactions and undesired surface-current coupling mechanisms [81]. In addition, the FSS superstrate contributes to stabilizing the electromagnetic field distribution above the antenna array, thereby maintaining stable isolation behavior despite the compact inter-element spacing. Overall, the simulated transmission responses confirm the suitability of the developed MIMO antenna system for high-isolation 5G millimeter-wave MIMO applications.

4.5.2 Gain and Radiation Patterns

The radiation characteristics of the proposed MIMO antenna were analyzed in terms of gain enhancement and radiation efficiency after integrating the Frequency Selective Surface (FSS) superstrate.

4.5.2.1 Gain

Figure 4.15 presents the simulated gain of the proposed MIMO antenna with and without the FSS superstrate positioned 7 mm above the antenna array.

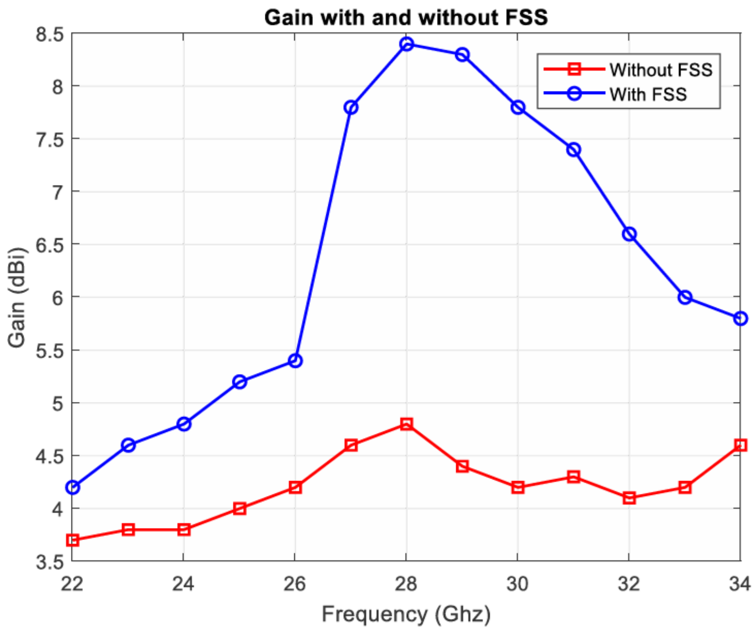

Figure 4.15: *Gain of the Proposed MIMO Antenna with and without FSS at 7 mm Separation Distance*

The obtained results show that the integration of the FSS significantly improves the antenna gain around the target 28 GHz operating frequency. Without the FSS layer, the antenna achieves a maximum gain of approximately 4.8 dBi, whereas the gain increases to nearly 8.4 dBi after integrating the FSS structure, corresponding to a gain enhancement of about 3.6 dBi. The observed improvement is mainly attributed to the partially reflective behavior of the FSS superstrate, which enhances electromagnetic field confinement and redirects the radiated energy toward the broadside direction. In addition, the optimized 7 mm separation distance enables constructive electromagnetic interference between the radiated and reflected waves, thereby improving radiation directivity and forward gain performance.

4.5.3 Radiation Efficiency

Figure 4.17a illustrates the simulated radiation efficiency of the proposed MIMO antenna with and without the FSS superstrate.

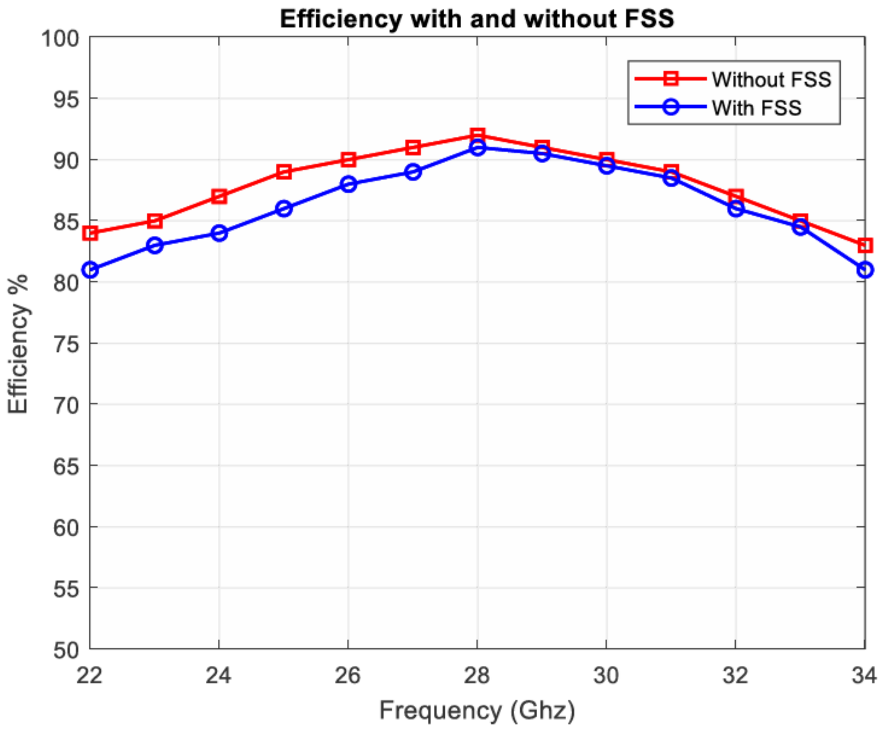

Figure 4.16: *Efficiency of the Proposed MIMO Antenna with and without FSS*

The obtained results indicate that the antenna maintains high radiation efficiency for both configurations. Without the FSS layer, the antenna achieves a maximum efficiency of approximately 92%, while the efficiency remains close to 91% after integrating the FSS structure.

Although a slight efficiency reduction is observed due to additional electromagnetic interactions and dielectric losses introduced by the FSS superstrate, the efficiency degradation remains limited compared with the significant gain enhancement achieved by the proposed configuration.

Overall, the obtained results confirm that the proposed FSS-integrated MIMO antenna achieves an effective balance between high gain, radiation efficiency, and compactness, making it suitable for 5G millimeter-wave communication applications

4.5.4 Radiation pattern

The radiation patterns of the proposed MIMO antenna were analyzed in the YOZ and XOZ planes at the target 28 GHz operating frequency. Figures 4.17a and 4.17b present the simulated co-polarization and cross-polarization radiation patterns evaluated at $\phi = 0^\circ$ and

$\phi = 90°$, corresponding to the XOZ and YOZ planes, respectively.

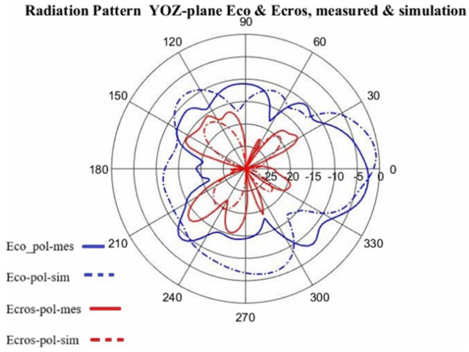

(a) *Radiation pattern in the YOZ plane at 28 GHz.*

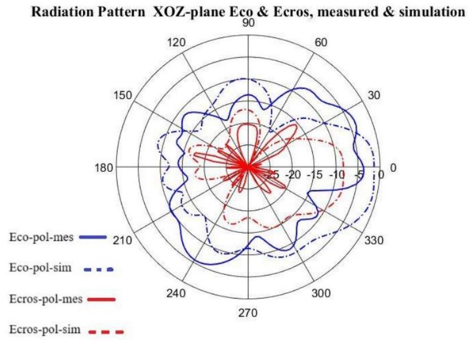

(b) *Radiation pattern in the XOZ plane at 28 GHz*

Figure 4.17: *Radiation patterns in the YOZ and XOZ planes at 28 GHz.*

The obtained results demonstrate that the proposed antenna exhibits stable broadside radiation characteristics in both principal planes around the target 28 GHz GHz operating frequency. As observed in Fig.4.17a, the co-polarization component in the YOZ plane reaches a maximum realized gain of approximately 8.4 dBi, while the cross-polarization level remains below −10 dB, confirming good polarization purity and stable directional radiation behavior. Similarly, Fig. 4.17b shows that the antenna maintains stable radiation characteristics in the XOZ plane, with dominant co-polarization and reduced cross-polarization levels for both $\phi = 0°$ and $\phi = 90°$. The absence of significant pattern distortion confirms the electromagnetic stability of the proposed MIMO-FSS configuration. The stable broadside radiation behavior is mainly attributed to the symmetrical arrangement of the antenna elements, the optimized current distribution, and the constructive electromagnetic interaction introduced by the FSS superstrate, which enhances forward radiation directivity and pattern stability. Overall, the obtained radiation patterns confirm the suitability of the proposed MIMO-FSS antenna configuration for directional 5G millimeter-wave communication applications.

4.5.5 Surface Current

The electromagnetic surface-current behavior of the proposed MIMO antenna was investigated at the target 28 GHz operating frequency in order to analyze the current propagation mechanisms and evaluate the effectiveness of the Mutual Coupling Reduction (MCR) structure.

The obtained results reveal that the surface currents are mainly concentrated around the feed lines and radiating patch edges, where strong electromagnetic excitation occurs. As illustrated in Fig. 4.18(a) and Fig. 4.18(d), Ports 1 and 4 exhibit the highest current densities, reaching approximately 231.79 A/m, respectively, indicating efficient electromagnetic energy transfer between the feeding structure and the radiating elements.

Similarly, Fig. 4.18(b) and Fig. 4.18(c) show that Ports 2 and 3 exhibit maximum current densities of approximately 164.09 A/m, respectively. The more uniform current distribution observed in these ports indicates reduced inter-element current propagation and improved electromagnetic isolation.

Furthermore, the reduced current concentration observed in the central coupling region confirms the effectiveness of the proposed MCR structure in suppressing undesired surface-current coupling mechanisms between adjacent antenna elements. This behavior is consistent with the transmission coefficients below −25 Db obtained in the S-parameter analysis.

In addition, the improved electromagnetic current confinement introduced by the FSS superstrate contributes to enhancing radiation efficiency and supports the achieved gain enhancement of approximately 3.6 dBi.

Overall, the obtained surface-current distributions confirm the effectiveness of the proposed MCR and FSS-integrated configuration in improving isolation performance and enhancing the electromagnetic radiation characteristics of the proposed 28 GHz mmWave MIMO antenna system

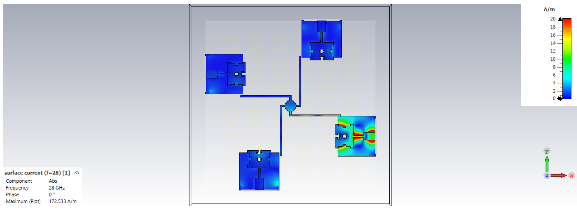

(a) *Port 1 (Max: 231.79 A/m)*

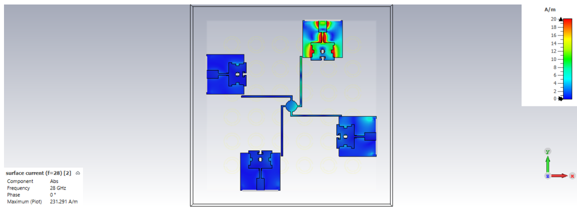

(b) *Port 2 (Max: 164.09 A/m)*

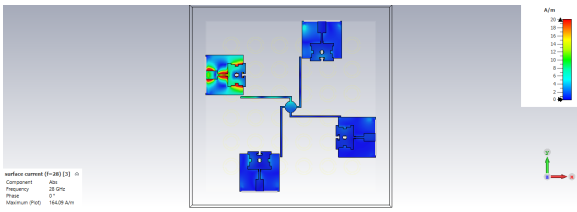

(c) *Port 3 (Max: 199.13 A/m)*

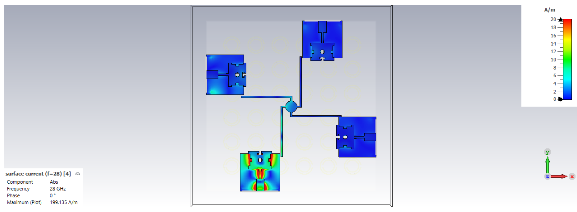

(d) *Port 4 (Max: 231.91 A/m)*

Figure 4.18: *Surface Current Distribution at 28 GHz for the Four Ports of the Proposed MIMO Antenna*

4.5.6 Envelope Correlation Coefficient (ECC)

The Envelope Correlation Coefficient (ECC) is an important performance parameter used to evaluate the diversity capability and mutual correlation between antenna elements in MIMO systems. Low ECC values are required to ensure independent antenna operation, improved spatial diversity, and enhanced channel capacity.

The ECC can be evaluated using either the radiation patterns or the scattering parameters of the antenna system. In this work, the ECC was calculated using the simulated S-parameters, which provide an accurate estimation of the correlation performance in rich isotropic scattering environments. The ECC is expressed as follows: [82]:

$$ECC = \frac{\left|S_{ii}^{*}S_{ij} + S_{ji}^{*}S_{jj}\right|^{2}}{\left(1 - |S_{ii}|^{2} - |S_{ji}|^{2}\right)\left(1 - |S_{jj}|^{2} - |S_{ij}|^{2}\right)} \tag{4.11}$$

where $S_i i$ and $S_j j$ represent the reflection coefficients, while Sij and Sji denote the transmission coefficients between antenna ports.

The obtained results indicate that the ECC remains below 0.04 throughout the operating frequency range, which is significantly lower than the conventional limit of 0.5 required for acceptable MIMO performance. The very low ECC values confirm that the proposed antenna elements operate with minimal correlation despite the compact inter-element spacing.

This low correlation behavior is mainly attributed to the orthogonal arrangement of the antenna elements and the effectiveness of the proposed Mutual Coupling Reduction (MCR) structure in suppressing electromagnetic coupling between adjacent ports. Furthermore, the high isolation performance below −25 dB obtained in the S-parameter analysis contributes directly to reducing the envelope correlation between the radiating elements.

Overall, the obtained ECC results validate the suitability of the proposed MIMO-FSS antenna configuration for compact high-isolation and low-correlation 5G millimeter-wave MIMO applications.

4.6 Fabrication and Measurement

To experimentally validate the electromagnetic performance and practical feasibility of the developed MIMO antenna system, a prototype of the proposed antenna integrated with the Frequency Selective Surface (FSS) was fabricated and experimentally characterized.The fabricated prototype was implemented using a Rogers RT/duroid 5880 substrate with a relative permittivity of $\epsilon_r = 2.2$ and a substrate thickness of 0.51 mm, according to the optimized geometrical dimensions obtained from CST Microwave Studio simulations. The experimental validation was conducted around the target 28 GHz operating frequency in order to verify the impedance-matching characteristics, isolation performance, and overall electromagnetic stability of the developed MIMO-FSS antenna system.

The experimental validation phase is particularly important for millimeter-wave antenna structures because fabrication tolerances, connector discontinuities, and dielectric losses may significantly influence the electromagnetic behavior at high frequencies.

4.6.1 Prototype Fabrication

The fabricated prototype of the proposed MIMO antenna is presented in Figs.4.19a and 4.19b in order to experimentally verify the practical feasibility and manufacturability of the developed antenna structure at millimeter-wave frequencies.

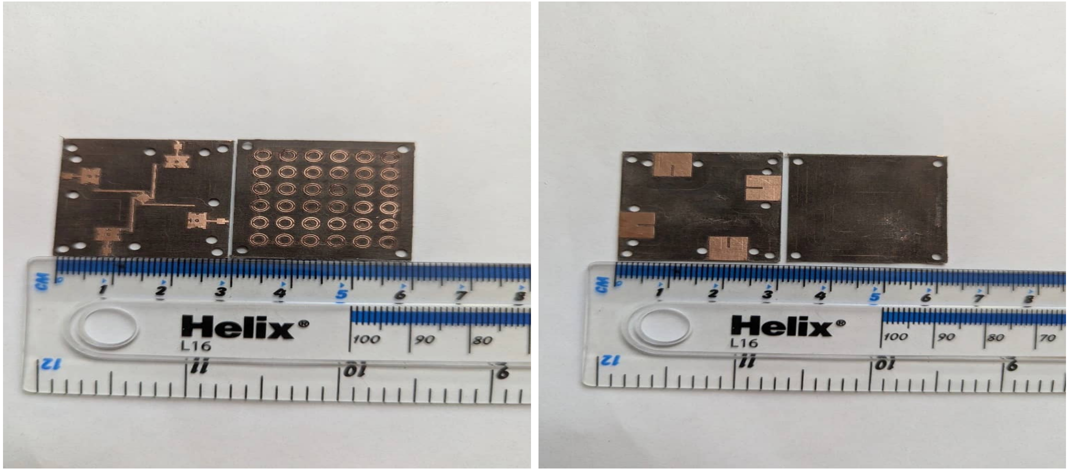

(a) (b)

Figure 4.19: *Fabricated prototype of the Proposed MIMO Antenna(a) Front view (b) back view.*

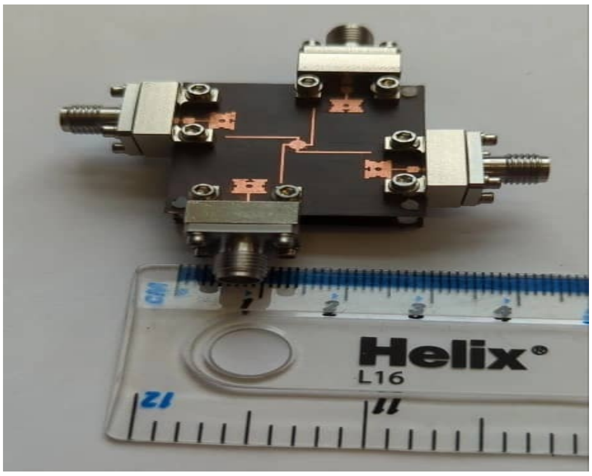

Figure 4.20: *Fabricated Four-Port MIMO Antenna Prototype*

As observed in Fig. 4.19a, the fabricated structure preserves the optimized compact dimensions of approximately $32.5{\times}32.5{\times}0.51\ mm3$, confirming the suitability of the developed configuration for compact 5G millimeter-wave applications. The front structure clearly shows the four radiating elements together with the integrated Mutual Coupling Reduction (MCR) structure positioned in the central region of the antenna array.

Furthermore, the fabricated FSS structure exhibits good geometrical uniformity and dimensional precision, which are essential for maintaining stable electromagnetic resonance behavior near 28 GHz. Figure 4.19b illustrates the backside metallization of the fabricated structure, confirming the accurate implementation of the ground-plane configuration required for stable electromagnetic operation. In addition, Fig. 4.20 presents the fully assembled antenna prototype integrated with high-frequency SMA connectors. The feeding connectors were carefully mounted to minimize parasitic discontinuities and impedance mismatch effects between the measurement ports and the antenna feed lines. Overall, the fabricated prototype confirms the practical manufacturability and feasibility of the proposed MIMO-FSS antenna system for compact 5G millimeter-wave communication applications.

4.6.2 Measurement Setup

The experimental measurement setup was established to validate the simulated electromagnetic performance of the developed MIMO-FSS antenna system under practical operating conditions at 28 GHz. The antenna measurements were performed using a Rohde and Schwarz ZVA24 Vector Network Analyzer (VNA) operating over the frequency range from 10 MHz to 40 GHz. The VNA was employed to measure the reflection and transmission coefficients of the fabricated antenna prototype with high measurement accuracy at millimeter-wave frequencies

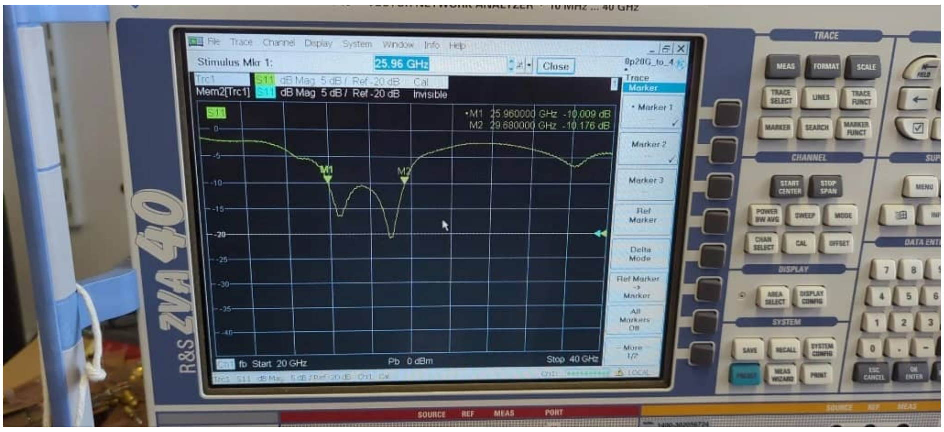

Figure 4.21: *graphic representation of S11*

As illustrated in Fig. 4.21, the fabricated antenna prototype was connected through high-frequency SMA connectors to experimentally evaluate the scattering parameters. The measured S11 response confirms stable resonance behavior near the target operating frequency.

4.6.3 Measured Reflection and Transmission Coefficients

The experimental scattering-parameter results of the fabricated MIMO antenna prototype are presented in Figs. 4.22a in order to validate the impedance-matching and isolation performance of the developped antenna system under practical operating conditions.

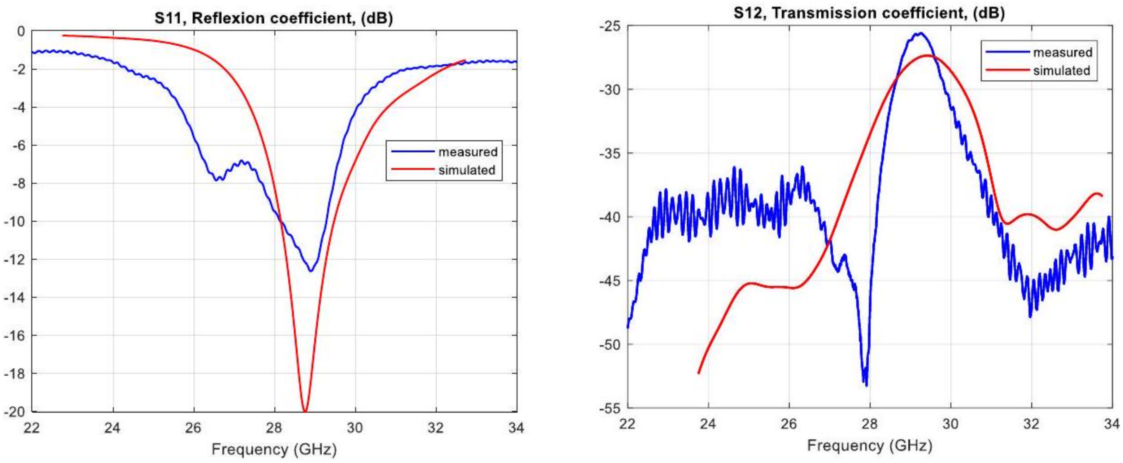

(a) *Simulated and Measured Reflection Coefficient (S11) of port 1*

(b) *Simulated and Measured Transmission Coefficient (S12) from port 1 to port 2.*

Figure 4.22: *Simulated and Measured Transmission Coefficient and Reflection Coefficient*

As observed in Fig. 4.22a, the fabricated antenna resonates near the target 28 GHz operating frequency with a measured impedance bandwidth of approximately 1.32 GHz, where the reflection coefficient remains below the conventional −10 dB criterion. In addition, Fig.4.22b shows that the measured transmission coefficient S12 remains close to −25 dB, confirming effective suppression of electromagnetic coupling between adjacent antenna elements.

The measured and simulated responses exhibit good overall agreement, while the slight discrepancies are mainly attributed to fabrication tolerances, SMA connector soldering imperfections, dielectric losses, and parasitic discontinuities introduced during the fabrication and assembly processes at millimeter-wave frequencies.

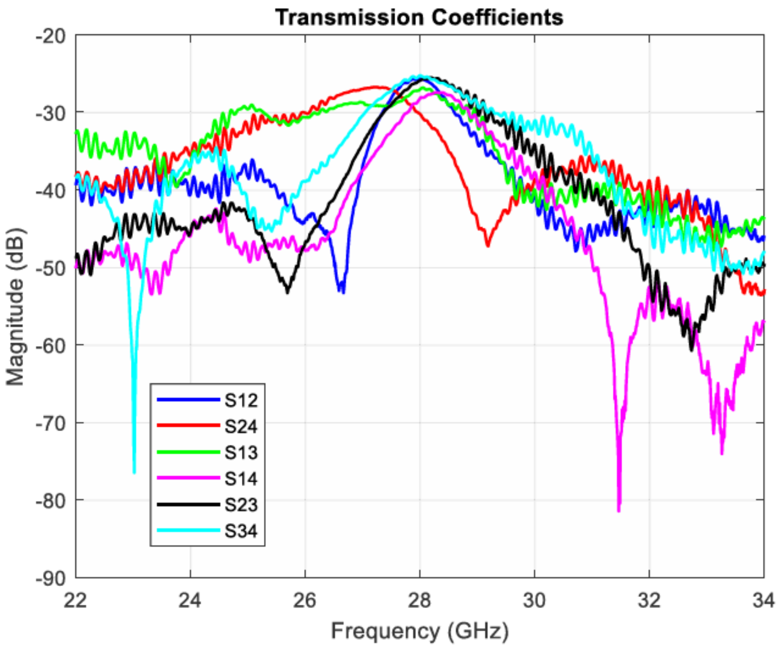

Figure 4.23: *Measured transmission coefficients*

The measured transmission coefficients presented in Fig.4.23 further confirm the high-isolation performance of the fabricated antenna prototype. The coupling coefficients S12, S23, and S34 remain below approximately −25 dB, whereas the cross-coupling coefficients S13, S14 , and S24 exhibit isolation levels better than −27 dB Overall, the measured results experimentally validate the effectiveness of the proposed Mutual Coupling Reduction (MCR) structure and confirm the practical feasibility of the developed MIMO-FSS antenna system for compact 28 GHz 5G millimeter-wave communication applications.

4.7 Discussion

This chapter presented the comprehensive development, optimization, and experimental validation of a four-port MIMO antenna operating at 28 GHz. The proposed design distinguishes itself by synergistically integrating a Frequency Selective Surface (FSS) alongside Mutual Coupling Reduction (MCR) techniques to satisfy the stringent requirements of 5G millimeter-wave (mmWave) communication systems. The key findings and discussions drawn from this contribution are detailed below:

4.7.1 Gain Enhancement Using the FSS Superstrate

The integration of the FSS superstrate proved to be highly effective in compensating for the severe free-space path loss typically encountered at millimeter-wave frequencies.

Without the FSS, the antenna achieved a maximum realized gain of approximately 4.8 dBi at 28 GHz. By positioning the FSS layer at the optimized distance of 7 mm above the antenna array, the gain increased to approximately 8.4 dBi, resulting in a gain enhancement of nearly 3.6 dBi.

The achieved gain improvement is mainly attributed to the partially reflective behavior of the FSS structure, which reinforces the forward-radiated electromagnetic fields and improves radiation directivity through constructive electromagnetic interference. Furthermore, the optimized 7 mm separation distance provides efficient electromagnetic coupling between the antenna array and the FSS superstrate while maintaining stable radiation characteristics and high radiation efficiency reaching approximately 91% These results confirm the effectiveness of the developed MIMO-FSS configuration for improving radiation performance in compact 5G millimeter-wave antenna systems.

4.7.2 Isolation Enhancement and mutual coupling Reduction

Achieving high isolation in compact multiport MIMO antennas represents a major electromagnetic challenge, particularly at millimeter-wave frequencies where strong near-field interactions may degrade the overall antenna performance. The obtained results confirm that the proposed MCR structure effectively suppresses undesired surface-current propagation and near-field electromagnetic coupling between adjacent antenna elements.

The surface-current distributions analyzed at 28 GHz demonstrated significant current suppression in the central coupling region, confirming the effectiveness of the developed MCR mechanism. Experimentally, the measured transmission coefficients S12, S23and S34 remained below approximately −25 dB, while the cross-coupling coefficients S13, S14, and S24 achieved isolation levels better than −27 dB.

The achieved high-isolation performance ensures stable independent operation of the antenna ports and contributes to improving spatial diversity and overall MIMO system performance.

4.7.3 Impedance Matching and MIMO Diversity Performance

The The fabricated antenna prototype resonated successfully around the target 28 GHz operating frequency with a measured impedance bandwidth of approximately 1.32 GHz, where all reflection coefficients remained below the conventional −10 dBimpedance-matching criterion. The stable impedance-matching performance is mainly attributed to the optimized antenna geometry, the orthogonal arrangement of the radiating elements, and the constructive electromagnetic interaction introduced by the FSS superstrate. In addition, the Envelope Correlation Coefficient (ECC) remained below 0.04, which is significantly lower than the conventional limit of 0.5 required for practical MIMO systems. The very low ECC values confirm efficient diversity performance and low signal correlation between the antenna ports despite the compact inter-element spacing, thereby validating the suitability of the proposed antenna structure for high-performance 5G millimeter-wave MIMO applications.

4.7.4 Reliability of the Experimental Validation

The experimental measurements performed using the Rohde and Schwarz ZVA24 Vector Network Analyzer showed good agreement with the full-wave electromagnetic simulations conducted in CST Microwave Studio. The measured reflection and transmission coefficients confirmed the reliability of the proposed antenna design methodology and validated the electromagnetic performance of the fabricated prototype at 28 GHz Although slight discrepancies were observed between the simulated and measured responses, the overall resonance and isolation behaviors remained consistent. These deviations are mainly attributed to fabrication tolerances, SMA connector soldering imperfections, dielectric losses, and parasitic discontinuities introduced during the fabrication and assembly processes. Overall, the experimental validation confirms the practical feasibility and electromagnetic stability of the developed MIMO-FSS antenna system for compact 5G millimeter-wave communication applications.

4.7.5 Trade-Off Analysis

The integration of the Frequency Selective Surface (FSS) significantly improved the antenna gain from approximately 4.8 dBi to 8.4 dBi at the optimized separation distance of 7 mm, mainly due to constructive electromagnetic interaction and enhanced forward-radiated field confinement. However, the FSS integration introduced additional electromagnetic interactions and dielectric losses, resulting in a slight radiation-efficiency reduction from approximately 92In addition, the proposed MIMO-FSS configuration increases fabrication and alignment complexity at 28 GHz, where small dimensional deviations and connector discontinuities may affect resonance stability and impedance matching. Nevertheless, the developed Mutual Coupling Reduction (MCR) structure maintained high isolation levels below approximately −25 dB and low ECC values below 0.04, confirming stable multiport operation despite the compact inter-element spacing. Overall, the proposed MIMO-FSS antenna system achieves an effective balance between compactness, high gain, high isolation, and stable electromagnetic performance for 28 GHz 5G millimeter-wave applications.

4.7.6 Comparative Analysis with Existing Works

Table 4.2 presents a comparative analysis between the proposed MIMO-FSS antenna system and recently reported millimeter-wave MIMO antennas operating around the 28 GHz band.

The comparison demonstrates that the proposed antenna achieves a favorable balance between bandwidth, gain enhancement, mutual-coupling reduction, and MIMO diversity performance compared with previously published designs.

In terms of bandwidth, the proposed antenna provides a significantly wider impedance bandwidth of approximately 28%, exceeding most reported works, which generally remain below 10%. This improvement confirms the effectiveness of the integrated FSS structure in enhancing the overall electromagnetic performance of the antenna system. The proposed configuration also achieves a realized gain of approximately 8.4 dBi, which remains competitive with existing mmWave MIMO antennas while maintaining compact integration and satisfactory radiation characteristics.

From the mutual-coupling perspective, the developed DGS–FSS configuration provides port-to-port isolation exceeding 25 dB, outperforming several previously reported compact MIMO designs. This strong isolation directly contributes to improved diversity performance and reduced electromagnetic interference between adjacent antenna elements.

The low ECC values obtained for the proposed antenna indicate weak correlation between the radiating elements, which ensures effective spatial diversity and reliable MIMO performance at millimeter-wave frequencies.

In summary, the proposed MIMO-FSS antenna architecture achieves an effective trade-off between compact integration, wide operational bandwidth, gain enhancement, and mutual-coupling suppression, making it a competitive candidate for 28 GHz 5G mmWave communication systems

Ref	Frequency (GHz)	Bandwidth (%)	Gain (dBi)	No. of ports	Dimensions (mm^3)	Isolation	ECC/dec. coeff.	Substrate
[83]	26	9.5	7.65/6.1	4	$11 \times 11 \times 0.32$	> 16	< 0.1285	FR4
[84]	38	7.1	5.27/7	8	$18.2 \times 34 \times 0.8$	> 20	< 0.1758	FR4
[82]	28, 30, 42	8.2	7.83/9	4	$0.97 \times 0.91 \times 0.045$	> 20	< 0.0185	FR4
[85]	32.5–37.5	25.8	7.84/8	2	$2.14 \times 2.14 \times 0.48$	> 31.5	< 0.0875	RT5880
[86]	28	3.1	7.94/9	4	$4.6 \times 6 \times 0.8$	> 16	< 0.0068	Rogers
[87]	36	3.5	7.85/9.7	2	$0.19 \times 0.15 \times 0.018$	> 13	< 0.00425	RO4350B
[88]	31	8	8.28/9	4	$0.22 \times 0.5 \times 0.015$	> 25	< 0.0456	Rogers RT 5880
This work	27.68 to 28.68	28	8.4/9.1	4	$32,5{\times}32,5{\times}0,51$ mm^3	> 25	< 0.04	Rogers RT/duroid 5880

Table 4.2: *Performance Comparison Between the Proposed MIMO-FSS Antenna System and Existing 28 GHz mmWave MIMO Antennas*

4.8 Conclusion

This work presented the design, optimization, fabrication, and experimental validation of a compact four-port MIMO antenna integrated with a Frequency Selective Surface (FSS) and a Mutual Coupling Reduction (MCR) structure for 28 GHz 5G millimeter-wave applications. The obtained results demonstrated that the integration of the FSS superstrate and the MCR structure significantly improves the electromagnetic performance of the antenna system in terms of gain enhancement, impedance matching, isolation performance, and MIMO diversity characteristics. The developed antenna achieved a realized gain improvement from approximately 4.8 dBi to 8.4 dBi after integrating the FSS layer at an optimized distance of 7 mm, resulting in a gain enhancement of approximately 3.6 dBi. In addition, the antenna maintained high radiation efficiency reaching approximately 91% Furthermore, the measured transmission coefficients remained below approximately −25 dB, while the Envelope Correlation Coefficient (ECC) remained below 0.04, confirming excellent isolation performance and efficient MIMO diversity behavior despite the compact antenna dimensions. The measured and simulated results exhibited good overall agreement, experimentally validating the reliability of the proposed antenna design methodology and confirming the practical feasibility of the developed MIMO-FSS antenna system for compact high-performance 28 GHz 5G millimeter-wave communication applications. Future work may focus on further optimization of the antenna structure, experimental radiation-pattern characterization, and real-world integration within next-generation wireless communication platforms[89–92].

Part III

Contribution 2 — ANN-Based Antenna Design

Chapter 5

ANN-Based Antenna Synthesis and Optimization

5.1 Introduction

Microstrip Patch Antennas (MPAs) have become essential components in modern wireless communication systems owing to their compact size, low-profile structure, lightweight characteristics, and compatibility with planar integrated circuits [20, 93].

These properties make MPAs particularly attractive for portable wireless devices and emerging fifth-generation (5G) and sixth-generation (6G) communication systems.

With the rapid deployment of millimeter-wave (mmWave) communication technologies, there is an increasing demand for compact antennas capable of supporting high data rates, low latency, and reliable wireless connectivity[6, 44, 94].

In this context, MPAs operating at 28 GHz offer several advantages, including high radiation efficiency, low power consumption, wide bandwidth, and enhanced gain performance[4, 95]. Rogers substrates are widely employed in such applications because of their low dielectric losses and stable electromagnetic behavior at high frequencies [44, 95].Despite these advantages, the design and optimization of mmWave antennas remain highly challenging due to the strong sensitivity of electromagnetic behavior to geometrical and substrate variations at high operating frequencies [96, 97].

Conventional Computational Electromagnetics (CEM) techniques such as the Finite Difference Time Domain (FDTD), Finite Element Method (FEM), and Method of Moments (MoM) generally require repeated full-wave simulations using commercial tools such as CST Microwave Studio, HFSS, and ADS [94]. Although these methods provide accurate electromagnetic analysis, they are computationally expensive and time-consuming during iterative antenna optimization.

To overcome these limitations, Machine Learning (ML) techniques, particularly Artificial Neural Networks (ANNs), have recently emerged as efficient alternatives for antenna synthesis and electromagnetic modeling. ANN-based approaches enable rapid prediction of key antenna parameters such as resonant frequency and geometrical dimensions while significantly reducing the number of required full-wave simulations.

However, purely data-driven ANN models often suffer from limited physical interpretability and reduced generalization capability. To address these limitations, this work adopts a physics-guided AI framework in which analytical Transmission-Line Model (TLM) equations are combined with CST Microwave Studio simulations to improve both computational efficiency and electromagnetic reliability.

The proposed methodology establishes an efficient antenna-design framework for 28 GHz mmWave microstrip patch antennas intended for next-generation 5G wireless communication systems.[98].

5.2 Problem Definition and Modeling

The design of Microstrip Patch Antennas (MPAs) operating at millimeter-wave frequencies, particularly around 28 GHz, represents a highly nonlinear and multi-variable electromagnetic optimization problem. The primary objective is to determine the optimal antenna dimensions capable of achieving resonance at the desired operating frequency while maintaining efficient radiation performance, wide bandwidth, and proper impedance matching for 5G wireless communication systems. At mmWave frequencies, the electromagnetic response of MPAs becomes extremely sensitive to geometrical dimensions, substrate properties, and feeding configurations. Consequently, small dimensional variations may significantly affect the resonant frequency, current distribution, radiation efficiency, and overall impedance behavior of the antenna system.

5.2.1 Analytical Modeling and Its Limitations

The conventional analytical framework widely used for the initial design of rectangular microstrip patch antennas is based on the Transmission-Line Model (TLM)[18]. The TLM provides closed-form equations that relate the antenna dimensions, particularly the patch width (Wp)) and patch length (Lp), to the substrate characteristics, including the relative permittivity (ϵ_r), substrate thickness (h), and the target resonant frequency (f_r). Although the TLM offers a rapid and physically interpretable antenna-design methodology, it relies on simplified quasi-static approximations and ideal electromagnetic assumptions. At millimeter-wave frequencies such as 28 GHz, the antenna dimensions become comparable to the substrate thickness, significantly increasing the influence of fringing-field extensions (ΔL), conductor losses, surface-wave excitation, and electromagnetic dispersion effects.

As a result, purely analytical models are generally unable to accurately capture the complex high-frequency electromagnetic interactions occurring within practical antenna structures, often leading to noticeable resonant-frequency deviations and reduced prediction accuracy under real operating conditions.

5.2.2 The Computational Electromagnetics (CEM) Bottleneck

To compensate for the limitations of analytical models, antenna designers commonly employ full-wave Computational Electromagnetics (CEM) solvers based on numerical techniques such as the Finite Integration Technique (FIT) and Finite Element Method (FEM), implemented in commercial software packages including CST Microwave Studio and HFSS.

Although these full-wave electromagnetic tools provide highly accurate analysis of antenna behavior, they remain computationally intensive, particularly during iterative optimization and parametric-sweep procedures. For 28 GHz 5G antenna applications, repeated full-wave simulations may require several hours or even days depending on mesh density, structural complexity, and optimization constraints [6, 7].

Furthermore, the inverse antenna-design problem remains particularly challenging because different geometrical configurations may produce similar electromagnetic responses, resulting in highly nonlinear relationships between the antenna dimensions and the corresponding performance characteristics.

Consequently, conventional optimization methodologies become computationally expensive, time-consuming, and strongly dependent on designer expertise, thereby limiting their efficiency in rapid antenna-development environments.

5.2.3 Physics-Guided ANN-Based Problem Formulation

To bridge the gap between the computational efficiency of analytical models and the accuracy of full-wave electromagnetic simulations, this work reformulates the antenna-design problem using a physics-guided Artificial Neural Network (ANN) framework. The overall workflow of the proposed physics-guided AI framework is illustrated in fig.5.1

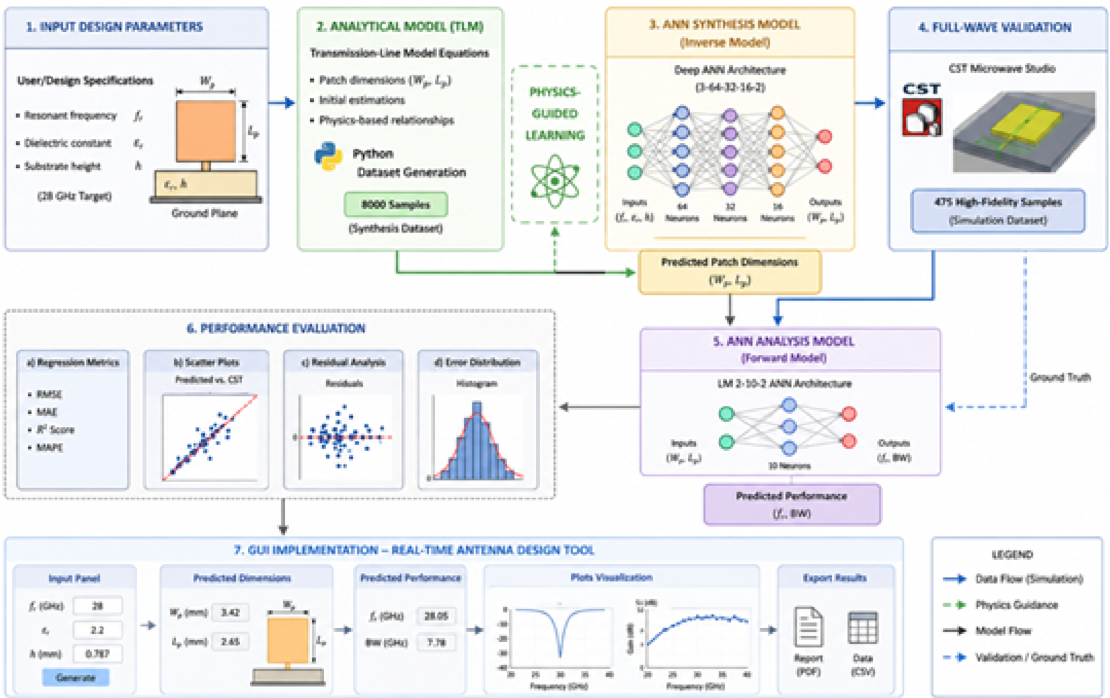

Figure 5.1: *Overall architecture of the proposed physics-guided AI framework for rapid 28 GHz antenna synthesis and electromagnetic prediction.*

As shown in fig.5.1, the proposed framework combines analytical Transmission-Line Model (TLM) equations, ANN-based inverse antenna synthesis, CST full-wave electromagnetic validation, and ANN-based forward electromagnetic prediction within a unified intelligent antenna-design workflow. The framework also integrates statistical performance evaluation and a GUI-based real-time implementation for rapid antenna synthesis and analysis. The proposed methodology decomposes the antenna-design process into two complementary electromagnetic modeling paradigms: •

- **Synthesis (Inverse Modeling):**
  This formulation addresses the inverse antenna-design problem by directly mapping the desired electromagnetic specifications, including the target resonant frequency (fr) and substrate parameters (εr,h), to the required antenna dimensions (Wp,Lp). One of the principal challenges of inverse electromagnetic modeling is the non-uniqueness problem, where multiple antenna geometries may generate similar resonant responses. To mitigate this limitation and improve physical consistency, the proposed synthesis framework incorporates datasets generated from analytical TLM equations, thereby embedding electromagnetic knowledge directly into the neural-network learning process instead of relying on purely black-box modeling.
- **Analysis (Forward Modeling):** This formulation acts as a fast electromagnetic surrogate model for full-wave CEM simulations. The developed ANN predicts the electromagnetic response of the antenna, particularly the reflection coefficient (S11) and operational bandwidth (BW), directly from the antenna geometrical parameters (Wp,Lp).

By combining these dual modeling strategies, the proposed physics-guided AI framework significantly reduces the dependence on conventional trial-and-error optimization procedures while maintaining accurate electromagnetic prediction capability for 28 GHz mmWave microstrip patch antenna design.

5.3 Physics-Guided Dataset Generation and Modeling Methodology

The reliability and robustness of the proposed physics-guided Artificial Neural Network (ANN) framework are fundamentally dependent on the construction of a high-fidelity electromagnetic dataset developed through a hybrid analytical–numerical methodology [99]. To overcome the limitations commonly associated with purely data-driven black-box models, the proposed approach combines analytical Transmission-Line Model (TLM) equations with full-wave electromagnetic simulations, thereby integrating physical knowledge directly into the learning process while maintaining high prediction accuracy [64].

The developed methodology employs two complementary datasets. The first dataset is analytically generated to train the inverse synthesis model, whereas the second dataset is constructed using CST Microwave Studio simulations to train and validate the forward electromagnetic analysis model.

5.3.1 Analytical Dataset Generation for Antenna Synthesis

To train the synthesis-oriented ANN operating as an inverse electromagnetic model, a large analytical dataset was generated using the Transmission-Line Model (TLM) equations implemented in Python [18]. Unlike conventional black-box learning approaches, the proposed framework embeds electromagnetic knowledge directly into the dataset generation process by enforcing the physical relationships between antenna dimensions, substrate properties, and resonant frequency. The generated dataset was constructed using three input parameters:

- Resonant frequency (fr)
- Substrate permittivity (ϵ_r)
- Substrate thickness (h)

The design space was sampled using random uniform distribution to ensure continuous and diverse coverage of the multidimensional antenna-design domain [100].

- Substrate permittivity (ϵ_r): $2.2 \leq \epsilon_r \leq 12.0$
- Substrate thickness (h): 0.5 mm $\leq h \leq 3.0$ mm
- Resonant frequency (f_r): 25 GHz $\leq f_r \leq$ 30 GHz

For each independent parameter combination, the corresponding patch width (Wp) and patch length (Lp) were calculated using the closed-form TLM equations [29]. This automated analytical procedure produced a large-scale dataset containing approximately N=8,000 antenna samples while avoiding the excessive computational cost associated with repeated full-wave electromagnetic simulations. To ensure reliable ANN training and evaluation, the generated dataset was divided into three subsets[29]:

- **Training Set:** 5,000 samples (63%)
- **Validation Set:** 1,500 samples (18.5%)
- **Testing Set:** 1,500 samples (18.5%)

The training dataset was used to optimize the neural-network parameters, whereas the validation dataset was employed for hyperparameter tuning and overfitting mitigation. The testing dataset remained completely isolated to evaluate the final prediction capability of the developed synthesis model.

5.3.2 High-Fidelity Dataset for Analysis and Validation (CST Microwave Studio)

Although the TLM equations provide a fast and physically interpretable antenna-design methodology, they remain based on simplified electromagnetic approximations. At millimeter-wave frequencies, these analytical models cannot fully capture complex electromagnetic effects such as fringing-field extensions (ΔL), surface-wave propagation, conductor losses, and electromagnetic dispersion phenomena.

To improve electromagnetic accuracy and validate the developed ANN framework, a secondary high-fidelity dataset was generated using CST Microwave Studio full-wave simulations. The dataset generation procedure consisted of three main stages:

1. **Parametric Antenna Simulation:**
   A parametric electromagnetic study was conducted in CST Microwave Studio by systematically varying the patch dimensions (Wp, Lp). A total of 475 high-fidelity antenna samples were generated. For each geometrical configuration, full-wave simulations provided the reflection coefficient (S11)) over the frequency range from 22 GHz to 32 GHz.
2. **Python-Based Electromagnetic Feature Extraction:** Following the simulations, a dedicated Python script was developed to automatically process the simulated S11 responses. The resonant frequency (fr) was identified as the frequency corresponding to the minimum S11 value.
3. **Operational Bandwidth Calculation:** The antenna bandwidth (BW) was automatically determined using the conventional −10 dB impedance-matching criterion according to: ($BW = f_U - f_L$). where fU and fL represent the upper and lower cutoff frequencies, respectively.

The generated CST-based dataset plays a critical role in improving the electromagnetic reliability of the proposed framework by enabling accurate prediction of the antenna reflection coefficient and bandwidth characteristics under realistic high-frequency operating conditions. By combining analytical TLM-based modeling with high-fidelity CST simulations, the proposed physics-guided methodology achieves an effective balance between computational efficiency and electromagnetic accuracy for 28 GHz mmWave antenna synthesis and analysis.

5.4 ANN Model Architecture

To implement the proposed physics-guided AI framework and reduce the limitations commonly associated with purely black-box learning approaches, a dual-network strategy was adopted. The developed framework decomposes the electromagnetic antenna-design problem into two complementary neural-network models: a synthesis model dedicated to inverse antenna design and an analysis model acting as a high-speed electromagnetic surrogate for full-wave simulations.

The proposed methodology combines analytical Transmission-Line Model (TLM) equations with high-fidelity CST Microwave Studio datasets in order to improve prediction stability, computational efficiency, and electromagnetic reliability for 28 GHz microstrip patch antenna design.

Unlike conventional purely data-driven ANN approaches, the developed framework integrates electromagnetic knowledge directly into the dataset generation and antenna synthesis process through analytical TLM equations and CST-based full-wave simulations.

5.4.1 Synthesis Model: Deep Learning for Dimensional Prediction

The synthesis model addresses the inverse antenna-design problem by predicting the antenna geometrical dimensions directly from the desired electromagnetic specifications. To capture the highly nonlinear relationships between substrate parameters, operating frequency, and antenna geometry, the model was implemented using the Keras deep-learning framework in Python. After empirical optimization, the most effective architecture was identified as a deep Feedforward Multilayer Perceptron (MLP) composed of:

- **Input Layer:** Three neurons corresponding to the resonant frequency (fr), substrate relative permittivity (ϵ_r), and substrate thickness (h).
- **Hidden Layers:**
  Three fully connected hidden layers containing 64, 32, and 16 neurons, respectively. The Rectified Linear Unit (ReLU) activation function was employed to efficiently model the nonlinear electromagnetic relationships within the antenna-design space. The progressive reduction of neurons from 64 to 16 enables hierarchical nonlinear feature extraction while reducing parameter redundancy and improving model generalization capability.
- **Output Layer:**

Two neurons corresponding to the predicted patch width (Wp) and patch length (Lp), using a linear activation function.

The network parameters were optimized using the Adam optimizer because of its adaptive learning-rate capability and efficient convergence behavior in deep neural architectures. In addition, L2 regularization with a coefficient of 0.01 was incorporated to reduce overfitting and improve model generalization performance. The use of a deep neural architecture is particularly suitable for the synthesis problem because the inverse mapping between the desired electromagnetic specifications and the antenna geometrical parameters presents higher nonlinear complexity than the forward electromagnetic analysis problem.

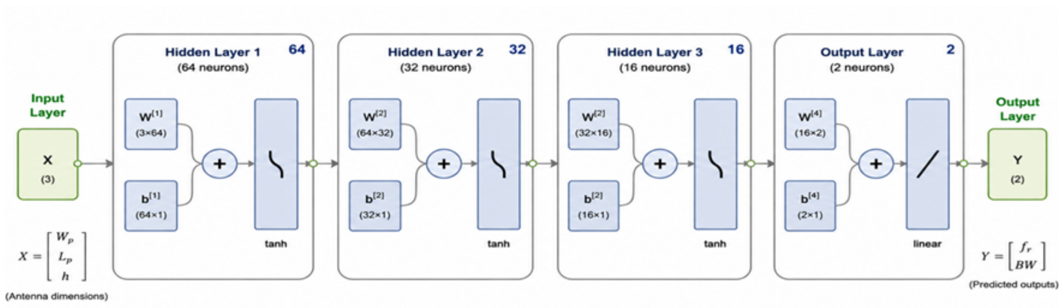

Figure 5.2: *Detailed Architecture of the Proposed Physics-Guided Synthesis ANN Model*

Figure 5.2 illustrates the architecture of the proposed synthesis model, including the three-input configuration, the 64-32-16-2 hidden-layer structure, and the two-dimensional output layer used for antenna-geometry prediction.

5.4.2 Analysis Model: High-Speed Electromagnetic Surrogate

The analysis model was developed to operate as a fast electromagnetic surrogate for full-wave CST simulations. Unlike the deep synthesis model, the analysis network was implemented from scratch using Python and NumPy in order to exploit the fast convergence capability of the Levenberg–Marquardt (LM) optimization algorithm, which is particularly efficient for shallow neural-network architectures. The developed feedforward ANN adopts a (2,10,2) configuration composed of:

– **Input Layer:** Two neurons corresponding to the antenna dimensions (W_p, L_p).
– **Hidden Layer:** One hidden layer containing 10 neurons using the hyperbolic tangent(tanh) activation function, selected to minimize the Mean Squared Error (MSE).
– **Output Layer:** Two neurons corresponding to the predicted resonant frequency (fr)and operational bandwidth (BW), using a linear activation function.

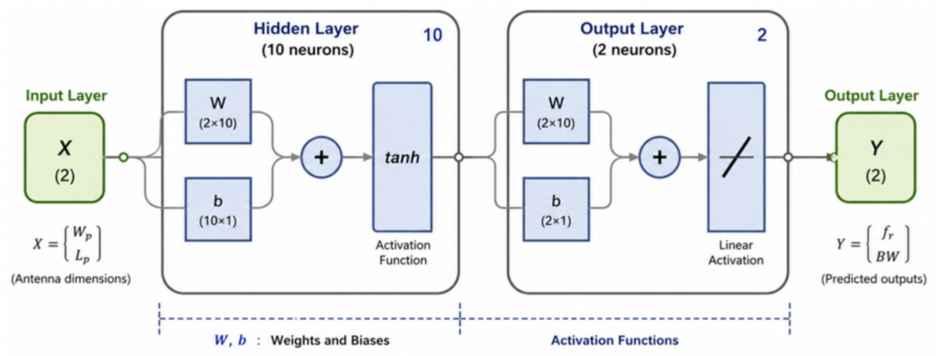

Figure 5.3: *ANN architecture of the proposed forward electromagnetic analysis model*

As illustrated in Fig.5.3, the antenna dimensions (Wp,Lp) are used as physical inputs to predict the corresponding resonant frequency (fr) and −10 dB operational bandwidth (BW). Compared with the inverse synthesis model, the forward electromagnetic analysis problem exhibits lower nonlinear complexity, allowing the use of a shallow ANN architecture with reduced computational cost and rapid convergence capability. The network was trained using a custom mathematical implementation of the Levenberg–Marquardt (LM) algorithm. The CST-generated high-fidelity dataset containing 475 antenna samples was divided into:

- Training set: 333 samples (70%)
- Validation set: 77 samples (15%)
- Testing set: 77 samples (15%)

This partitioning strategy ensured reliable training, robust generalization capability, and accurate evaluation of the developed electromagnetic surrogate model on previously unseen antenna configurations. By combining deep inverse synthesis modeling with fast forward electromagnetic prediction, the proposed physics-guided AI framework establishes an efficient and reliable methodology for 28 GHz mmWave microstrip patch antenna design while significantly reducing the dependence on repeated full-wave electromagnetic simulations.

5.5 Training Strategy and Optimization

To ensure reliable model training and statistically valid performance evaluation, the generated datasets were divided into three independent subsets:

- **Training set**:Used to optimize the neural-network weights and biases (63% for the synthesis model and 70% for the analysis model).
- **Validation set**:Used for hyperparameter tuning, training monitoring, and overfitting mitigation (18.5% for the synthesis model and 15% for the analysis model).
- **Testing set**:Completely isolated during training and exclusively used to evaluate the final prediction capability of the developed ANN models on previously unseen data (18.5% for the synthesis model and 15% for the analysis model).

Prior to training, Min–Max normalization was applied to all input and output variables in order to scale the heterogeneous electromagnetic parameters, including frequencies (GHz) and antenna dimensions (mm), into a normalized numerical range.

This preprocessing stage improves numerical stability during backpropagation, prevents gradient instability, and ensures balanced weight updates throughout the optimization process.[7].

5.5.1 Comparative Optimization Strategy: Adam vs. Levenberg-Marquardt

A major contribution of this methodology is the tailored selection of optimization algo-rithms, highlighting the complementary roles of the Adam optimizer for deep architec-tures and the Levenberg-Marquardt (LM) algorithm for shallow networks in microwave engineering problems.

- **Synthesis Model Optimization Using Adam**: The deep synthesis model with a 3-64-32-16-2 architecture was trained using the Adaptive Moment Estimation (Adam) optimizer. Adam was selected because of its adaptive learning-rate mechanism and stable convergence behavior in deep neural networks. The inverse antenna-synthesis problem exhibits strong nonlinear complexity and multidimensional parameter interactions, making Adam particularly suitable for stable optimization over large-scale datasets containing 8,000 analytical antenna samples. In addition, Adam avoids the excessive computational burden associated with second-order Hessian-matrix approximations, thereby improving computational efficiency during long training procedures extending up to 5,000epochs.
- **Analysis Model Optimization Using Levenberg-Marquardt:**
  Conversely, the shallow analysis network (featuring a 2-10-2 configuration) was trained using the Levenberg-Marquardt (LM) algorithm.
  Because the forward electromagnetic prediction problem exhibits lower nonlinear complexity and a smaller parameter space, the LM algorithm provides extremely rapid second-order convergence and highly accurate Mean Squared Error (MSE) minimization for CST-based electromagnetic surrogate modeling.
  The LM algorithm was therefore particularly suitable for learning the high-fidelity CST dataset containing 475 antenna samples.

5.5.2 Convergence Analysis and Overfitting Mitigation

The training process of both ANN models was performed by minimizing the Mean Squared Error (MSE) cost function, which evaluates the difference between the predicted and target electromagnetic parameters.

$$MSE = \frac{1}{N}\sum_{i=1}^{N}(y_i - \hat{y}_i)^2 \tag{5.1}$$

where y_i represents the target value, $\hat{y}_i$ denotes the predicted ANN output, and N corresponds to the total number of training samples.

One of the principal challenges in electromagnetic machine-learning applications is overfitting, where the neural network memorizes the training data instead of learning the underlying physical relationships governing the antenna behavior.

To mitigate this issue, L2 regularization with a coefficient of $\lambda = 0.01$ was incorporated into the synthesis-model training procedure in order to penalize excessively large synaptic weights and enforce smoother electromagnetic mappings.

During the 5,000-epoch training process, both the training-loss and validation-loss curves exhibited rapid convergence within the early training stages while maintaining stable overlap throughout the optimization procedure.

The absence of significant divergence between the training and validation losses confirms that the developed framework achieved stable generalization capability without severe overfitting behavior.

Furthermore, the stable convergence behavior demonstrates that the proposed physics-guided AI framework successfully learned the electromagnetic relationships derived from the analytical Transmission-Line Model (TLM) equations and CST-generated full-wave datasets rather than merely memorizing the training samples.

By combining physics-guided dataset generation, adaptive optimization strategies, and overfitting mitigation techniques, the proposed methodology establishes a reliable and computationally efficient framework for 28 GHz mmWave microstrip patch antenna synthesis and electromagnetic prediction.

5.6 Results and Electromagnetic Performance Evaluation

5.6.1 Synthesis Results

This section presents the performance evaluation of three machine-learning models — Artificial Neural Network (ANN), Support Vector Regression (SVR), and Random Forest (RF) — developed for the synthesis of rectangular microstrip patch antennas operating at 28 GHz. The objective of the synthesis stage is to accurately predict the antenna geometrical dimensions, namely the patch width (Wp) and patch length (Lp), expressed in millimetres.

The comparative analysis includes convergence behavior, prediction accuracy, residual distribution, and statistical performance metrics in order to identify the most suitable model for electromagnetic antenna synthesis applications

5.6.1.1 ANN Training and Validation Loss

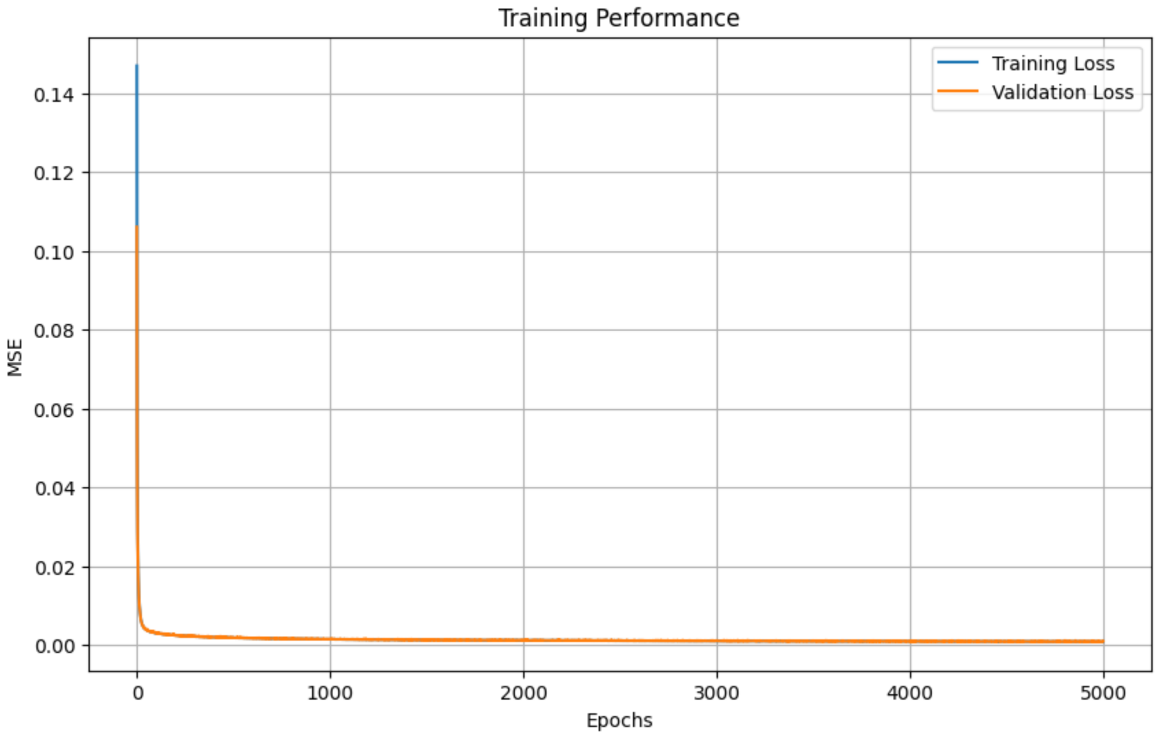

Figure 5.4: *ANN Training and Validation Loss over 5,000Epochs Using the Mean Squared Error (MSE).*

The convergence behavior of the proposed ANN synthesis model was evaluated using the Mean Squared Error (MSE) computed over the training and validation datasets during the 5, ,000-epoch optimization process.

The training loss initially starts at approximately 0.146 and decreases rapidly during the early training stages before converging toward values close to zero. Similarly, the validation loss follows a comparable trajectory while remaining consistently close to the training-loss curve throughout the optimization procedure.

The absence of significant divergence between the two curves confirms that the developed ANN model achieves stable generalization capability without severe overfitting behavior. The final MSE converges to the order of 10−6, demonstrating the high prediction precision of the proposed synthesis model. These convergence characteristics validate the effectiveness of the adopted optimization strategy, including the Adam optimizer, Min–Max normalization, and L2 regularization, in ensuring stable deep-network training for 28 GHz microstrip patch antenna synthesis.

5.6.1.2 Actual vs. Predicted Values

The prediction capability of the developed ANN, SVR, and RF models was evaluated by comparing the predicted antenna dimensions against the corresponding target values for both the patch width (Wp) and patch length (Lp).

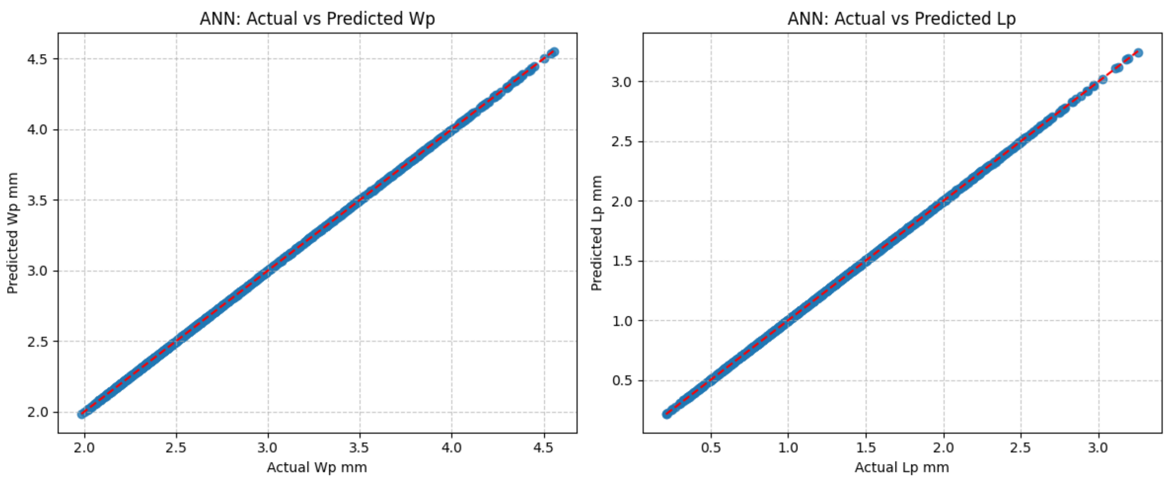

Figure 5.5: *ANN: Actual vs. Predicted W_p (left) and L_p (right)*

The ANN results presented in Fig.5.5 show that nearly all data points are tightly distributed around the ideal diagonal line for both Wp and Lp. This strong correlation confirms that the proposed ANN model accurately captures the nonlinear electromagnetic relationships governing the antenna geometrical dimensions.

The minimal scatter observed around the diagonal further demonstrates the high prediction stability and generalization capability achieved by the deep synthesis ANN model.

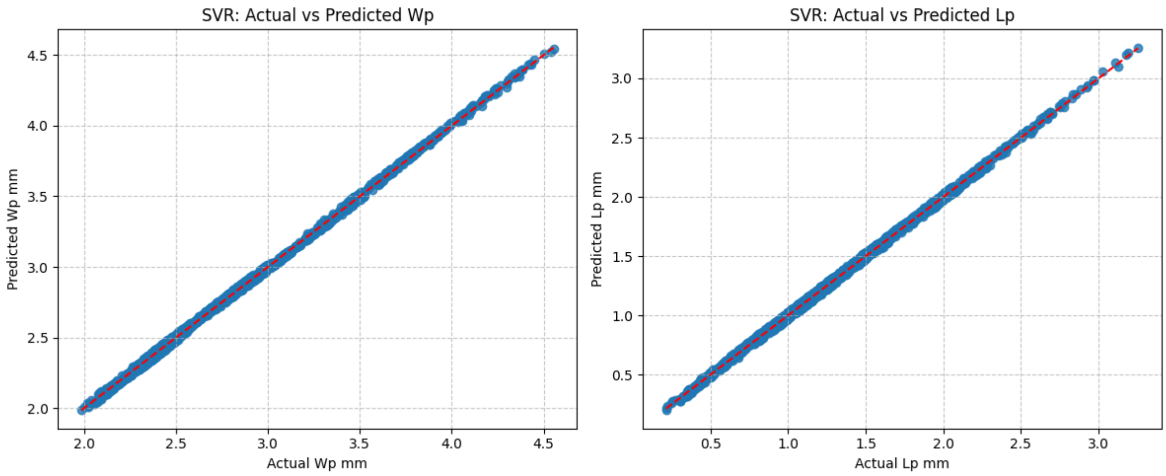

Figure 5.6: *SVR: Actual vs. Predicted W_p (left) and L_p (right).*

The SVR model also exhibits good agreement between the predicted and actual values, particularly for the patch width (Wp). However, a slightly larger dispersion appears for the patch length (Lp), especially near the lower and upper regions of the prediction range. This behavior indicates a moderate reduction in prediction accuracy compared with the ANN model and suggests that the SVR model is less effective in capturing the highly nonlinear inverse electromagnetic relationships associated with the antenna synthesis problem.

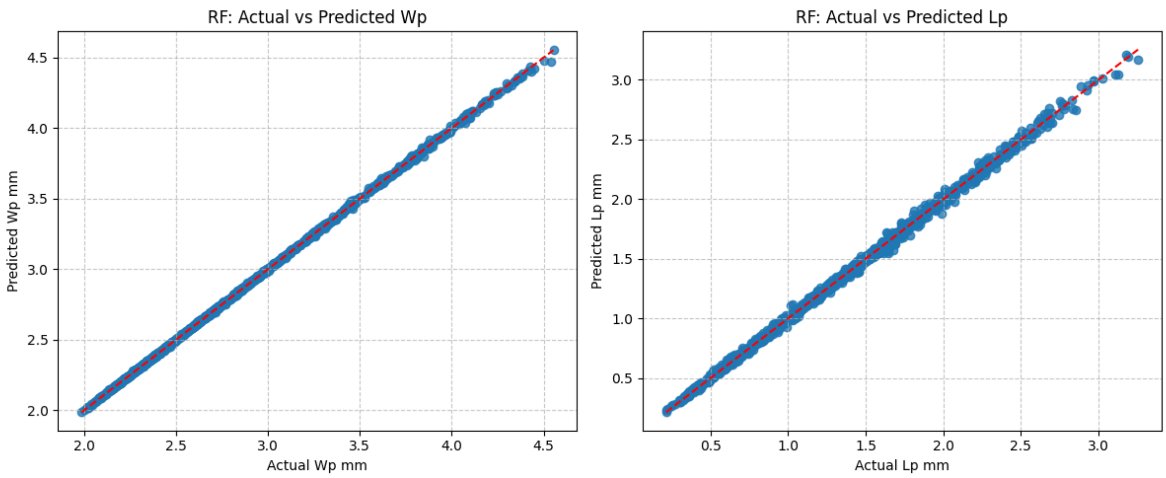

Figure 5.7: *RF: Actual vs. Predicted W_p (left) and L_p (right).*

The RF model exhibits a wider prediction scatter, particularly for the Lp parameter in the intermediate range of values. This behavior is characteristic of ensemble tree-based models, which may introduce discretization effects and reduced smoothness when estimating continuous electromagnetic parameters.

Compared with ANN RF and SVR, the ANN model demonstrates lower prediction consistency, confirming its reduced capability in modeling the continuous nonlinear relationships governing the 28 GHz microstrip patch antenna synthesis process. The superior alignment achieved by the ANN model confirms its stronger capability to capture the continuous non-linear electromagnetic relationships governing the antenna synthesis problem compared with SVR and RF models.

5.6.1.3 ANN Residual Distribution

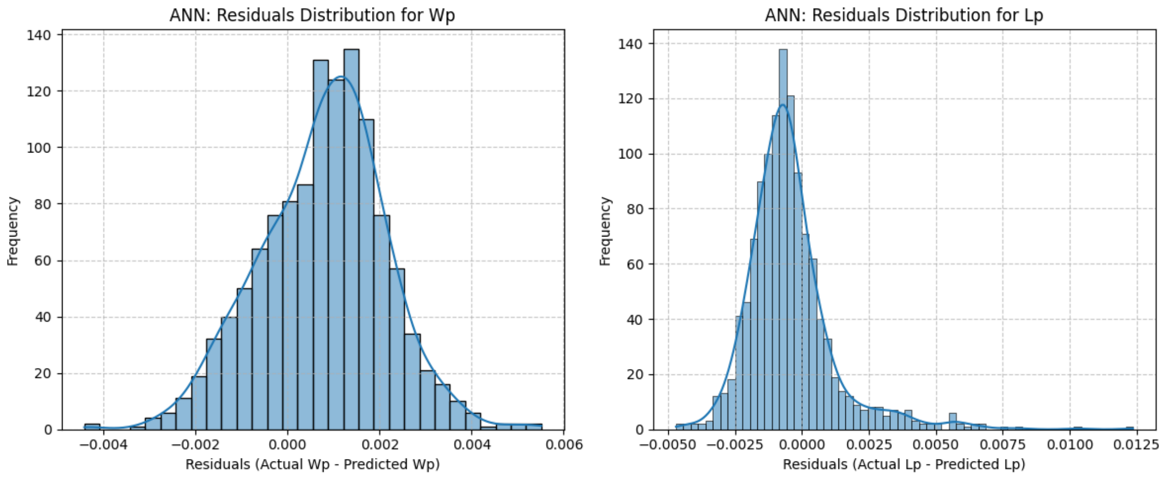

Figure 5.8: *ANN: Residual distributions for W_p (left) and L_p (right).*

The statistical behavior of the ANN prediction errors was analyzed through the residual distributions presented in Fig. 5.8 in order to evaluate the accuracy and robustness of the developed synthesis model. For the patch width (Wp), the residuals exhibit an approximately Gaussian distribution centered near zero, with a slight positive skew corresponding to a mean residual of approximately +0.001 mm. The relatively symmetric distribution and limited dispersion indicate stable prediction performance across the investigated design range.

For the patch length (Lp), the residual distribution is more sharply concentrated around zero, exhibiting a leptokurtic behavior with a slight negative skew and an extended positive tail. Despite this moderate asymmetry, the majority of prediction errors remain strongly confined near zero.

Most residual values remain within a very narrow interval of approximately ±0.003 mm for Wp and ±0.005 mm for Lp, confirming the high precision achieved by the proposed ANN model. These prediction errors remain significantly smaller than the standard PCB fabrication tolerances commonly encountered in millimeter-wave antenna manufacturing processes (±0.1 mm), confirming the practical applicability of the proposed ANN framework for 28 GHz microstrip patch antenna synthesis.

Furthermore, the absence of strong asymmetry, multimodal distributions, or significant dispersion confirms that the developed ANN model maintains stable statistical behavior and reliable electromagnetic prediction capability throughout the investigated antenna-design space. The narrow residual distributions further demonstrate the robustness of the proposed ANN model in preserving the electromagnetic accuracy required for 28 GHz mmWave antenna synthesis applications.

5.6.1.4 Comparative Performance Metrics

A quantitative comparison between the ANN, SVR, and RF models was conducted using the Root Mean Squared Error (RMSE), Mean Absolute Error (MAE), and coefficient of determination (R^2) metrics. The comparative results are presented in Figs. 5.9-5.11.

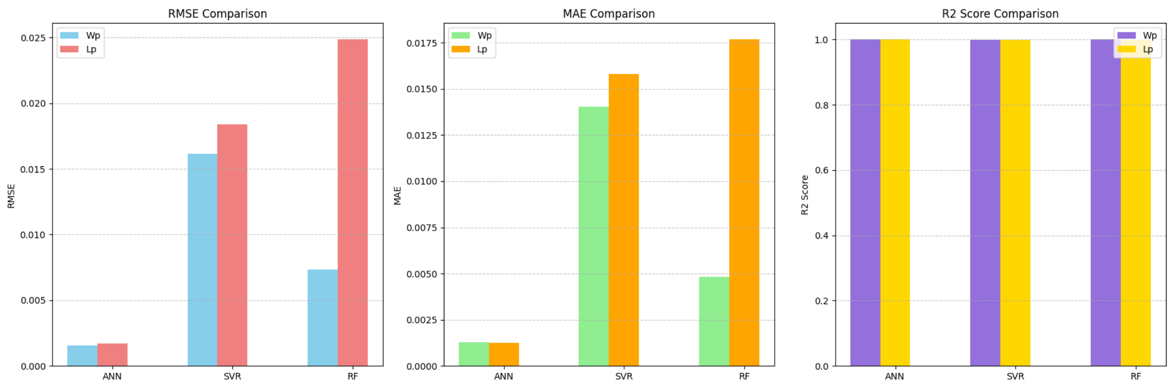

Figure 5.9: *Combined comparison of RMSE, MAE, and R^2 for ANN, SVR, and RF Models*

The ANN model achieves the lowest prediction errors for both antenna dimensions. For the patch width (Wp)), the ANN reaches an RMSE of approximately 0.00156 mm, while the corresponding value for the patch length (Lp) remains close to 0.00169 mm.

Compared with SVR, the ANN reduces the RMSE by nearly one order of magnitude for both outputs. In addition, the RF model exhibits the largest prediction error for Lp, with an RMSE approaching 0.025 mm, indicating reduced prediction stability for this parameter.

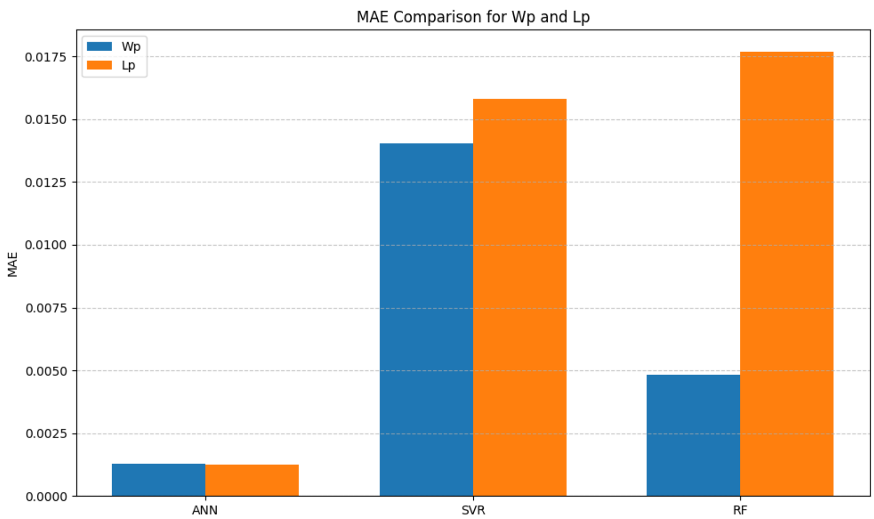

Figure 5.10: *MAE comparison for W_p and L_p across ANN, SVR, and RF.*

The MAE results further confirm the superior prediction capability of the ANN model.

The obtained MAE values remain close to 0.00129 mm for Wp and 0.00124 mm for Lp, demonstrating highly accurate average prediction performance. By contrast, both SVR and RF produce significantly larger MAE values, particularly for Lp, where the prediction errors become more pronounced.

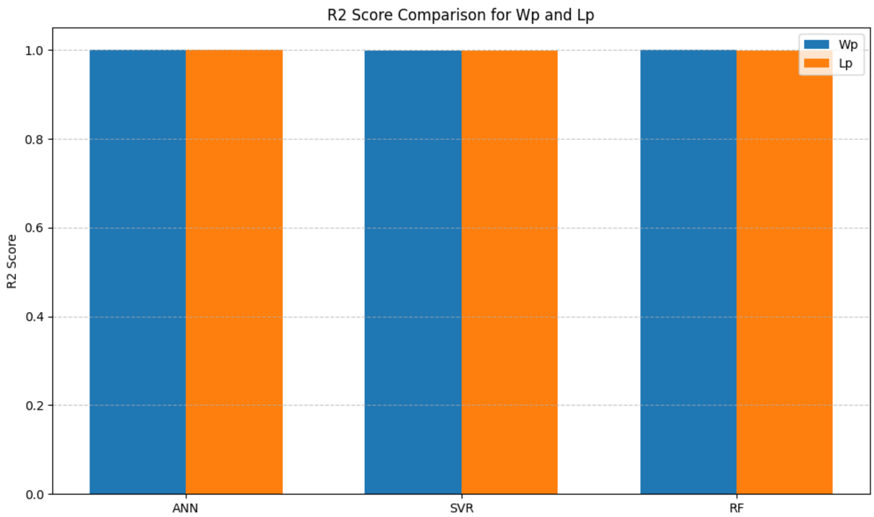

Figure 5.11: *R^2 score comparison for W_p and L_p across ANN, SVR, and RF.*

All three machine-learning models achieve R2 values approaching 1.00 for both antenna dimensions, indicating that the developed models successfully capture most of the variance within the target electromagnetic parameters.

However, because the prediction errors remain extremely small in absolute magnitude, the R2 metric alone becomes insufficient to clearly discriminate between the three models. Consequently, the RMSE and MAE metrics provide a more reliable quantitative assessment of prediction accuracy for the antenna synthesis problem.

Overall, the comparative analysis confirms that the ANN model provides the highest prediction precision, the lowest statistical error, and the strongest nonlinear modeling capability among the investigated machine-learning approaches.

Furthermore, the superior performance achieved by the ANN model demonstrates its enhanced capability to accurately learn the continuous electromagnetic relationships governing the 28 GHz microstrip patch antenna synthesis process compared with SVR and RF models.

The final performance metrics of the selected ANN synthesis model are presented in Section 5.6.1.5

5.6.1.5 Selected ANN Model Performance

The comparative evaluation identifies the ANN model as the most accurate and reliable approach for the synthesis of 28 GHz rectangular microstrip patch antenna dimensions.

All RMSE and MAE values are expressed in millimetres. The selected ANN model achieves a mean R^2value of 0.99999, together with a mean RMSE of approximately 0.00156 mm

Performance Metric	(Wp)	(Lp)	Mean Value
RMSE (mm)	0.00156	0.00169	0.001628
MAE (mm)	0.001286	0.001244	0.001265
(R^2) Score	0.99999	0.99999	0.99999

and a mean MAE of approximately 0.001286 mm respectively.

These extremely low prediction errors confirm the high accuracy, practical reliability, and electromagnetic suitability of the proposed ANN-based synthesis methodology for rapid 28 GHz microstrip patch antenna design applications.

5.6.1.6 summary

The obtained results demonstrate that all investigated machine-learning models are capable of accurately predicting the geometrical dimensions (Wp,Lp) of rectangular microstrip patch antennas operating at 28 GHz.

Among the evaluated approaches, the ANN model consistently achieves the highest prediction accuracy, the lowest RMSE and MAE values, and the strongest statistical stability while maintaining R2 values approaching unity.

In addition, the residual distributions remain narrowly centered around zero, and the convergence behavior confirms stable learning without significant overfitting.

Based on these findings, the ANN model is selected as the optimal and most reliable synthesis approach for 28 GHz microstrip patch antenna design applications.

5.6.2 Analysis Results

This section presents the performance evaluation of the developed ANN-based electromagnetic surrogate model with an LM 2-10-2 architecture. The network was trained using the Levenberg–Marquardt optimization algorithm to predict the resonant frequency (fr) and operational bandwidth (BW) of the 28 GHz rectangular microstrip patch antenna.

The evaluation includes convergence analysis, electromagnetic validation on both training and testing datasets, residual-error analysis, and comparative performance assessment against SVR and RF models.

5.6.2.1 Training Convergence — Levenberg–Marquardt Algorithm

The convergence behavior of the proposed ANN surrogate model was evaluated using the normalized Mean Squared Error (MSE) computed for both the training and testing datasets over 200 epochs.

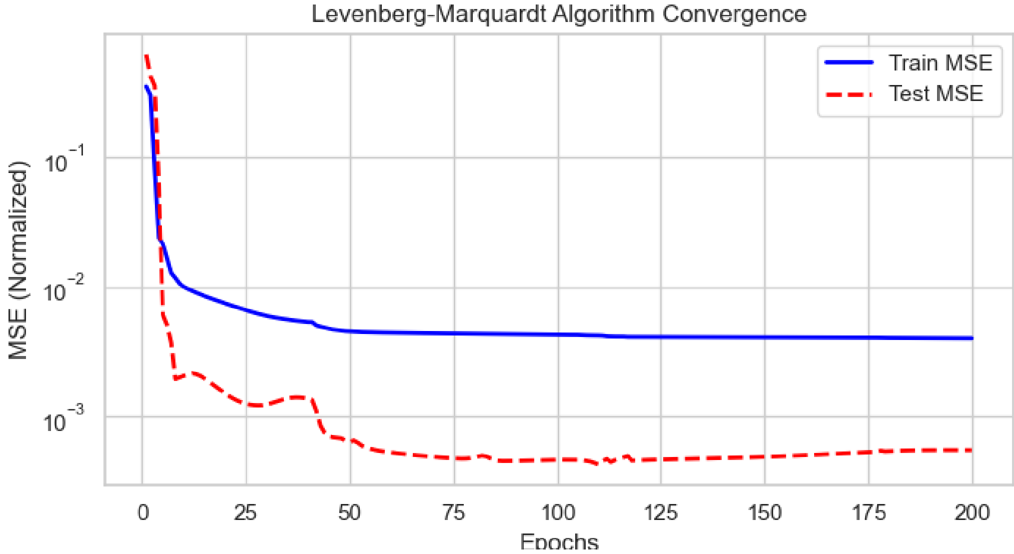

Figure 5.12: *Convergence of the Levenberg–Marquardt algorithm for training and testing MSE over 200 epochs.*

As illustrated in Fig. 5.12, the Levenberg–Marquardt optimization algorithm exhibits rapid initial convergence, where both MSE curves decrease by more than two orders of magnitude during the first 50 epochs. The training MSE progressively stabilizes around 7×10^{-4}, while the testing MSE converges toward a slightly higher plateau close to 3×10^{-3}. The absence of divergence between the training and testing curves confirms that the developed ANN model achieves strong generalization capability without significant overfitting behavior. Furthermore, the fact that the testing error remains consistently above the training error throughout the optimization process demonstrates the robustness and stability of the developed surrogate model when evaluated on previously unseen electromagnetic data. This convergence behavior highlights the effectiveness of the Levenberg–Marquardt algorithm for compact electromagnetic ANN architectures, where the Jacobian-based second-order optimization mechanism enables rapid and stable convergence with reduced computational complexity.

5.6.2.2 Electromagnetic Validation — Training Set

The electromagnetic prediction capability of the developed ANN surrogate model was first evaluated using the CST-generated training dataset.

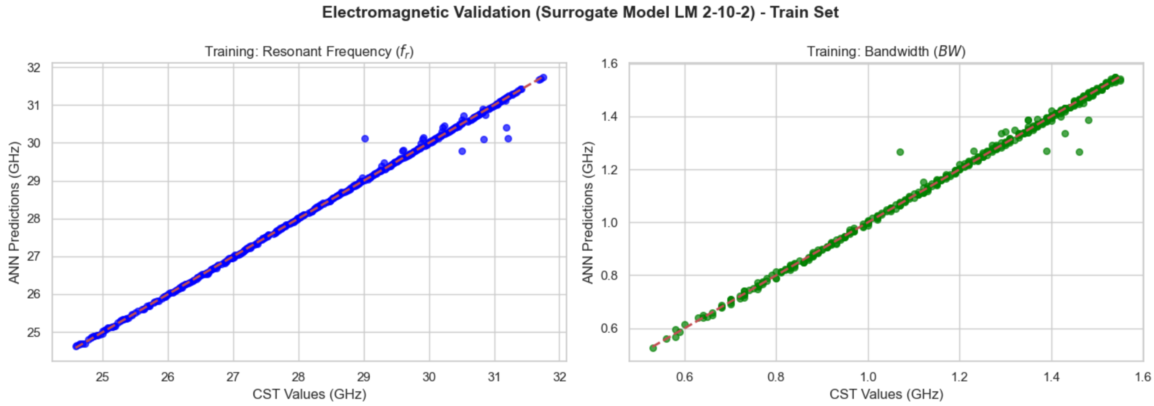

Figure 5.13: *Surrogate model LM 2-10-2: ANN predictions vs. CST-simulated values for fr (left) and BW (right) on the training set.*

As illustrated in Fig. 5.13, the predicted resonant frequency (fr) values remain strongly aligned with the CST reference data across the operating range of approximately 24.7–32 GHz, with only a few isolated deviations near the upper-frequency region. Similarly, the bandwidth (BW) predictions exhibit strong agreement with the CST-simulated results over the range of approximately 0.5–1.55 GHz, where most data points remain tightly concentrated around the ideal diagonal.

These results confirm that the proposed LM 2-10-2 ANN architecture accurately captures the nonlinear electromagnetic relationships between the antenna dimensions (Wp,Lp) and the output parameters (fr,BW) while maintaining stable and reliable prediction performance.

5.6.2.3 Electromagnetic Validation — Test Set

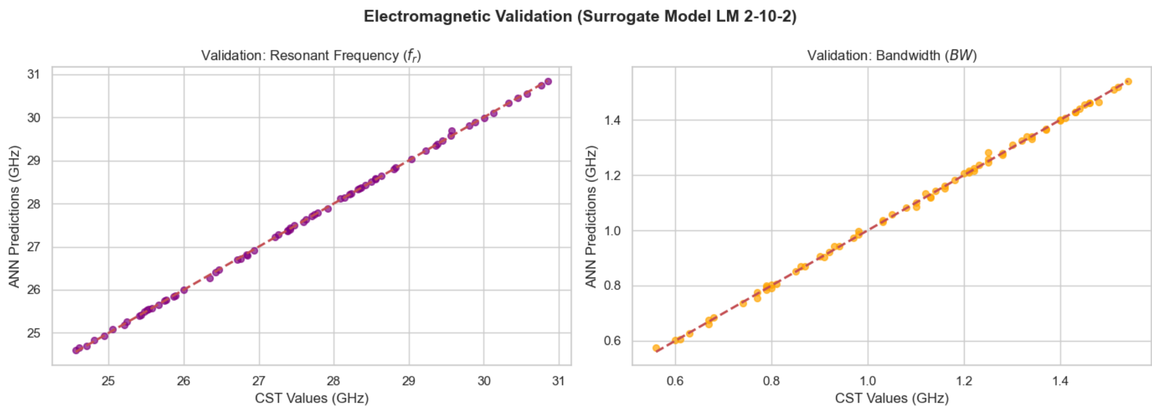

Figure 5.14: *Surrogate model LM 2-10-2: ANN predictions vs. CST-simulated values for fr (left) and BW (right) on the test set*

The generalization capability of the developed ANN surrogate model was evaluated using the independent testing dataset, which was completely excluded from the training process.

As illustrated in Fig.5.14, the predicted resonant frequency (fr) values remain closely aligned with the CST reference data across the operating range of approximately 24.7–31 GHz, with only minimal prediction dispersion.

Similarly, the bandwidth (BW) predictions exhibit strong agreement with the CST-simulated results over the range of approximately 0.6–1.5 GHz, where most data points remain tightly concentrated around the ideal diagonal.

The strong prediction accuracy obtained on previously unseen data — consistent with the low testing MSE observed in Fig. 5.12 — confirms that the developed ANN surrogate model successfully captures the nonlinear electromagnetic mapping without significant underfitting or overfitting behavior.

These results validate the robustness, reliability, and generalization capability of the proposed LM 2-10-2 ANN architecture for rapid electromagnetic prediction and surrogate-based antenna-analysis applications.

5.6.2.4 Residual Analysis

Figures 5.15 and 5.16 provide a detailed residual analysis of the developed ANN surrogate model.

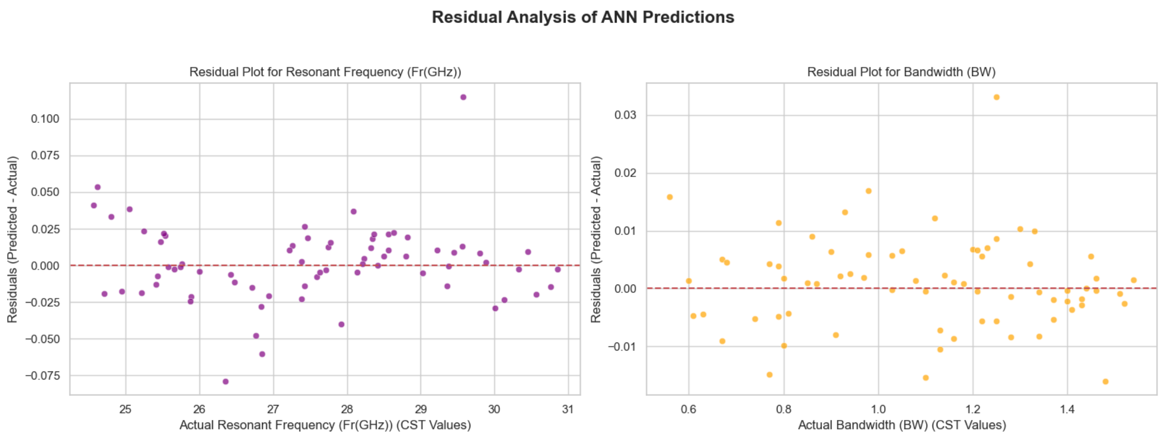

Figure 5.15: *Residual Errors (Predicted Actual) for fr (left) and BW (right)*

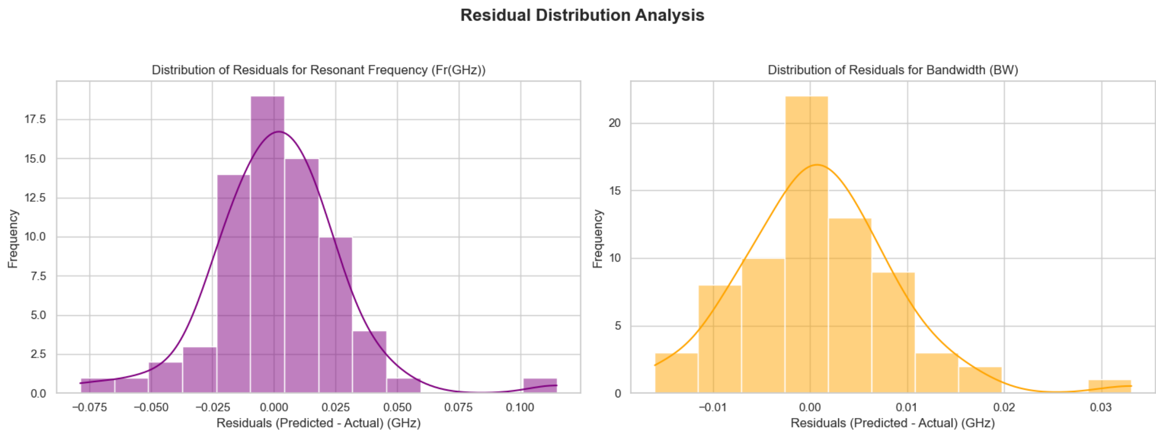

Figure 5.16: *Residual distributions for fr (left) and BW (right).*

As illustrated in Fig. 5.15, the residuals associated with the resonant frequency (fr)remain randomly distributed around zero across the investigated frequency range, with most prediction errors confined within approximately ±0.05 GHz. Only a limited number of isolated outliers reach values between approximately ±0.08 and ±0.11 GHz.

For the bandwidth (BW), the residuals remain more tightly bounded, where the majority of prediction errors stay within approximately ±0.015 GHz, with only a few isolated outliers approaching ±0.03 GHz.

No significant systematic trend or heteroscedastic behavior is observed in either case, confirming the absence of structural prediction bias within the developed ANN model.

As shown in Fig. 5.16, the residual distributions remain approximately centered around zero with near-Gaussian behavior. The fr residuals exhibit a slight positive skew caused by isolated outliers, whereas the BW residuals appear more symmetric and sharply concentrated around zero.

Overall, the majority of residual values remain confined within one standard deviation from zero, confirming the statistical robustness, electromagnetic consistency, and prediction reliability of the proposed ANN surrogate model.

5.6.2.5 Comparative Model Performance

A comparative performance evaluation was conducted between the ANN, SVR, and RF models using the Root Mean Squared Error (RMSE) metric for both the resonant frequency (fr) and operational bandwidth (BW).

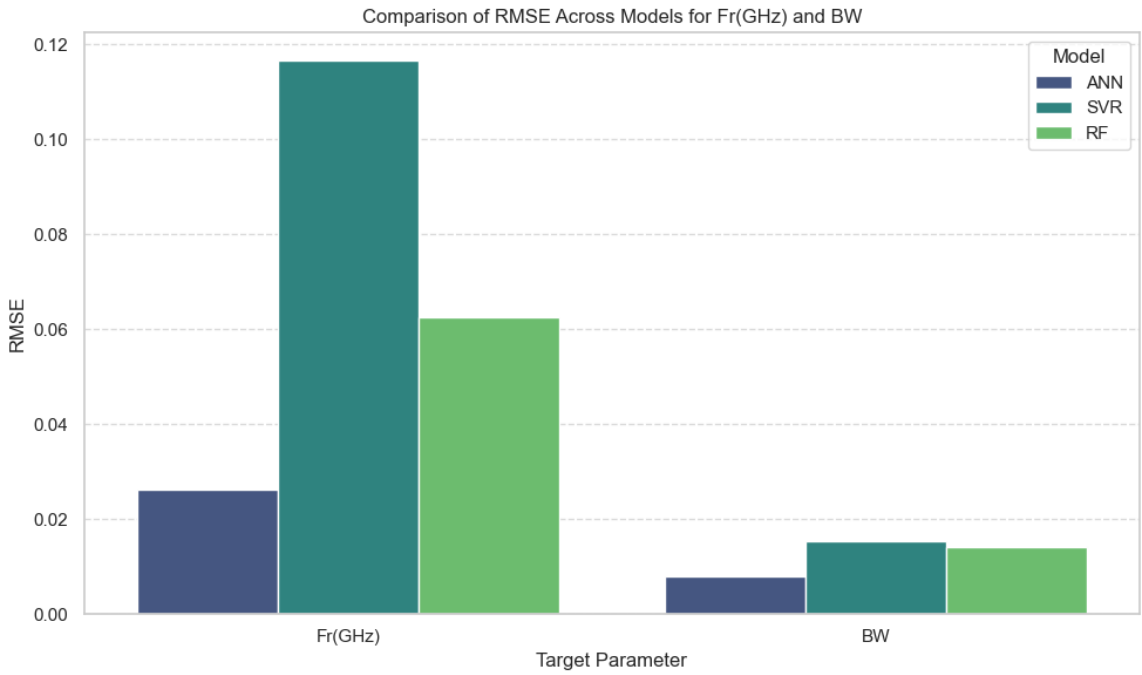

Figure 5.17: *RMSE comparison for ANN, SVR, and RF for fr and BW*

As illustrated in Fig.5.17 and summarized in Table 5.1, the ANN model achieves the lowest prediction errors for both electromagnetic parameters.

Table 5.1: *RMSE comparison for fr and BW across all models.*

Model	RMSE — f_r (GHz)	RMSE — BW (GHz)
ANN	≈ 0.026	≈ 0.008
SVR	≈ 0.116	≈ 0.016
RF	≈ 0.063	≈ 0.015

For the resonant frequency (fr), the ANN model achieves an RMSE of approximately 0.026 GHz, which is nearly 4.5× lower than both the RF and SVR models. The SVR model exhibits the largest prediction error for fr, likely due to the sensitivity of radial-basis-function kernels to nonlinear electromagnetic feature distributions and parameter scaling. For the bandwidth (BW), the ANN model again achieves the lowest RMSE value of approximately 0.008 GHz, which remains nearly half the error obtained using SVR and RF models. Overall, the comparative analysis confirms that the ANN model provides the highest electromagnetic prediction accuracy and the strongest nonlinear modeling capability among the investigated machine-learning approaches.

5.6.2.6 Summary

The obtained results demonstrate that the developed LM 2-10-2 ANN surrogate model can accurately predict both the resonant frequency and operational bandwidth of the 28 GHz rectangular microstrip patch antenna directly from its geometrical dimensions. The Levenberg–Marquardt optimization algorithm achieves rapid and stable convergence without significant overfitting, while the residual analysis confirms strong statistical stability and minimal prediction bias. In addition, the ANN model consistently outperforms SVR and RF approaches across all comparative performance metrics. Overall, the developed ANN surrogate model establishes a reliable, accurate, and computationally efficient alternative to conventional full-wave CST simulations for rapid millimeter-wave antenna analysis and optimization applications. Future work may investigate multi-band antenna synthesis, transfer learning strategies, and physics-constrained neural architectures for more complex mmWave antenna configurations.

5.7 Validation (Comparison with Analytical Models and CST Simulations)

The analytical Transmission-Line Model (TLM) provides an efficient first-order approximation for microstrip patch antenna design and was therefore employed during the dataset-generation stage. However, because the TLM is based on simplified quasi-static assumptions, its prediction accuracy becomes limited at millimeter-wave frequencies, where complex electromagnetic phenomena such as conductor losses, surface-wave propagation, and fringing-field extensions (ΔL) significantly influence antenna behavior [18].

To validate the electromagnetic accuracy and practical reliability of the proposed physics-guided AI framework, the antenna dimensions synthesized by the ANN model were reimplemented and analyzed using CST Microwave Studio, a high-fidelity 3D full-wave electromagnetic simulator based on the Finite Integration Technique (FIT).

A comparative validation was conducted between the ANN predictions and CST full-wave simulation results using several randomly selected antenna configurations. Table 5.2 summarizes the synthesized antenna dimensions together with the corresponding resonant frequency (fr) and −10 dB bandwidth (BW) obtained from both ANN predictions and CST simulations.

. The relative prediction error for the resonant frequency was calculated using:

$$Error(\%) = \frac{|f_{r(CST)} - f_{r(ANN)}|}{f_{r(CST)}} \times 100 \tag{5.2}$$

As presented in Table 5.2, the proposed ANN framework achieves excellent agreement with the CST full-wave simulations. For most antenna configurations, the resonant-frequency pre-

Table 5.2: *Comparison between CST Full-Wave Simulations and ANN Predictions for Resonant Frequency and Bandwidth*

Synthesized Dimensions		**Resonant Frequency (f_r)**			**Bandwidth (BW)**		
W_p **(mm)**	L_p **(mm)**	**CST (GHz)**	**ANN (GHz)**	**Error (%)**	**CST (GHz)**	**ANN (GHz)**	**Error (%)**
3.13	4.18	27.92	28.01	0.34	1.28	1.32	3.36
2.79	2.91	31.21	30.67	1.75	1.46	1.35	7.27
2.83	2.91	30.87	30.60	0.88	1.42	1.36	4.57
2.87	2.91	30.53	30.51	0.08	1.37	1.35	1.54
2.91	2.91	30.24	30.37	0.42	1.32	1.33	0.97
2.95	2.91	29.92	30.16	0.81	1.27	1.30	2.66
2.99	2.91	29.61	29.88	0.90	1.21	1.26	4.09
3.03	2.91	29.31	29.52	0.72	1.15	1.20	4.44
2.91	2.95	31.18	30.40	2.51	1.48	1.37	7.61

diction error remains below 1%, demonstrating strong electromagnetic prediction capability and high model generalization performance.

The minimum prediction error reaches only 0.08%, corresponding to the 30.53 GHz CST configuration predicted at 30.51 GHz by the ANN model. Even under the most challenging validation conditions, the maximum resonant-frequency error remains limited to approximately 2.51% Similarly, the predicted −10 dB bandwidth values remain in close agreement with the CST full-wave results despite the strong nonlinear electromagnetic behavior associated with millimeter-wave microstrip antenna radiation mechanisms.

Overall, this validation study confirms that the proposed ANN-based surrogate framework successfully preserves the electromagnetic fidelity of full-wave CST simulations while significantly reducing computational complexity and prediction time. Consequently, the developed framework provides a reliable, accurate, and computationally efficient alternative for rapid 28 GHz microstrip patch antenna synthesis and electromagnetic analysis applications.

5.8 Implementation: GUI-Based Design Tool

Although the developed ANN framework demonstrates high electromagnetic prediction accuracy, its practical applicability ultimately depends on its accessibility and usability within real antenna-design workflows [12].To facilitate practical deployment, a standalone desktop-based computer-aided design (CAD) application was developed to integrate the trained ANN models into an interactive and user-friendly engineering environment [23].

The developed application enables rapid synthesis and electromagnetic evaluation of 28 GHz rectangular microstrip patch antennas without requiring direct interaction with full-wave electromagnetic simulators or machine-learning programming environments.

5.8.1 Software Development and Integration

The Graphical User Interface (GUI) was developed using the Python Tkinter library. The optimised synthesis model — originally trained using the Keras deep-learning framework — was exported and embedded directly within the application. The asso-ciated data scalers, derived from the Min-Max normalisation preprocessing stage, were also integrated. This ensures that user inputs are correctly normalised before being fed into the network, and that the network outputs are accurately denormalised back into physical dimensions in millimetres [69].

5.8.2 User Interface and Workflow

The developed GUI provides an intuitive design environment in which users interact exclusively with the antenna-design parameters without requiring access to the underlying ANN architecture, optimization algorithms, or Python source code [12].

As illustrated in Fig.5.18, the synthesis interface requires the user to specify the primary design constraints associated with the targeted 5G antenna application, namely:

- Target resonant frequency (f_r)
- Relative permittivity (ε_r)
- Substrate height (h)

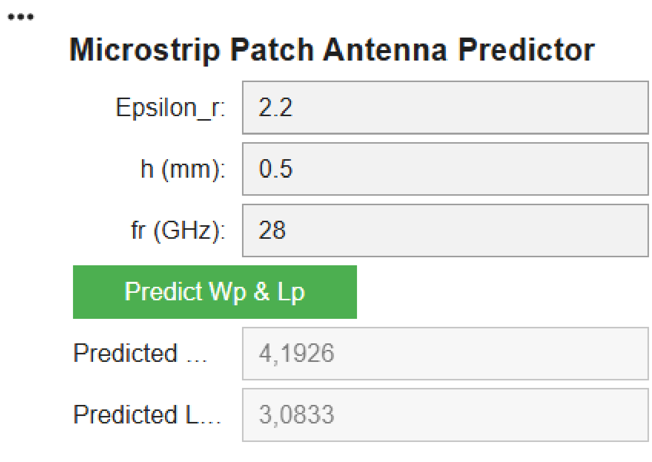

Figure 5.18: *Python-Based GUI for Real-Time Antenna Dimension Prediction*

Once the prediction process is executed, the application automatically performs the following sequential operations:

1. Normalization of the user-defined input parameters using the saved Min–Max scalers.
2. Real-time ANN inference using the trained synthesis network[69].
3. Output denormalization and display of the predicted antenna dimensions (Wp,Lp) in millimetres.

This automated workflow significantly simplifies the antenna-design process while preserving the electromagnetic accuracy of the developed ANN synthesis framework.

5.8.3 Forward Analysis Interface: Real-Time Electromagnetic Prediction

In addition to the synthesis module, the developed GUI integrates the LM 2-10-2 ANN analysis model as a real-time electromagnetic surrogate for rapid antenna-performance evaluation [23]. As illustrated in Fig.5.19, the user can interactively adjust the antenna dimensions (Wp,Lp) using dedicated sliders, after which the application automatically predicts the resonant frequency (fr) and operational bandwidth (BW) in real time [69].

As illustrated in Figure 5.19, the analysis module prompts the user to input the patch dimensions via intuitive sliders:

- Patch width (W_p, in mm)
- Patch length (L_p, in mm)

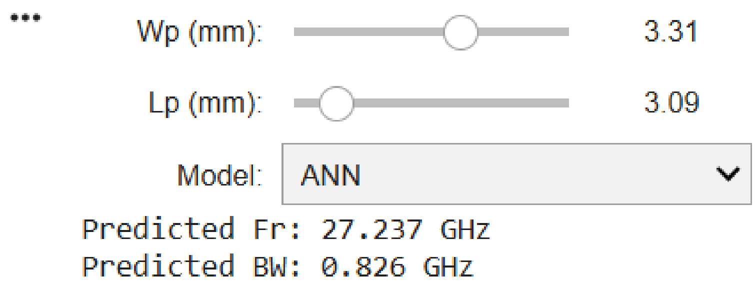

Figure 5.19: *Real-Time Electromagnetic Prediction Interface for Resonant Frequency and Bandwidth Estimation*

A practical validation test using Wp=3.31 mm and Lp=3.09 mm produced a predicted resonant frequency of approximately 27.237 GHz and a bandwidth of approximately 0.826 GHz These results demonstrate the capability of the proposed GUI to provide rapid, reliable, and computationally efficient electromagnetic prediction for real-time 28 GHz microstrip patch antenna design and analysis applications.

5.9 Discussion

The obtained results demonstrate that the proposed ANN framework provides an effective alternative to conventional trial-and-error methodologies commonly used in millimeter-wave antenna design. Beyond the achieved prediction accuracy, the developed framework highlights the potential of machine-learning techniques to significantly accelerate electromagnetic modeling and antenna optimization processes

5.9.1 Accuracy–Efficiency Trade-Off

Conventional full-wave electromagnetic solvers such as CST Microwave Studio and HFSS remain highly accurate but computationally expensive, particularly for iterative optimization problems involving 28 GHz antenna structures [6, 7].

The developed ANN framework substantially reduces this computational complexity by enabling near-instantaneous prediction of the antenna dimensions (Wp,Lp), resonant frequency (fr), and operational bandwidth (BW) after the training stage.

Despite this acceleration, the developed models maintain strong electromagnetic fidelity. Validation against CST full-wave simulations demonstrated resonant-frequency prediction errors below 1% for most investigated antenna configurations, with a minimum error of approximately 0.08%

These results confirm that ANN-based surrogate modeling can successfully combine rapid prediction capability with reliable electromagnetic accuracy for mmWave antenna applications.

5.9.2 Physics-Guided Learning, Practical Implications, and Limitations

Unlike purely data-driven approaches, the proposed framework combines analytical Transmission-Line Model (TLM) equations with CST-generated datasets to improve electromagnetic consistency, prediction stability, and model generalization.

The comparative analysis further demonstrates that the ANN model outperforms SVR and RF approaches because of its stronger capability to learn the continuous nonlinear electromagnetic relationships governing microstrip patch antenna behavior.

The integration of the trained ANN models into a standalone GUI-based application additionally demonstrates the practical applicability of the proposed framework for real-time antenna synthesis and electromagnetic prediction.

Nevertheless, the developed models remain limited to the investigated 28 GHz rectangular microstrip patch antenna configurations and depend strongly on the quality and diversity of the generated datasets. Future work may extend the proposed methodology toward more complex antenna structures, including MIMO systems, phased arrays, reconfigurable antennas, and metamaterial-based designs for next-generation wireless communication systems.

5.10 Conclusion

In This chapter presented a physics-guided AI framework for the rapid synthesis and electromagnetic analysis of 28 GHz rectangular microstrip patch antennas for 5G millimeter-wave applications.

The developed ANN models achieved high prediction accuracy, with dimensional RMSE values of approximately 0.00156 mm for Wp and 0.00169 mm for Lp. Validation against CST full-wave simulations further confirmed strong electromagnetic fidelity, with resonant-frequency prediction errors remaining below 1% for most investigated antenna configurations and reaching a minimum error of approximately 0.08%

In addition to the achieved accuracy, the proposed framework significantly reduced the computational cost associated with conventional full-wave optimization by replacing time-consuming CST simulations with near-instantaneous ANN-based predictions.

The integration of the trained ANN models into a standalone GUI-based application also demonstrated the practical applicability of the proposed framework for real-time antenna synthesis and electromagnetic prediction.

Despite these promising results, the developed models remain limited to the investigated 28 GHz rectangular microstrip patch antenna configurations and depend strongly on the quality of the generated datasets.

Future work may extend the proposed framework toward more complex antenna structures, including MIMO systems, phased arrays, reconfigurable antennas, and metamaterial-based designs, while exploring advanced physics-constrained and multi-objective AI optimization techniques for next-generation wireless communication systems.

Chapter 6

General Conclusion and Future Work

6.1 General Overview

This doctoral thesis presented a rigorous investigation into the design and optimization of advanced antenna systems for fifth-generation (5G) and beyond wireless communication applications. The proposed research combined computational electromagnetics, artificial intelligence (AI), and electromagnetic optimization techniques to address the increasing complexity associated with millimeter-wave antenna engineering.

By integrating full-wave electromagnetic simulations with physics-guided AI modeling approaches, this work demonstrated the capability of AI-assisted methodologies to significantly accelerate antenna synthesis and electromagnetic prediction while preserving high electromagnetic accuracy and reliability.

6.2 Main Contributions of This Thesis

The principal scientific contributions of this thesis are summarized as follows:

1. **High-Isolation 28 GHz MIMO Antenna Design** A compact four-element MIMO antenna operating at 28 GHz was designed, optimized, fabricated, and experimentally validated for 5G millimeter-wave applications. By integrating Defected Ground Structures (DGS) and Frequency Selective Surfaces (FSS), the proposed antenna achieved inter-element isolation exceeding 25 dB across the 24–40 GHz frequency range.
2. **Development of a Physics-Guided AI Framework** A physics-guided AI framework combining analytical Transmission-Line Model (TLM) equations with CST-generated full-wave datasets was developed for rapid antenna synthesis and electromagnetic prediction. This hybrid methodology improved electromagnetic consistency and reduced the limitations commonly associated with purely data-driven black-box models.
3. **Computational Acceleration of Electromagnetic Design** The developed ANN models significantly reduced the computational complexity of antenna optimization by

replacing repetitive full-wave simulation procedures with near-instantaneous ANN-based predictions. The obtained framework achieved resonant-frequency prediction errors below 1% for most investigated configurations, with minimum errors approaching 0.08% while maintaining sub-millimeter dimensional prediction accuracy.

4. **Real-Time GUI-Based Antenna Design Tool** The trained ANN synthesis and analysis models were successfully integrated into a standalone GUI-based application capable of performing real-time antenna synthesis and electromagnetic prediction within an intuitive engineering environment.

6.3 Scientific Impact

The contributions of this thesis extend beyond conventional antenna optimization and provide broader implications for computational electromagnetics and AI-assisted engineering methodologies.

First, this work demonstrates that ANN-based surrogate models trained using physics-guided electromagnetic datasets can accurately learn highly nonlinear antenna behaviors while preserving strong electromagnetic consistency.

Second, the proposed framework illustrates a transition from conventional trial-and-error optimization methodologies toward rapid data-driven and goal-oriented antenna-design strategies.

Third, the substantial reduction in computational complexity enables faster exploration of antenna-design spaces and accelerates the development cycle of advanced millimeter-wave communication systems.

Finally, the implementation of the developed ANN models within a practical GUI-based application highlights the feasibility of deploying AI-assisted electromagnetic prediction tools within real engineering workflows.

6.4 Limitations

Despite the promising results achieved in this research, several limitations remain.

1. The developed ANN models strongly depend on the quality, diversity, and physical consistency of the generated datasets.
2. The proposed framework was specifically trained for rectangular microstrip antenna configurations operating around the 28 GHz band, which may limit prediction capability outside the investigated design space.
3. The proposed FSS and DGS structures remain passive and non-reconfigurable, limiting adaptability under dynamically changing operational conditions.
4. More complex electromagnetic structures may require larger datasets and more advanced learning architectures to ensure stable generalization capability.

These limitations highlight the need for continued investigation into scalable and adaptive AI-assisted electromagnetic-design methodologies.

6.5 Future Research Directions

Several promising research directions may further extend the work presented in this thesis.

1. **Reconfigurable and Tunable Electromagnetic Structures** Future studies may investigate dynamically tunable FSS and DGS structures using graphene, liquid crystals, or varactor-based technologies for adaptive antenna optimization.
2. **Advanced Artificial Intelligence Architectures** The integration of more advanced AI models, including Convolutional Neural Networks (CNNs), deep reinforcement learning, and transfer-learning techniques, may further improve electromagnetic prediction capability while reducing dataset-generation requirements.
3. **Extension Toward 6G and Terahertz Systems** The proposed framework may be extended toward sixth-generation (6G) and Terahertz (THz) antenna systems involving ultra-massive MIMO architectures, metasurfaces, and holographic electromagnetic structures.
4. **Digital Twins and Intelligent Electromagnetic Optimization** Future research may also explore the integration of ANN-assisted electromagnetic prediction within digital twin environments and automated fabrication systems for real-time intelligent antenna optimization and deployment.

6.6 Final Remarks

Overall, this research demonstrates the strong potential of physics-guided artificial intelligence techniques to transform future electromagnetic design methodologies for next-generation wireless communication systems. The obtained results confirm that AI-assisted electromagnetic modeling can simultaneously achieve high prediction accuracy, reduced computational complexity, and practical engineering applicability, thereby establishing a promising foundation for future intelligent antenna-design frameworks.

Appendix A

Python Source Codes for ANN Models

This appendix provides the complete Python implementations for the artificial neural network (ANN) frameworks developed in Chapter 5. The codes rely on standard machine learning libraries, including TensorFlow/Keras and Scikit-Learn, as well as NumPy for custom matrix operations.

A.1 Synthesis Model (PINN) - Deep Learning Architecture

The following script implements the Physics-Informed Neural Network (PINN) utilized for the dimensional synthesis of the 28 GHz microstrip patch antenna. It includes the automated generation of the 8000-sample dataset using analytical Transmission-Line Model (TLM) equations and the deep feedforward Multilayer Perceptron training process over 5000 epochs.

Listing A.1: *Python script for the PINN Synthesis Model.*

```
# ================================================================================
# SYNTHESE D'ANTENNE 28 GHz - RESEAU DE NEURONES
# N_samples = 8000 | Epochs = 5000 (FORCE)
# ================================================================================
import numpy as np
import pandas as pd
import matplotlib.pyplot as plt
import seaborn as sns
import joblib
import warnings
import tensorflow as tf
from tensorflow.keras.models import Sequential
from tensorflow.keras.layers import Dense, Dropout, Input
from tensorflow.keras.optimizers import Adam
from tensorflow.keras.callbacks import ReduceLROnPlateau
from sklearn.model_selection import train_test_split
from sklearn.preprocessing import MinMaxScaler
from sklearn.metrics import mean_squared_error, r2_score

warnings.filterwarnings('ignore')

# ====================== REPRODUCTIBILITE ======================
tf.random.set_seed(42)
```

```python
np.random.seed(42)

# ====================== 1. GENERATION DU DATASET ======================
N_samples = 8000
c = 3e11 # mm/s
fr = np.random.uniform(25e9, 30e9, N_samples)
er = np.random.uniform(2.2, 12.0, N_samples)
h = np.random.uniform(0.5, 3.0, N_samples)

def tlm_forward(fr, er, h):
Wp = (c / (2 * fr)) * np.sqrt(2 / (er + 1))
E_eff = ((er + 1) / 2) + ((er - 1) / 2) * (1 + 12 * (h / Wp))**(-0.5)
num = (E_eff + 0.3) * (Wp / h + 0.264)
den = (E_eff - 0.258) * (Wp / h + 0.8)
Delta_L = 0.412 * h * (num / den)
Lp = (c / (2 * fr * np.sqrt(E_eff))) - 2 * Delta_L
return Wp, Lp, E_eff

Wp, Lp, E_eff = tlm_forward(fr, er, h)
df = pd.DataFrame({'fr_GHz': fr / 1e9, 'er': er, 'h_mm': h, 'Wp_mm': Wp, 'Lp_mm': Lp, 'E_eff': E_eff})
df.to_csv('antenna_dataset_8000.csv', index=False)

# ====================== 2. PRETRAITEMENT ======================
X = df[['fr_GHz', 'er', 'h_mm']].values
y = df[['Wp_mm', 'Lp_mm']].values

scaler_X = MinMaxScaler()
scaler_y = MinMaxScaler()
X_scaled = scaler_X.fit_transform(X)
y_scaled = scaler_y.fit_transform(y)

X_train, X_test, y_train, y_test = train_test_split(X_scaled, y_scaled, test_size=0.15,
    random_state=42)

# ====================== 3. MODELE KERAS ======================
model = Sequential([
Input(shape=(3,)),
Dense(256, activation='relu'),
Dropout(0.25),
Dense(128, activation='relu'),
Dropout(0.25),
Dense(64, activation='relu'),
Dense(2, activation='linear')
])

model.compile(optimizer=Adam(learning_rate=0.001), loss='mse')

reduce_lr = ReduceLROnPlateau(monitor='val_loss', factor=0.5, patience=60, min_lr=1e-7,
    verbose=1)

history = model.fit(X_train, y_train, validation_split=0.2, epochs=5000, batch_size=128, callbacks=[reduce_lr], verbose=1)
model.save('antenna_synthesis_model_8000_5000epochs.h5')

# ====================== 4. EVALUATION FINALE ======================
y_pred_scaled = model.predict(X_test, verbose=0)
y_pred = scaler_y.inverse_transform(y_pred_scaled)
y_test_real = scaler_y.inverse_transform(y_test)
```

```python

def calculate_metrics(y_true, y_pred):
rmse = np.sqrt(mean_squared_error(y_true, y_pred))
mre = np.mean(np.abs((y_true - y_pred) / y_true)) * 100
r2 = r2_score(y_true, y_pred)
return rmse, mre, r2

rmse_wp, mre_wp, r2_wp = calculate_metrics(y_test_real[:, 0], y_pred[:, 0])
rmse_lp, mre_lp, r2_lp = calculate_metrics(y_test_real[:, 1], y_pred[:, 1])

# ====================== 5. EXPORT ET PLOT ======================
metrics_dict = {'Parametre': ['Wp', 'Lp'], 'RMSE (mm)': [rmse_wp, rmse_lp], 'MRE (%)': [mre_wp, mre_lp], 'R2 Score': [r2_wp, r2_lp]}
metrics_df = pd.DataFrame(metrics_dict)
metrics_df.to_csv('metrics_results_8000_5000epochs.csv', index=False)
```

A.2 Analysis Model - Levenberg-Marquardt Implementation

Because standard deep learning libraries lack native support for the Levenberg-Marquardt (LM) algorithm for shallow architectures, the following script provides a rigorous, from-scratch mathematical implementation using NumPy. It calculates the Jacobian matrix and updates the synaptic weights to act as a high-speed surrogate model for the full-wave CST solver.

Listing A.2: *Python script for the Analysis Model (Levenberg-Marquardt).*

```python
# ============================================================================
# SCRIPT : MODELE D'ANALYSE (LEVENBERG-MARQUARDT 2-10-2)
# ============================================================================
import argparse
import logging
from pathlib import Path
from typing import Tuple
import numpy as np
import pandas as pd
import matplotlib.pyplot as plt
import seaborn as sns

INPUT_COLUMNS = ["Wp", "Lp"]
TARGET_COLUMNS = ["Fr(GHz)", "BW", "S11Min(dB)"]

logging.basicConfig(level=logging.INFO, format="%(asctime)s | %(levelname)s | %(message)s", datefmt="%Y-%m-%d %H:%M:%S")
logger = logging.getLogger(__name__)

def train_test_split_indices(n_samples, test_size, seed):
rng = np.random.default_rng(seed)
indices = rng.permutation(n_samples)
n_test = max(1, int(round(n_samples * test_size)))
return indices[n_test:], indices[:n_test]

def standardize(train_values, test_values):
mean = train_values.mean(axis=0)
std = train_values.std(axis=0)
std[std < 1e-8] = 1.0
train_scaled = (train_values - mean) / std
test_scaled = (test_values - mean) / std
return train_scaled, test_scaled, mean, std

def pack_params(w1: np.ndarray, b1: np.ndarray, w2: np.ndarray, b2: np.ndarray) -> np.ndarray:
return np.concatenate([w1.ravel(), b1.ravel(), w2.ravel(), b2.ravel()])

def unpack_params(params: np.ndarray, n_inputs: int, n_hidden: int, n_outputs: int) -> Tuple[np.ndarray, np.ndarray, np.ndarray, np.ndarray]:
offset = 0
w1 = params[offset : offset + n_inputs * n_hidden].reshape(n_inputs, n_hidden)
offset += n_inputs * n_hidden
b1 = params[offset : offset + n_hidden]
offset += n_hidden
```

```python
w2 = params[offset : offset + n_hidden * n_outputs].reshape(n_hidden, n_outputs)
offset += n_hidden * n_outputs
b2 = params[offset : offset + n_outputs]
return w1, b1, w2, b2

def forward(x: np.ndarray, params: np.ndarray, n_hidden: int, n_outputs: int) -> Tuple[np.ndarray, np.ndarray]:
n_inputs = x.shape[3]
w1, b1, w2, b2 = unpack_params(params, n_inputs, n_hidden, n_outputs)
z1 = x @ w1 + b1
a1 = np.tanh(z1)
y_hat = a1 @ w2 + b2
return y_hat, a1

def residuals(x: np.ndarray, y: np.ndarray, params: np.ndarray, n_hidden: int) -> np.ndarray:
y_hat, _ = forward(x, params, n_hidden, y.shape[3])
return (y_hat - y).ravel()

def jacobian(x: np.ndarray, params: np.ndarray, n_hidden: int, n_outputs: int) -> np.ndarray:
n_samples, n_inputs = x.shape
_, _, w2, _ = unpack_params(params, n_inputs, n_hidden, n_outputs)
y_hat, a1 = forward(x, params, n_hidden, n_outputs)
da_dz = 1.0 - a1**2
n_params = n_inputs * n_hidden + n_hidden + n_hidden * n_outputs + n_outputs
j_mat = np.zeros((n_samples * n_outputs, n_params), dtype=float)

w1_offset = 0
b1_offset = n_inputs * n_hidden
w2_offset = b1_offset + n_hidden
b2_offset = w2_offset + n_hidden * n_outputs

for i in range(n_samples):
for k in range(n_outputs):
row = i * n_outputs + k
for h in range(n_hidden):
common = w2[h, k] * da_dz[i, h]
for m in range(n_inputs):
j_mat[row, w1_offset + m * n_hidden + h] = common * x[i, m]
j_mat[row, b1_offset + h] = common
j_mat[row, w2_offset + h * n_outputs + k] = a1[i, h]
j_mat[row, b2_offset + k] = 1.0
return j_mat

def train_lm(x_train, y_train, hidden_neurons, max_epochs, seed):
rng = np.random.default_rng(seed)
n_inputs, n_outputs = x_train.shape[3], y_train.shape[3]

w1 = rng.normal(0.0, 0.4, (n_inputs, hidden_neurons))
b1 = np.zeros(hidden_neurons)
w2 = rng.normal(0.0, 0.4, (hidden_neurons, n_outputs))
b2 = np.zeros(n_outputs)
params = pack_params(w1, b1, w2, b2)

mu = 1e-3
mu_inc, mu_dec = 10.0, 0.1
min_grad = 1e-9
history = []
```

```python

for epoch in range(1, max_epochs + 1):
err = residuals(x_train, y_train, params, hidden_neurons)
mse = float(np.mean(err**2))
j_mat = jacobian(x_train, params, hidden_neurons, n_outputs)
gradient = j_mat.T @ err
grad_norm = float(np.linalg.norm(gradient, ord=np.inf))

accepted = False
for _ in range(15):
lhs = j_mat.T @ j_mat + mu * np.eye(len(params))
try:
step = np.linalg.solve(lhs, -gradient)
except np.linalg.LinAlgError:
step = np.linalg.lstsq(lhs, -gradient, rcond=None)

candidate_params = params + step
candidate_err = residuals(x_train, y_train, candidate_params, hidden_neurons)
candidate_mse = float(np.mean(candidate_err**2))

if candidate_mse < mse:
params = candidate_params
mu = max(mu * mu_dec, 1e-12)
mse = candidate_mse
accepted = True
break
else:
mu = min(mu * mu_inc, 1e12)

history.append({"epoch": epoch, "train_mse_scaled": mse, "mu": mu})
if grad_norm < min_grad:
break

return params, history

def main():
parser = argparse.ArgumentParser()
parser.add_argument("--csv", type=Path, default=Path("Dataset.csv"))
parser.add_argument("--hidden", type=int, default=12)
parser.add_argument("--epochs", type=int, default=300)
parser.add_argument("--test-size", type=float, default=0.2)
parser.add_argument("--seed", type=int, default=42)
args, _ = parser.parse_known_args()

data = pd.read_csv(args.csv)[INPUT_COLUMNS + TARGET_COLUMNS].dropna().reset_index(drop=True)
X = data[INPUT_COLUMNS].to_numpy(dtype=float)
Y = data[TARGET_COLUMNS].to_numpy(dtype=float)

train_idx, test_idx = train_test_split_indices(len(data), args.test_size, args.seed)
x_train, x_test, _, _ = standardize(X[train_idx], X[test_idx])
y_train, y_test, _, _ = standardize(Y[train_idx], Y[test_idx])

params, history = train_lm(x_train, y_train, args.hidden, args.epochs, args.seed)
logger.info("Entrainement termine avec succes !")

if __name__ == "__main__":
main()
```

Bibliography

[1] Y. Niu, Y. Li, D. Jin, L. Su, and A. V. Vasilakos, "A survey of millimeter wave communications (mmWave) for 5G: Opportunities and challenges," *Wireless Networks*, vol. 21, no. 8, pp. 2657–2676, Nov. 2015.

[2] J. Zhang, E. Bjornson, M. Matthaiou, D. W. K. Ng, H. Yang, and D. J. Love, "Prospective Multiple Antenna Technologies for Beyond 5G," *IEEE J. Select. Areas Commun.*, vol. 38, no. 8, pp. 1637–1660, Aug. 2020.

[3] W. Hong, Z. H. Jiang, C. Yu, D. Hou, H. Wang, C. Guo, Y. Hu, L. Kuai, Y. Yu, Z. Jiang, Z. Chen, J. Chen, Z. Yu, J. Zhai, N. Zhang, L. Tian, F. Wu, G. Yang, Z.-C. Hao, and J. Y. Zhou, "The Role of Millimeter-Wave Technologies in 5G/6G Wireless Communications," *IEEE Journal of Microwaves*, vol. 1, no. 1, pp. 101–122, Jan. 2021.

[4] T. S. Rappaport, S. Sun, R. Mayzus, H. Zhao, Y. Azar, K. Wang, G. N. Wong, J. K. Schulz, M. Samimi, and F. Gutierrez, "Millimeter Wave Mobile Communications for 5G Cellular: It Will Work!" *IEEE Access*, vol. 1, pp. 335–349, 2013.

[5] P. Tiwari, J. K. Rai, A. K. Dwivedi, V. Gahlaut, P. Ranjan, R. Chowdhury, and A. Pandey, "A high isolated, high gain millimeter wave quad-port MIMO antenna array for wideband 5G new radio application," *Scientific reports*, vol. 15, no. 1, p. 34484, Oct. 2025.

[6] M. O. Akinsolu, K. K. Mistry, B. Liu, P. I. Lazaridis, and P. Excell, "Machine Learning-assisted Antenna Design optimization: A Review and the State-of-the-art," in *2020 14th European Conference on Antennas and Propagation (EuCAP)*. Copenhagen, Denmark: IEEE, Mar. 2020, pp. 1–5.

[7] Q. Wu, Y. Cao, H. Wang, and W. Hong, "Machine-learning-assisted optimization and its application to antenna designs: Opportunities and challenges," *China Communications*, vol. 17, no. 4, pp. 152–164, Apr. 2020.

[8] S. A. Ali, M. Wajid, A. Kumar, and M. Shah Alam, "Design Challenges and Possible Solutions for 5G SIW MIMO and Phased Array Antennas: A Review," *IEEE access : practical innovations, open solutions*, vol. 10, pp. 88 567–88 594, 2022.

[9] A. Ramos, T. Varum, and J. N. Matos, “A Review on Mutual Coupling Reduction Techniques in mmWaves Structures and Massive MIMO Arrays,” *IEEE Access*, vol. 11, pp. 143 143–143 166, 2023.

[10] N. H. Jemaludin, A. J. A. Al-Gburi, R. H. Elabd, T. Saeidi, M. F. Akbar, I. M. Ibrahim, and Z. Zakaria, “A comprehensive review on MIMO antennas for 5G smartphones: Mutual coupling techniques, comparative studies, SAR analysis, and future directions,” *Results in Engineering*, vol. 23, p. 102712, Sep. 2024.

[11] M. M. Khan, S. Hossain, P. Mozumdar, S. Akter, and R. H. Ashique, “A review on machine learning and deep learning for various antenna design applications,” *Heliyon*, vol. 8, no. 4, p. e09317, Apr. 2022.

[12] N. Sarker, P. Podder, M. R. H. Mondal, S. S. Shafin, and J. Kamruzzaman, “Applications of Machine Learning and Deep Learning in Antenna Design, Optimization, and Selection: A Review,” *IEEE Access*, vol. 11, pp. 103 890–103 915, 2023.

[13] M. N. A. Siddiky, M. E. Rahman, M. S. Uzzal, and H. M. D. Kabir, “A Comprehensive Exploration of 6G Wireless Communication Technologies,” *Computers*, vol. 14, no. 1, p. 15, Jan. 2025.

[14] T. Raj, R. Mishra, P. Kumar, and A. Kapoor, “Advances in MIMO Antenna Design for 5G: A Comprehensive Review,” *Sensors*, vol. 23, no. 14, p. 6329, Jul. 2023.

[15] R. Chataut, M. Nankya, and R. Akl, “6G Networks and the AI Revolution—Exploring Technologies, Applications, and Emerging Challenges,” *Sensors*, vol. 24, no. 6, p. 1888, Mar. 2024.

[16] M. Alsabah, M. A. Naser, B. M. Mahmmod, S. H. Abdulhussain, M. R. Eissa, A. Al-Baidhani, N. K. Noordin, S. M. Sait, K. A. Al-Utaibi, and F. Hashim, “6G Wireless Communications Networks: A Comprehensive Survey,” *IEEE access : practical innovations, open solutions*, vol. 9, pp. 148 191–148 243, 2021.

[17] K. Rasilainen, T. D. Phan, M. Berg, A. Pärssinen, and P. J. Soh, “Hardware Aspects of Sub-THz Antennas and Reconfigurable Intelligent Surfaces for 6G Communications,” *IEEE J. Select. Areas Commun.*, vol. 41, no. 8, pp. 2530–2546, Aug. 2023.

[18] C. A. Balanis, *Antenna Theory: Analysis and design$nElektronische Ressource*, 3rd ed. Hoboken, N.J: Wiley-Interscience, 2005.

[19] U. B. Shukurillaevich, R. O. Sattorivich, and R. U. Amrillojonovich, “5g Technology Evolution,” in *2019 International Conference on Information Science and Communications Technologies (ICISCT)*. Tashkent, Uzbekistan: IEEE, Nov. 2019, pp. 1–5.

[20] D. Pozar, “Microstrip antennas,” *Proceedings of the IEEE*, vol. 80, no. 1, pp. 79–91, Jan. 1992.

[21] Kai-Fong Lee and Kin-Fai Tong, “Microstrip Patch Antennas—Basic Characteristics and Some Recent Advances,” *Proceedings of the IEEE*, vol. 100, no. 7, pp. 2169–2180, Jul. 2012.

[22] I. Singh and D. V. S. Tripathi, “Micro strip Patch Antenna and its Applications: A Survey,” vol. 2, 2011.

[23] V. S. Kushwah and G. S. Tomar, “Design and Analysis of Microstrip Patch Antennas Using Artificial Neural Network,” in *Trends in Research on Microstrip Antennas*, S. Chattopadhyay, Ed. InTech, Nov. 2017.

[24] M. Rahim, Z. Low, P. Soh, A. Asrokin, M. Jamaluddin, and T. Masri, “Aperture Coupled Microstrip Antenna with Different Feed Sizes and Aperture Positions,” in *2006 International RF and Microwave Conference*. Putra Jaya: IEEE, Sep. 2006, pp. 31–35.

[25] A. Majumder, “Rectangular Microstrip Patch Antenna Using Coaxial Probe Feeding Technique to Operate in S-Band,” *International Journal of Engineering Trends and Technology*, 2013.

[26] R. Rodrigo, “Fundamental Parameters of Antennas.”

[27] WANG. Junjun, “Antenna Theory and Design.”

[28] 1Assisttant Professr, Asansol Engineering College 2Student, Asansol Engineering College and S. Karmakar, “Study of Multiband Microstrip Patch Antenna Design for Wireless Communication,” *International Scientific Journal of Engineering and Management*, vol. 04, no. 06, pp. 1–9, Jun. 2025.

[29] S. E. El Aoud, H. Abbaoui, L. Aguni, Z. El Ouadi, S. Ibnyaich, A. Ghammaz, A. Zeroual, and H. Belahrach, “Design, Optimization and Prediction of the Performances for a Multi-band Patch Antenna Using Artificial Neural Network (ANN),” in *Smart Mobility and Industrial Technologies*, B. El Bhiri, R. Saidi, M. Essaaidi, and N. Kaabouch, Eds. Cham: Springer Nature Switzerland, 2024, pp. 55–64.

[30] S. R. Best and D. L. Hanna, “A Performance Comparison of Fundamental Small-Antenna Designs,” *IEEE Antennas and Propagation Magazine*, vol. 52, no. 1, pp. 47–70, Feb. 2010.

[31] B. S. Da Silva, A. L. P. D. S. Campos, and A. G. Neto, “Equivalent circuit model for analysis of frequency selective surfaces with ring and double concentric ring apertures,” *IET Microwaves, Antennas & Propagation*, vol. 14, no. 7, pp. 600–607, Jun. 2020.

[32] A. Sibille, C. Oestges, and A. Zanella, *MIMO: From Theory to Implementation*. Burlington, MA: Academic Press/Elsevier, 2011.

[33] L. Malviya, R. K. Panigrahi, and M. V. Kartikeyan, *MIMO Antennas for Wireless Communication: Theory and Design*, first edition ed. Boca Raton, FL: CRC Press, 2021.

[34] A. Paulraj, D. Gore, R. Nabar, and H. Bolcskei, “An Overview of MIMO Communications—A Key to Gigabit Wireless,” *Proceedings of the IEEE*, vol. 92, no. 2, pp. 198–218, Feb. 2004.

[35] A. Es-saleh, M. Bendaoued, S. Lakrit, S. Das, and A. Faize, “Design aspects of MIMO antennas and its applications: A comprehensive review,” *Results in Engineering*, vol. 25, p. 103797, Mar. 2025.

[36] A. Christina Josephine Malathi and D. Thiripurasundari, “Review on Isolation Techniques in MIMO Antenna Systems,” *Indian Journal of Science and Technology*, vol. 9, no. 35, Sep. 2016.

[37] S. K. Ibrahim, M. J. Singh, S. S. Al-Bawri, H. H. Ibrahim, M. T. Islam, M. S. Islam, A. Alzamil, and W. M. Abdulkawi, “Design, Challenges and Developments for 5G Massive MIMO Antenna Systems at Sub 6-GHz Band: A Review,” *Nanomaterials*, vol. 13, no. 3, p. 520, Jan. 2023.

[38] S. H. Kiani, A. Altaf, M. R. Anjum, S. Afridi, Z. A. Arain, S. Anwar, S. Khan, M. Alibakhshikenari, A. Lalbakhsh, M. A. Khan, R. A. Abd-Alhameed, and E. Limiti, “MIMO Antenna System for Modern 5G Handheld Devices with Healthcare and High Rate Delivery,” *Sensors*, vol. 21, no. 21, p. 7415, Nov. 2021.

[39] X. Chen, P. J. Soh, and M. S. Sharawi, *MIMO Antenna Systems for 5G and Beyond*. Hoboken, New Jersey: Wiley, 2025.

[40] J. G, I. Singh, and D. K. Choudhary, “Gain and isolation improvement techniques for MIMO antenna: A compendious survey,” *Results in Engineering*, vol. 25, p. 104482, Mar. 2025.

[41] P. Sharma, R. N. Tiwari, P. Singh, P. Kumar, and B. K. Kanaujia, “MIMO Antennas: Design Approaches, Techniques and Applications,” *Sensors*, vol. 22, no. 20, p. 7813, Oct. 2022.

[42] M. A. Haque, J. H. Nirob, K. H. Nahin, N. M. Jizat, M. A. Zakariya, R. A. Ananta, W. M. Abdulkawi, K. Aljaloud, and S. S. Al-Bawri, “Machine learning-based technique for gain prediction of mm-wave miniaturized 5G MIMO slotted antenna array with high isolation characteristics,” *Scientific Reports*, vol. 15, no. 1, p. 276, Jan. 2025.

[43] A. N. Uwaechia and N. M. Mahyuddin, “A Comprehensive Survey on Millimeter Wave Communications for Fifth-Generation Wireless Networks: Feasibility and Challenges,” *IEEE access : practical innovations, open solutions*, vol. 8, pp. 62 367–62 414, 2020.

[44] S. Ershadi, A. Keshtkar, A. H. Abdelrahman, and H. Xin, “WIDEBAND HIGH GAIN ANTENNA SUBARRAY FOR 5G APPLICATIONS,” *Progress In Electromagnetics Research C*, vol. 78, pp. 33–46, 2017.

[45] D. A. Sehrai, M. Abdullah, A. Altaf, S. H. Kiani, F. Muhammad, M. Tufail, M. Irfan, A. Glowacz, and S. Rahman, “A Novel High Gain Wideband MIMO Antenna for 5G Millimeter Wave Applications,” *Electronics*, vol. 9, no. 6, p. 1031, Jun. 2020.

[46] B. Aghoutane, S. Das, M. El Ghzaoui, B. Madhav, and H. El Faylali, “A novel dual band high gain 4-port millimeter wave MIMO antenna array for 28/37 GHz 5G applications,” *AEU - International Journal of Electronics and Communications*, vol. 145, p. 154071, Feb. 2022.

[47] S. Ghosh, G. S. Baghel, and M. Swati, “Design of a highly-isolated, high-gain, compact 4-port MIMO antenna loaded with CSRR and DGS for millimeter wave 5G communications,” *AEU - International Journal of Electronics and Communications*, vol. 169, p. 154721, Sep. 2023.

[48] I. Khouyaoui, M. Elbathaoui, M. Hamdaoui, and J. Foshi, “Design, simulation, and fabrication of high-gain microstrip patch antenna arrays for 28 GHz millimeter-wave 5G applications,” *Physica Scripta*, vol. 100, no. 4, p. 045218, Apr. 2025.

[49] H. A. Mohamed, M. Edries, M. A. Abdelghany, and A. A. Ibrahim, “Millimeter-Wave Antenna With Gain Improvement Utilizing Reflection FSS for 5G Networks,” *IEEE Access*, vol. 10, pp. 73 601–73 609, 2022.

[50] D. Choi, M. A. Sufian, J. Lee, W. A. Awan, Y. Choi, and N. Kim, “Advanced Metamaterial-Integrated Dipole Array Antenna for Enhanced Gain in 5G Millimeter-Wave Bands,” *Applied Sciences*, vol. 14, no. 19, p. 9138, Oct. 2024.

[51] M. Shaban, “Development and Implementation of High-Gain, and High-Isolation Multi-Input Multi-Output Antenna for 5G mmWave Communications,” *Telecom*, vol. 6, no. 1, p. 14, Feb. 2025.

[52] M. A. Haque, M. S. Ahammed, R. A. Ananta, K. Aljaloud, N. M. Jizat, W. M. Abdulkawi, K. H. Nahin, and S. S. Al-Bawri, “Broadband high gain performance MIMO antenna array for 5 G mm-wave applications-based gain prediction using machine learning approach,” *Alexandria Engineering Journal*, vol. 104, pp. 665–679, Oct. 2024.

[53] I. Nadeem and D.-Y. Choi, “Study on Mutual Coupling Reduction Technique for MIMO Antennas,” *IEEE Access*, vol. 7, pp. 563–586, 2019.

[54] G. A. Fadehan, Y. O. Olasoji, and K. B. Adedeji, “Mutual Coupling Effect and Reduction Method with Modified Electromagnetic Band Gap in UWB MIMO Antenna,” *Applied Sciences*, vol. 12, no. 23, p. 12358, Dec. 2022.

[55] R. Selvaraju, M. H. Jamaluddin, M. R. Kamarudin, J. Nasir, and M. H. Dahri, “COMPLEMENTARY SPLIT RING RESONATOR FOR ISOLATION ENHANCEMENT IN 5G COMMUNICATION ANTENNA ARRAY,” *PIER C*, vol. 83, pp. 217–228, 2018.

[56] M. Li, L. Jiang, and K. L. Yeung, “Novel and Efficient Parasitic Decoupling Network for Closely Coupled Antennas,” *IEEE Trans. Antennas Propagat.*, vol. 67, no. 6, pp. 3574–3585, Jun. 2019.

[57] W. Afzal, M. Z. Baig, A. Ebrahimi, M. R. Robel, M. T. A. Rana, and W. Rowe, “Frequency Selective Surfaces: Design, Analysis, and Applications,” *Telecom*, vol. 5, no. 4, pp. 1102–1128, Nov. 2024.

[58] I. Troudi, C. Baccouch, B. Chibani, A. Zouinkhi, A. Flah, C. Z. El-Bayeh, H. Kraiem, and M. Oueder, “Integration of frequency selective surfaces with MIMO antennas for enhanced performance in IoT and V2V communication systems,” *Scientific Reports*, vol. 15, no. 1, p. 35545, Oct. 2025.

[59] K. Katoch, N. Jaglan, and S. D. Gupta, “A Review on Frequency Selective Surfaces and its Applications,” in *2019 International Conference on Signal Processing and Communication (ICSC)*. NOIDA, India: IEEE, Mar. 2019, pp. 75–81.

[60] Hsing-Yi Chen and Yu Tao, “Antenna gain and bandwidth enhancement using frequency selective surface with double rectangular ring elements,” in *Proceedings of the 9th International Symposium on Antennas, Propagation and EM Theory*. Guangzhou, China: IEEE, Nov. 2010, pp. 271–274.

[61] F. Costa, A. Monorchio, and G. Manara, “Efficient Analysis of Frequency-Selective Surfaces by a Simple Equivalent-Circuit Model,” *IEEE Antennas and Propagation Magazine*, vol. 54, no. 4, pp. 35–48, Aug. 2012.

[62] G. H. Dadashzadeh, M. H. Amini, and A. R. Mallahzadeh, “Equivalent Circuit Model for Square Ring Slot Frequency Selective Surface.”

[63] N. Türker, F. Güneş, and T. Yildirim, “Artificial Neural Design of Microstrip Antennas,” 2006.

[64] P. P. Bhagat, D. Pujara, and D. Adhyaru, “Analysis and synthesis of microstrip patch antenna using Artificial Neural Networks,” in *2012 IEEE Asia-Pacific Conference on Antennas and Propagation*. Singapore, Singapore: IEEE, Aug. 2012, pp. 120–121.

[65] H. M. E. Misilmani and T. Naous, “Machine Learning in Antenna Design: An Overview on Machine Learning Concept and Algorithms,” in *2019 International Conference on High Performance Computing & Simulation (HPCS)*. Dublin, Ireland: IEEE, Jul. 2019, pp. 600–607.

[66] M. Abdi and T. Aguili, “Resonance Frequency Prediction of Aperture Coupled Microstrip Antenna Based on Artificial Neural Network:,” Sousse, Tunisia, 2022.

[67] N. Türker, F. Güneş, and T. Yildirim, “Artificial Neural Networks Applied to the Design of Microstrip Antennas,” 2006.

[68] M. V. V. P. Kantipudi, S. Vemuri, S. Sreenath Kashyap, R. Aluvalu, and Y. Satish Kumar, “Modeling of Microstrip Patch Antenna Using Artificial Neural Network Algorithms,” in *Advanced Informatics for Computing Research*, A. K. Luhach, D. S. Jat, K. H. Bin Ghazali, X.-Z. Gao, and P. Lingras, Eds. Singapore: Springer Singapore, 2021, vol. 1394, pp. 27–36.

[69] T. Khan and A. De, “Modeling of microstrip antennas using neural networks techniques: A review: Modeling of MSAs Using NN Techniques,” *International Journal of RF and Microwave Computer-Aided Engineering*, vol. 25, no. 9, pp. 747–757, Nov. 2015.

[70] P. A. Gajbhiye, S. P. Singh, and M. K. Sharma, “A comprehensive review of AI and machine learning techniques in antenna design optimization and measurement,” *Discover Electronics*, vol. 2, no. 1, p. 46, Jun. 2025.

[71] H. Tataria, M. Shafi, A. F. Molisch, M. Dohler, H. Sjöland, and F. Tufvesson, “6G Wireless Systems: Vision, Requirements, Challenges, Insights, and Opportunities,” *Proceedings of the IEEE*, vol. 109, no. 7, pp. 1166–1199, Jul. 2021.

[72] J. L. A. De Guzman and A. C. C. V. Guzman, “Design and Optimization of Microstrip Patch Antennas for Wireless Communication Systems– A Literature Review,” *International Journal of Research Publication and Reviews*, vol. 5, no. 7, pp. 573–580, Jul. 2024.

[73] M. K. ElAbbasi, M. Madi, K. Y. Kabalan, and J. Salah, “Optimizing microstrip patch antenna performance: Leveraging machine learning for comparative analysis of antenna di-mensions and slot structures,” *Results in Engineering*, vol. 28, p. 107523, Dec. 2025.

[74] J. G. Andrews, S. Buzzi, W. Choi, S. V. Hanly, A. Lozano, A. C. K. Soong, and J. C. Zhang, “What Will 5G Be?” *IEEE Journal on Selected Areas in Communications*, vol. 32, no. 6, pp. 1065–1082, Jun. 2014.

[75] R. N. Tiwari, D. Sharma, P. Singh, and P. Kumar, “A flexible dual-band 4 × 4 MIMO antenna for 5G mm-wave 28/38 GHz wearable applications,” *Scientific reports*, vol. 14, no. 1, p. 14324, Jun. 2024.

[76] M. Y. Zeain, M. Abu, A. A. Althuwayb, H. Alsariera, A. J. A. Al-Gburi, A. A. Abdulbari, and Z. Zakaria, “A New Technique of FSS-Based Novel Chair-Shaped Compact MIMO Antenna to Enhance the Gain for Sub-6GHz 5G Applications,” *IEEE access : practical innovations, open solutions*, vol. 12, pp. 49 489–49 507, 2024.

[77] M. Lashab, J. Kosha, F. Abdussalam, M. Belattar, L. Djouablia, C. Zebiri, F. Benabdelaziz, and R. Abd-Alhameed, “Design and Optimization of Electromagnetic Sensor Based On CRLH Resonator,” in *Loughborough Antennas & Propagation Conference 2018 (LAPC 2018)*. Loughborough, UK: Institution of Engineering and Technology, 2018, pp. 68 (4 pp.)–68 (4 pp.).

[78] A. M. Salem, H. Djellab, M. Lashab, O. Allaoua, M. A. Elwanis, C. H. See, and R. A. Abd-Alhameed, “High Isolation and High Gain of MIMO Antennas With FSS for 5G mm-wave Applications,” *Micro & Optical Tech Letters*, vol. 68, no. 1, p. e70499, Jan. 2026.

[79] T. Khan and A. De, “Design of Circular/Triangular Patch Microstrip Antennas using a Single Neural Model.”

[80] I. Ud Din, M. Alibakhshikenari, B. S. Virdee, R. K. R. Jayanthi, S. Ullah, S. Khan, C. H. See, L. Golunski, and S. Koziel, “Frequency-Selective Surface-Based MIMO Antenna Array for 5G Millimeter-Wave Applications,” *Sensors*, vol. 23, no. 15, p. 7009, Aug. 2023.

[81] M. M. Hasan, M. T. Islam, M. Samsuzzaman, M. H. Baharuddin, M. S. Soliman, A. Alzamil, I. I. M. Abu Sulayman, and M. S. Islam, “Gain and isolation enhancement of a wideband MIMO antenna using metasurface for 5G sub-6 GHz communication systems,” *Scientific Reports*, vol. 12, no. 1, p. 9433, Jun. 2022.

[82] I. Khan, K. Zhang, L. Ali, and Q. Wu, "A Compact FSS-Based Four-Port MIMO Antenna for Low Mutual Coupling," *IEEE Antennas and Wireless Propagation Letters*, vol. 22, no. 12, pp. 2836–2840, Dec. 2023.

[83] M. Bilal, R. Saleem, Hammad. H. Abbasi, M. F. Shafique, and A. K. Brown, "An FSS-Based Nonplanar Quad-Element UWB-MIMO Antenna System," *IEEE Antennas and Wireless Propagation Letters*, vol. 16, pp. 987–990, 2017.

[84] R. K. Mistri, A. K. Singh, S. K. Mahto, R. Sinha, A. J. A. Al-Gburi, M. M. Ismail, and K. Alhassoon, "An Eight-element MIMO Antenna System Supporting Dual Bands for 5G Mobile, FSS, and DBS Communication," *Progress In Electromagnetics Research B*, vol. 107, pp. 125–137, 2024.

[85] A. Desai, H.-T. Hsu, Y.-F. Tsao, B. M. Yousef, and A. A. Ibrahim, "FSS based high gain optically transparent MIMO antenna for Sub-6 GHz 5G mid-band applications," *Optik*, vol. 307, p. 171829, Jul. 2024.

[86] T. Raj, R. Mishra, P. Kumar, A. Kapoor, and P. Kuchhal, "Design and development of a FSS backed high gain UWB MIMO planar antenna for FR-II NR bands," *Results in Engineering*, vol. 26, p. 105034, Jun. 2025.

[87] R. Saleem, M. Bilal, H. T. Chattha, S. Ur Rehman, A. Mushtaq, and M. F. Shafique, "An FSS Based Multiband MIMO System Incorporating 3D Antennas for WLAN/WiMAX/5G Cellular and 5G Wi-Fi Applications," *IEEE Access*, vol. 7, pp. 144 732–144 740, 2019.

[88] S. M. Gaber, R. A. Kareem, and A. A. Ibrahim, "Antenna loaded with FSS for 5G."

[89] A. M. Salem, H. Djellab, and A. Oumaima, "Boosting Gain and bandwidth in 5G Wireless Communication Systems."

[90] A. M. Salem, H. Djellab, M. Lashab, and A. Oumaima, "Defected ground microstrip antenna for 5G."

[91] ——, "Design and optimization of Microstrip Patch Antenna at 28GHz for 5G wireless applications," in *2024 6th International Conference on Pattern Analysis and Intelligent Systems (PAIS)*. EL OUED, Algeria: IEEE, Apr. 2024, pp. 1–5.

[92] A. M. Salem, H. Djellab, M. Lashab, and O. Allaoua, "Enhancing Gain and Bandwidth in 5G Wireless Communication Systems," in *13th International Conference on Information Systems and Advanced Technologies "ICISAT 2023"*, M. R. Laouar, V. E. Balas, V. Piuri, D. Rad, Z. Touati Hamad, and A. Cheddad, Eds. Cham: Springer Nature Switzerland, 2024, vol. 981, pp. 11–20.

[93] V. V. Thakare and P. Singhal, “Microstrip antenna design using artificial neural networks: Microstrip Antenna Design Using ANN,” *Int J RF and Microwave Comp Aid Eng*, vol. 20, no. 1, pp. 76–86, Jan. 2010.

[94] S. R. Shakya, M. Kube, and Z. Zhou, “A comparative analysis of machine learning approach for optimizing antenna design,” *Int. J. Microw. Wireless Technol.*, vol. 16, no. 3, pp. 487–497, Apr. 2024.

[95] M. Attaran, “The impact of 5G on the evolution of intelligent automation and industry digitization,” *Journal of Ambient Intelligence and Humanized Computing*, vol. 14, no. 5, pp. 5977–5993, May 2023.

[96] D. Alvarez Outerelo, A. V. Alejos, M. Garcia Sanchez, and M. Vera Isasa, “Microstrip antenna for 5G broadband communications: Overview of design issues,” in *2015 IEEE International Symposium on Antennas and Propagation & USNC/URSI National Radio Science Meeting*. Vancouver, BC, Canada: IEEE, Jul. 2015, pp. 2443–2444.

[97] R. Tiwari, R. Sharma, and R. Dubey, “Microstrip Patch Antenna Parameter Optimization Prediction Model using Machine Learning Techniques,” *IJRITCC*, vol. 10, no. 9, pp. 53–59, Sep. 2022.

[98] A. K. Pandey and M. P. Singh, “Antenna Optimization using Machine Learning Algorithms and their Applications: A Review,” *Journal of Engineering Science and Technology Review*, vol. 17, no. 2, pp. 128–144, Apr. 2024.

[99] M. Mushaib, D. A. Kumar, and D. R. K. Singh, “Designing and Validation of Micro strip Patch Antenna Using Artificial Neural Networks,” vol. 6, no. 06, 2024.

[100] Department of Electrical Engineering, Universitas Trisakti, DKI Jakarta 11440, Indonesia, N. Kurniawati, A. Fahmi, and S. Alam, “Predicting Rectangular Patch Microstrip Antenna Dimension Using Machine Learning,” *Journal of Communications*, pp. 394–399, 2021.